FOSSIL ENERGY

330
7-22-81
Jwa

(2)

Rec. - 330
Bins - 216
NTIS-25

Dr. 2860

DOE/ET/15602-T4

MHD AIR HEATER TECHNOLOGY DEVELOPMENT

Annual Technical Progress Report for the Period January 1—December 31, 1980

March 1981

Work Performed Under Contract No. AC01-80ET15602

FluiDyne Engineering Corporation
Minneapolis, Minnesota

U. S. DEPARTMENT OF ENERGY

DISCLAIMER

DISCLAIMER

Available from the National Technical Information Service, U. S. Department of Commerce, Springfield, Virginia 22161.

Price: Printed Copy A10
Microfiche A01

DOE/ET/15602-T4
Distribution Categories UC-90g and UC-93

MHD AIR HEATER TECHNOLOGY DEVELOPMENT

Annual Technical Progress Report
For the Period
January 1, 1980 - December 31, 1980

Prepared for

United States Department of Energy
Office of Magnetohydrodynamics
Under Contract # DE-AC01-80ET15602

Prepared by

FluiDyne Engineering Corporation
5900 Olson Memorial Highway
Minneapolis, Minnesota 55422

FluiDyne Job 1228
March 1981

TABLE OF CONTENTS

U.S. DEPARTMENT OF ENERGY

FORM DOE 535
(1/78)

MILESTONE SCHEDULE AND STATUS REPORT

1. Contract Identification	2. Reporting Period	3. Contract Number
MHD AIR HEATER TECHNOLOGY	1 Jan 1980 through 31 Dec 1980	DE-AC01-80ET15602

4. Contractor (name, address)
FluiDyne Engineering Corporation
5900 Olson Memorial Highway
Minneapolis, MN 55422

5. Contract Start Date: November 26,1979

6. Contract Completion Date: November 25, 1980 *

7. Identification Number	8. Reporting Category (e.g., contract line item or work breakdown structure element)	9. Fiscal Years and Months: FY 80 (N D J F M A M J J A S) / FY 81 (O N D)	10. Percent Complete a) Planned	10. Percent Complete b) Actual
1.1.1	Material Selection			100
1.1.2	Property Determination			100
1.1.3	Liaison			100
1.1.4	Specifications			100
1.1.5	Materials Analyses			100
1.1.6	Thermal Stress Criteria			100
1.2.1.1	MTF Inst./Data Acq.			100
1.2.1.2	MTF Modifications			100
1.2.1.3	MTF Testing			100
1.2.1.4	MTF Analysis/Reporting			100
1.2.2.1	VTF Inst./Data Acq.			100
1.2.2.2	VTF Modifications			100
1.2.2.3	VTF Testing			100
1.2.2.4	VTF Analysis/Reporting			100

11. Remarks
Detail by WBS

* Additional efforts begun under Contract Mod A001; completion date changed to May 31, 1983

12. Signature of Contractor's Project Manager and Date
D. B. DeCrane 3-26-81

13. Signature of Government Technical Representative and Date

U.S. DEPARTMENT OF ENERGY

FORM DOE 635 (1/78)

MILESTONE SCHEDULE AND STATUS REPORT

1. Contract Identification	2. Reporting Period	3. Contract Number
MHD AIR HEATER TECHNOLOGY	1 Jan 1980 through 31 Dec 1980	DE-AC01-80ET15602

4. Contractor (name, address)	5. Contract Start Date	6. Contract Completion Date
FluiDyne Engineering Corporation 5900 Olson Memorial Highway Minneapolis, MN 55422	November 26,1979	November 25, 1980 *

7. Identification Number	8. Reporting Category (e.g., contract line item or work breakdown structure element)	9. Fiscal Years and Months: FY 80 (N D J F M A M J J A S) FY 81 (O N D)	10. Percent Complete a) Planned	10. Percent Complete b) Actual
1.2.3	Emissions Measurements			100
1.2.4	Creep Testing Apparatus			100
1.2.5	Effluent Air Stream			100
1.3.1	Size/Cost	*		100
1.3.2	SCAMP	*		100
1.3.3	Layout Drawings	*		100
1.3.4	Cost Estimates	*		100
1.3.5	Control Systems	*		100
1.3.6	Matrix Support Test Facility	*		100
1.3.7	Alternative Heater Systems			100
1.3.8	Electrical Isolation			100

11. Remarks
Detail by WBS * Additional efforts begun under Contract Mod A001; completion date changed to 31 May, 1983

12. Signature of Contractor's Project Manager and Date	13. Signature of Government Technical Representative and Date
D. G. DeCorso 3-26-81	

MILESTONE LOG

Identification Number	Description	Completion Date Planned	Completion Date Actual	Comments
1.1.1A	Select. Matls for Full-Scale	Jan 80	Jan 80	
1.1.1B	Select. Matls. for Matrix Test	May 80	Jun 80	Addt'l matl's selected
1.1.1	Materials Selection	Sep 80	Sep 80	
1.1.2	Property Determinations	Nov 80	Nov 80	
1.1.3	Liaison	Nov 80	Nov 80	
1.1.4	Specifications	Nov 80	Nov 80	
1.1.5A	Analysis of Matrix and Valve Test Samples. Heat 202, VTF 1&2	Dec 79	Dec 79	
1.1.5B	Analysis of Valve Test Samples	July 80	July 80	
1.1.5C	Analysis of Matrix Test Samples	Oct 80	Oct 80	
1.1.5	Materials Samples Analyses	Nov 80	Nov 80	
1.1.6	Thermal Stress Criteria	Nov 80	Nov 80	
1.2.1.1	Instrumentation/Data Acquisition	Aug 80	Sep 80	Completion delayed due to technician manpower scheduling
1.2.1.2A	Design Hot Gas Supply Duct	Jun 80	Jun 80	
1.2.1.2B	Test Hot Gas Supply Duct	Jul 80	Jul 80	
1.2.1.2	Reassemble Matrix	Aug 80	Sep 80	
1.2.1.3	Matrix Test	Sep 80	Oct 80	Delayed due to MTF ass'y delays
1.2.1.4	Matrix Analysis/Reporting	Nov 80	Nov 80	
1.2.2.1	Instrumentation/Data Acquisition	May 80	May 80	
1.2.2.2A	Replace Valve Castable	Dec 79	Dec 79	
1.2.2.2	Reassemble VTF	Feb 80	Feb 80	Addt'l mods. required to complete valve test.
1.2.2.3	Valve Test	May 80	Jun 80	
1.2.2.4	Valve Analysis/Reporting	Nov 80	Nov 80	
1.2.3A	Assemble Hardware	Aug 80	Aug 80	
1.2.3	Emissions Measurements	Sep 80	Oct 80	Completion delayed due to delayed start of Heat 203
1.2.4	Creep Testing Apparatus	Nov 80	Sep 80	
1.2.5A	Assemble Hardware	Aug 80	Aug 80	
1.2.5B	Measurements	Sep 80	Oct 80	
1.2.5	Characterize Effluent Air Stream	Nov 80	Nov 80	

Identification Number	Description	Completion Date Planned	Actual	Comments
1.3.1A	Define Base Case Dimensions	Dec 79	Dec 79	
1.3.1	Complete Parametric Studies	Nov 80	Sep 80	
1.3.2A	Design Point Performance	Feb 80	Feb 80	
1.3.2B	Off Design Performance	Aug 80	Aug 80	
1.3.2	Complete Performance Studies	Nov 80	Sep 80	
1.3.3	Critical Component Design Concepts - Base Case	Nov 80	Sep 80	
1.3.3A	Layout Drawings	Apr 80	Apr 80	
1.3.4	Cost Estimate	Nov 80	Nov 80	
1.3.5	Control Concepts	Nov 80	Sep 80	
1.3.6	Matrix Support Test Facility	Nov 80	Nov 80	
1.3.7	Alternate Heater Systems	Nov 80	Nov 80	
1.3.8	Electrical Isolation	Nov 80	Sep 80	

1.0 OBJECTIVE AND SCOPE OF WORK

Work to be done under this Contract will continue the technology development of the directly-fired high temperature air heater (HTAH) for MHD power plants. The work will extend the efforts begun under previous ERDA/DOE contracts, the most recent being Contract DE-AC01-78ET10814. The Statement of Work specifies work to be done under three tasks as described in the following.

Task 1 - Materials Selection, Evaluation, and Development

The objective of this task is to continue development of ceramic materials technology for the directly-fired HTAH. The scope of the work under Task 1 will include compilation of materials data, materials selection for testing and design studies, materials property determination, liaison with refractory manufacturers and other organizations to encourage development of materials and fabrication technology, establishment of preliminary HTAH material specifications, analyses of test materials, and development of criteria for thermal stress limits for crack-tolerant refractory materials.

Task 2 - Operability, Performance, and Materials Testing

The objectives of this task are to demonstrate the technical feasibility of operating a directly-fired HTAH (including both the heater matrix and valves), to continue obtaining information on life and corrosion resistance of HTAH materials, and to obtain design information for full-scale studies and future design work. The scope of the work will include tests in the Matrix Test Facility (MTF) and Valve Test Facility (VTF) built and operated under contracts EX-76-C-01-2254 and DE-AC01-78ET10814, emissions measurements in the MTF and VTF, design of a dilatometer for performing creep measurements in the directly-fired HTAH environment, and characterization of the effluent air stream from the MTF.

Task 3 - Full-Scale Design Concepts

The objectives of this task are to begin the identification of HTAH control requirements and control system needs, and to continue full-scale study efforts incorporating updated materials and design information in order to identify development needs for the HTAH development program. The scope of the work will include size/cost analyses and parametric studies of design options using a size/cost code and other computer codes developed and refined under Contracts EX-76-C-01-2254 and DE-AC01-78ET10814, dynamic HTAH system performance calculations using the SCAMP (System Cyclic Analysis of Multiple Preheaters) computer code developed under contract DE-AC01-78ET10814, preparation of system layouts and cost estimates, screening and definition of control systems and determination of operating methods, definition of requirements for a future test facility to test matrix support concepts at nearly full-scale, and development of design concepts for alternative heater systems and electrical isolation of the air duct from the MHD combustor.

2.0 SUMMARY

During the reporting period from January 1 through December 31, 1980, work was continued on all three tasks. The objectives and milestones of the contract as originally written were achieved prior to November 26, 1980. The contract has been modified to include additional efforts on certain subtasks delineated in the original contract and to extend the period of performance until May 31, 1983. The format of this report will follow the work plan submitted to DOE under the original contract, including work done after November 26, 1981. Future reports will follow the work plan submitted to DOE following the contract modification.

The major activities during the reporting period were conducted under Task 2, and included the running of one test each in the Matrix Test Facility (MTF) and Valve Test Facility (VTF). The MTF simulates the performance of a matrix of cored bricks in a directly-fired HTAH. This facility was operated cyclically with a reheat gas flow containing potassium sulfate seed and Montana Rosebud ash for 300 hours during the test denoted as Heat 203, following the numbering sequence used under the previous contract. Fused cast magnesia-spinel material continued to show good resistance to the HTAH conditions as a matrix material. Several other materials were also tested in various matrix locations, including spinel castable, sintered spinel, and fused cast chromia. The spinel materials, used in the lower portions of the matrix, appear to have held up well while the fused cast chromia was badly degraded at the top of the matrix. Performance of these materials will be characterized through materials analyses. Accumulation of deposits in the matrix flow passages was observed over the course of the 300 hour test. No attempt was made to remove the deposits through operation

in a "cleanout" mode; the MTF was operated under conditions simulating normal operation of a directly-fired HTAH. Measurements of NO_x concentration in the reheat gas flow and of potassium carryover in the effluent air stream were also made during the test.

The VTF simulates the performance of a directly-fired HTAH gas inlet valve. The test of the VTF during the reporting period was denoted as Test 3, again continuing the numerical sequence established under the previous contract. The facility was operated for a total of 532 hours, including 375 total valve cycles. During 154 hours and 282 cycles, the gas flow included potassium sulfate seed and Montana Rosebud ash. Problems were encountered with the VTF hot gas supply duct, requiring two intermediate shutdowns for modifications to this portion of the facility. No problems were encountered with the test valve during Test 3, however. Leakage of the test valve remained small, and operation of the valve was not inhibited by exposure to the simulated radiant boiler exhaust gas stream. Calcium aluminate bonded spinel castable continued to perform well as insulation in the water cooled test valve. In addition, no evidence of degradation of insulation materials in the VTF due to pressure cycling was detected.

Design of refractory creep testing apparatus to perform creep measurements in the simulated HTAH environment was also completed under the Task 2 activities. Fabrication and testing of this apparatus was not authorized under this contract but is anticipated at some future date.

Activities under Task 1 continued the development of ceramic materials technology for the directly-fired HTAH. Materials were selected for evaluation in the HTAH test facilities, and materials were selected and layup schemes were developed for evaluation in full-scale studies. Analysis of materials from tests in the MTF and VTF under this and the previous contract was continued. Liaison efforts with refractory manufacturers were continued and material samples produced through developmental programs at various companies were supplied for test evaluation at FluiDyne and at Montana State University (MSU). Meetings and discussions were held with personnel at MSU, MERDI, and Montana College of Mineral Science and Technology, all of whom are doing HTAH materials work under contract to DOE. Guidance and coordination was provided to the Montana personnel with regard to priority rankings for the various property measurements and as to materials and test conditions for which measurements are desired. Compilation of these property measurements and other HTAH materials data in a formal data base and development of procedures for establishing specifications for HTAH materials were begun.

Studies of full-scale heater systems were continued under Task 3. An example HTAH for a 1000 MW_e power plant was developed and used as a focal point for the full-scale studies. This example system was used to make cost studies in which the cost effectiveness of various material and insulation schemes was examined. Four runs of the SCAMP computer code were also made, examining dynamic performance and response to a control technique for the example HTAH. Direction was given by DOE to focus the full-scale studies on a 600 MW_e plant instead of the 1000 MW_e example, and a new example HTAH is being developed.

Studies of specific concerns related to the use of a directly-fired HTAH were also made during the reporting period, including an examination of the effect of valve life assumptions on HTAH reliability and an evaluation of the effect of valve leakage on the performance of the MHD plant.

In addition to these major efforts under Task 3, a concept was developed for a test facility to evaluate matrix support concepts at nearly full-scale, and concepts were studied for alternative air heaters, specifically including an intermediate temperature air heater (ITAH) and an upflow-type HTAH, and for electrically isolating the HTAH from the MHD combustor.

Details of the technical progress during the reporting period are presented in Section 3, and conclusions drawn from the HTAH development work during the reporting period are discussed in Section 4.

3.0 DESCRIPTION OF TECHNICAL PROGRESS

3.1 Task 1 - Materials Selection, Evaluation, and Development

3.1.1 Materials, Selection and Data Base

During the reporting period, selection of refractory materials was made for test evaluation in both the MTF and VTF. Materials schemes were also proposed for full-scale studies of the directly-fired HTAH and of a so-called intermediate temperature air heater (ITAH). In addition to these material selection activities, work under this subtask included beginning to compile HTAH material properties in a formal data base.

Materials Selection - Test Valve

Insulation material for HTAH hot gas inlet valves must be resistant to attack by corrosion and erosion due to the seed/ash-laden radiant boiler exhaust gases. Two insulation materials had been tested in the test valve of the VTF during Valve Tests 1 and 2 (Ref 6). One of these materials, a calcium aluminate bonded stoichiometric spinel castable (Norton LS-812), had shown good performance in the first tests. This material was selected for further evaluation in the test valve. All of the castable insulation in the test valve was removed and replaced with the Norton LS-812 castable before valve testing was resumed, as described in Section 3.2.2. No additional materials were selected for evaluation in the test valve itself during the reporting period.

Materials Selection - Hot Gas Supply Ducts

Each of the test facilities, MTF and VTF, includes a hot gas supply duct having a length on the order of 3.7 m (12 ft) which is required to properly simulate the HTAH reheat gas and deliver it to the test matrix or test valve. Gas temperatures of 2030 K (3200 F) or greater and presence of solid and liquid seed and ash particles (as the injected seed vaporizes and ash melts) combine to produce more severe corrosion/erosion conditions than will exist in an actual directly-fired HTAH. Materials used as the high temperature liner in these ducts have generally performed poorly, and this has been a major difficulty in conducting tests with the MTF and VTF. The size and configuration of the hot liner and the refractory material used have been found to affect its performance during tests.

Based on the good performance of the Norton LS-812 castable in the test valve and in previous tests as a matrix hot liner in the MTF, this material was selected for use in a portion of the VTF hot gas supply duct. However, in this application, the LS-812 castable showed significant reaction with and depletion by the gas stream. It was deemed unsuitable for use in the hot gas supply duct near the point of seed/ash injection.

Rebonded fused grain magnesia chrome (Corhart RFG) has demonstrated the best corrosion/erosion resistance in the hot gas supply ducts. RFG was selected for use in the VTF tests, replacing the spinel castable material, and in the MTF test work during the reporting period. Test specimens of fused cast chromia (Carborundum Monofrax E), fused cast stoichiometric

spinel (Carborundum Monofrax LS) and eutectic spinel (Carborundum Monofrax LE), fused cast magnesia-spinel (Corhart X-317), an alumina chrome ramming mix (A.P. Green Jade Ram), and the LS-812 castable coated with an alumina chrome mortar (A.P. Green Jade Set) were also evaluated in the hot gas supply duct of the VTF, but none of these materials performed as well as the RFG.

Materials Selection - MTF

Several materials were selected for evaluation in the MTF test run during the reporting period. In order to minimize the cost of a full-scale HTAH, it will be desirable to use the most inexpensive materials which will provide sufficient resistance to the service conditions. Since the severity of these conditions varies somewhat in the various regions of the HTAH, it will be desirable to use the most cost effective materials for each region of the heater. The materials selected for evaluation in the MTF during the reporting period were chosen to begin addressing this "materials stratification" question, evaluating different materials in different areas.

Above the cored brick matrix in the MTF is a so-called "target area," which serves as a means for redirecting the horizontally flowing reheat gas from the hot gas supply duct vertically downward into the cored bricks. This target area is subjected to severe erosion by the liquid ash particles as well as corrosive attack by the seed and ash in the gas. Fused cast chromia (Carborundum Monofrax E) was selected for evaluation in the target area; this material was expected to have superior erosion resistance compared to materials previously used in this area. Although this type of material

is relatively expensive, if used only in certain high erosion erosion areas of a full-scale HTAH the effect on total system cost would not be prohibitive. The Monofrax E was also selected for use in the uppermost 0.23 m (9 in) of the cored brick matrix, which had shown a relatively high degree of erosion in earlier tests.

During test evaluation in the MTF, the Monofrax E demonstrated excellent performance in the target region, bearing out expectations for its erosion resistance. The Monofrax E matrix bricks, however, were severely attacked and depleted. At this time, it appears that the Monofrax E material is suitable for use as an erosion wear surface, but is not suitable for use as a cored brick, where a large surface/volume ratio exists. Further analysis of the material is underway.

The use of castable materials where possible has been shown through full-scale studies to result in significant HTAH cost reduction. Thus it is desirable to evaluate the performance of castable materials in the test facilities. Norton LS-812 castable was selected for use as the liner surrounding the matrix over the entire length of the matrix. This material had been evaluated in the matrix liner application in previous tests (Ref 6), but not in such a large quantity. LS-812 castable was also selected for use as the inner hot liner enclosing the gas stream in the regions above and below the cored brick matrix. The service conditions in these regions are not as severe as in the hot gas duct liner for which the LS-812 had proved unsuitable as discussed above. The performance of the LS-812 castable appeared to be generally acceptable, but post test evaluation is still underway.

Fused cast magnesia-spinel (Corhart X-317) is the material which has shown the best performance as a matrix material in previous tests (Ref 6). This material was selected for use as the bulk of the cored brick matrix. Previously tested X-317 matrix bricks were reused, and some unused X-317 was also used. Preliminary results indicate that the X-317 material performed satisfactorily, but substantial alteration of the bricks immediately below the Monofrax E matrix bricks was observed. Further analysis of the X-317 material is underway.

Sintered spinel bricks (Norton SX-471) were selected for evaluation at the bottom of the cored brick matrix. The thermal conditions are least severe in this region and the superior properties of fusion cast material may not be required Thus, evaluation of the relatively inexpensive sintered brick was desired. Post-test analysis of this material is underway.

The matrix support mechanism for the directly-fired HTAH is of major importance. The material used must be capable of withstanding the severe thermal and corrosive conditions as well as the mechanical loads imposed by the need to support the weight of the entire cored brick matrix. Complex brick shapes may also be required, as in one concept which involves a perforated support dome. LS-812 castable was selected for evaluation as the matrix support brick in the MTF in order to begin evaluating materials and construction methods for the more complex structure needed for a full-scale HTAH.

A method was developed for casting the MTF support brick in one piece with flow passages to match the matrix flow passages. The mold developed for this purpose is shown in Fig 1.

Wooden dowel inserts were initially used for the flow passages. This approach proved ineffective, however, because of swelling of the dowels which caused cracking of the support brick. Cardboard tubes were then chosen for the flow passage inserts. The tubes were soaked in paint to provide sufficient rigidity under the moist working conditions during casting, while remaining flexible enough not to inhibit expansion of the castable material. This approach was successful, and a support brick with minimal cracking was produced as shown in Fig 2. The support brick is shown being installed in Fig 3.

This method could be used for producing pieces for a full-scale HTAH matrix support from a spinel castable. Significant cost savings could be realized by casting matrix support pieces rather than requiring hot pressed or sintered bricks in the complex shapes with flow passages required for a dome type matrix support. Evaluation of the performance of cast matrix support pieces in HTAH test facilities will help define whether this approach to the matrix support is viable.

Materials Selection - Full-Scale HTAH Studies

Materials and insulation layups were selected for an entire full-scale HTAH system. The selection was made using materials which had been tested in subscale HTAH test facilities or for which sufficient data was available to make judgments of performance in the HTAH environment. Layups were chosen to allow reasonable installation techniques. The purpose of this material selection exercise was to provide an updated choice of materials and layups for full-scale HTAH systems, against which the size and cost effectiveness of different materials and layups can be measured through full-scale studies. This is done periodically in the course of the HTAH development program in order to identify development needs for materials and installation techniques.

A summary of the 21 areas for which materials and layups were selected is given in Table 1. An example of one of these areas, the gas inlet duct, is shown in Table 2 in order to illustrate the type of materials chosen and the extent of the selection process.

Materials Selection - Full-Scale ITAH Studies

Materials were also selected for use in full-scale studies of alternate heater systems (see Section 3.3.7). In particular refractory insulation schemes were selected for use in the gas and air inlet and outlet manifolds and ducts of an intermediate temperature air heater (ITAH). The materials are delineated in Table 3. The materials specified are generally more conventional than the materials proposed for the HTAH application except for the inner liner in the gas inlet manifolds and ducts. Spinel castable is proposed in this area for seed resistance. Since the materials temperatures in the ITAH are much lower than for the HTAH, development needs would be considerably reduced for a ceramic ITAH.

Data Base

Work was begun during the reporting period on a formal data base for compiling engineering data on HTAH materials. The data base will be arranged in a format such that it is accessible by FluiDyne's size/cost and performance computer codes and is readily accessible for editing whenever new or updated data is available. The first information stored in the data base includes, for each of the materials compiled:

1. Manufacturer's designation
2. Generic designation
3. ASTM designation (if any)
4. Method of fabrication

5. Manufacturer's name and address
6. HTAH application (including service condition restrictions)
7. Experience to date in MHD testing
8. Composition
9. Mixing and curing instructions (for castables)
10. Data source and estimate of validity for engineering calculations
11. Cost information
12. Materials properties including density; porosity; temperature dependent values of modulus of elasticity, Poisson's ratio, thermal conductivity, specific heat, thermal stress limit, thermal expansion coefficient, electrical conductivity, modulus of rupture, compressive strength, critical stress intensity factor (K_{1C}); and load and temperature dependent values of creep rate.

This information will provide the basis for size/cost and performance studies under Task 3 and for future design of HTAH systems.

Much of this data has been compiled for five materials as shown in Tables 4-8. These materials are Corhart X-317, Norton LS-812 castable, and Johns-Manville Yuma, C-22Z, and Superex 2000. Corhart X-317 is a fusion cast magnesia-spinel proposed for the directly-fired heater matrix and hot liners. Norton LS-812 is a stoichiometric spinel castable proposed for hot liners , matrix support, or for the matrix at temperatures below 1589 K (2400 F). The Johns-Manville materials are possible backup insulation, if no contact with the directly-fired reheat gas is allowed. The data was extracted from Refs 1-5. If no reference is indicated in Tables 4-8, the values represent estimates by FluiDyne.

Information on these and other materials will be added to the data base as it becomes available. The information will be continually reviewed and updated.

3.1.2,6 Property Determination and Thermal Stress Criteria

The objectives of these subtasks are to define needs and test conditions for HTAH material property determination work carried out at FluiDyne or at other laboratories, to interpret the results in terms of the HTAH materials data base, and to develop criteria relating stress and fracture to thermal cycling.

A priority system was established in order to provide basic goals for the overall property determination efforts. The suggested priority rankings of properties to be determined and types of materials for which they are needed is given in Table 9. The need dates given in this table reflect the need to obtain materials data for development of the HTAH in a program which will move from the present testing scale (0.25 - 0.5 MW_{th}) to a Technology Development Unit of about 5 MW_{th}, in which all HTAH components of a single heater are tested, and finally to design of HTAH systems at progressively larger scale, for example at the CDIF and ETF MHD facilities. The work being carried out at this time and in the near future will be directed at meeting the Priority One requirements as specified in Table 9.

Discussions were held with personnel at Montana College of Mineral Science and Technology, Montana State University (MSU), and Montana Energy and MHD Research and Development Institute (MERDI) to review and coordinate materials property work being done in support of the directly-fired HTAH development program. The most recent meetings took place

December 10-12, 1980. Following these meetings, the Montana personnel were provided with priority rankings concerning the work now underway and to be carried out in the current fiscal year. The priority rankings given the Montana personnel are:

Montana Tech

1. Refractory creep under thermal cycling conditions
   a. X-317, fused cast magnesia-spinel
   b. LS-812, stoichiometric spinel castable, calcium aluminate bond phase

2. Determination of elastic properties using mechanical technique at elevated temperatures
   a. X-317
   b. LS-812

3. Isothermal creep testing - anticipate work done in parallel with 1 or 2
   a. X-317 - additional data points in range of 1.4 - 2.8 MPa (200-400 psi) load and 1823-1923 K (2800-3000 F) temp.
   b. LS-812 - additional data at intermediate temperature and load points to better determine creep model
   c. Carborundum developmental materials - only after some thermal expansion under load results available
   d. Insulating brick - only if all of 1,2, and 3 above have been completed

4. Castable refractory QA procedures for MSU testing

5. Hot compressive strength or hot modulus of rupture - not needed at present; will have importance in future years.

Montana State University

1. Electrical conductivity measurements at elevated temperatures
   a. X-317
   b. LS-812

2. Thermal expansion under load
   a. LS-812 if needed to support Montana Tech creep work
   b. Carborundum developmental materials - prior to creep work

3. X-ray diffraction work as required to determine compositions in a timely fashion

4. Electrical conductivity cell for MTSFF refractories

5. Investigate refractory material interactions for potential areas such as stratified matrix, dome/hot liner, etc.

MERDI

1. Pre- and Post-test microstructural analyses
   a. SEM
   b. Thin section work

2. Pre- and Post-test phase composition work; X-ray diffraction

3. Insulating castable development

4. Thermal diffusivity/conductivity measurements for new materials

5. Fracture toughness (K_{1c}) at elevated temperatures

These priority rankings will be continually reviewed and updated to insure that the property measurement work is meeting the needs of the HTAH development program.

High temperature creep measurements at Montana Tech have been completed for fused cast magnesia spinel (Corhart X-317) and calcium aluminate bonded spinel castable (Norton LS-812). The results of the X-317 measurements are shown in Figs 4 and 5. The experimental data is presented in terms of measured steady state creep rate vs. applied stress. As seen in Fig 4, when plotted in this manner, the creep rate appears to be independent of temperature; in fact, additional measurements will be required at stress levels on the order of 1.4-2.8 MPa (200-400 psi) at temperatures in the range of 1823-1923 K (2800-3000 F) to determine temperature dependence of the creep rate.

The results do indicate that at stresses less than 1 MPa (145 psi) no measurable steady state creep was observed even at temperatures as high as 1923 K (3001 F). Mechanical stresses in HTAH refractory materials have been shown to be less than about 1 MPa (145 psi) at temperatures up to 1978 K (3100 F) in upper dome regions and less than about 1.4 MPa (200 psi) in lower temperature regions in full-scale designs considered to date. Various concepts for design of large refractory ducts or heater domes, or so called "alternative heater concepts" (see Section 3.3.7), may involve stresses and temperatures in the range specified above for additional measurements.

Possible allowable creep rates are indicated in Fig 5. The Montana Tech measurements indicate that under compressive stress below about 3.25 MPa (470 psi) refractory pieces constructed from Corhart X-317 would deform less than 1% over a 75,000 hour operating life. Thus, Corhart X-317 appears to be a suitable material for use in HTAH designs from the standpoint of required mechanical loads. Results of the measurements on Norton LS-812 are still being analyzed.

Cyclic thermal stresses in the HTAH cored bricks may have magnitudes many times greater than the mechanical loads. An experiment was designed during the reporting period to be carried out at Montana Tech in order to investigate the effects of cyclic thermal stresses on candidate HTAH cored brick materials. The experiment was designed to produce thermal stresses in a cylindrical sample of refractory material by immersing it in a furnace whose temperature is varied in a cyclic manner. The prescribed temperature cycle and the resulting induced thermal stress are shown in Fig 6. The thermal stress levels approximate the stresses which would be experienced in the webs of a cored brick during normal operation of a HTAH.

A furnace was built and 25 mm (1 in) diameter cylinders of Corhart X-317 were tested in the furnace. Lamé constants, which may be used to determine the elastic properties of materials, were ultrasonically measured before and after the exposure to thermal cycling. However, due to the nature of the material (microstructurally very dense with large macroporosity) the ultrasonic measurements could not be interpreted, and the technique had to be abandoned. For future thermal cycling work, the material properties will be measured mechanically.

The emphasis of the thermal cycling measurements will also be changed. In order to study the interaction of a steady applied load and cyclic thermal stresses, as would exist in an actual HTAH, creep measurements will be undertaken at Montana Tech in which refractory samples are loaded mechanically while being subjected to cyclic thermal stress as shown in Fig 6.

3.1.3 Liaison

Liaison with refractory manufacturers and other organizations is conducted primarily to encourage development of suitable materials, as well as manufacturing and installation techniques, for use in the directly-fired HTAH. The most important results of these efforts during the reporting period were from the Norton Co. and the Carborundum Co.

Norton Co. began development work on a sintered spinel brick type material, and supplied bricks which were tested in the MTF as the lowermost matrix bricks. The material has properties similar to other high temperature materials manufactured by Norton with the additional advantage of the

spinel composition, which has been shown in earlier test work to be resistant to the corrosive directly-fired HTAH environment. The material is more easily shaped and would be less expensive than fused cast materials. Preliminary test results have indicated good performance in the lowest matrix temperature range as discussed in Section 3.1.1.

Carborundum Co. has undertaken development programs concerning fused cast materials for use in directly-fired MHD air heaters. One of these programs involves development of new fused cast material compositions. Fused cast materials have proved to be the most resistant to the corrosive HTAH environment, but many fused cast materials, which have very high density, do not have sufficient thermal stress cycling resistance for use in the HTAH. An exception has been Corhart X-317, in the MgO-Al_2O_3 system, whose microstructure gives this fused cast material good resistance to propagation of cracks induced by cyclic thermal stresses. The intent of the Carborundum efforts is to develop a material combining the higher melting point of fused cast chromia with the better microstructure of fused cast magnesia-alumina. Several samples were produced under the Carborundum program during the reporting period. They did not become available in time to be tested in the MTF, however. The samples were then delivered to Montana State University because a simulated directly-fired HTAH matrix will be tested at MSU before the next test of the MTF is run at FluiDyne. The test programs at MSU and FluiDyne are designed to complement each other and provide more information on the directly-fired HTAH than would be available from either test program alone.

Development efforts are also underway at Carborundum for the production of cored brick shapes from fused cast materials. This is of great importance to the HTAH development program, since the costs of machining and drilling fused cast materials for full-scale heater matrix bricks may be economically prohibitive. The ability to obtain matrix bricks with the proper flow passages

and shapes at reasonable cost will insure that the use of fused cast materials is economically feasible.

Liaison efforts also included a number of other refractory manufacturers concerning the development needs for the directly-fired HTAH. Information was also shared with Babcock and Wilcox and Argonne National Laboratory, regarding refractory material for use in the HRSR project. The primary goal of future liaison work will be to encourage development of materials resistant to corrosion and thermal cycling, manufacturing techniques for fusion cast materials, and castable insulation suitable for the HTAH.

3.1.4 Specifications

The objective of this subtask is to develop preliminary specifications for the refractory materials needed in the directly-fired HTAH. These preliminary specifications will be updated as additional information becomes available from property measurements as described in Section 3.1.2, and from test evaluation at FluiDyne and MSU.

In order to determine the level of detail required for preliminary material specifications, procurement specifications for other refractory heaters were reviewed. The objective of work under this subtask is to prepare such specifications for the various materials required in a directly-fired HTAH in order to identify what information is required for HTAH materials and to lay the foundation for future HTAH design work. These specifications will be revised and upgraded as more information on materials requirements and material properties becomes available over the course of the heater development program.

A quality assurance program was initiated at FluiDyne's laboratory for use initially with spinel castable materials. An outline of the procedures involved in this program is shown in Table 10. These procedures are of the type which would be followed to assure quality of material purchased for use in construction of a HTAH. The procedures will be followed as part of FluiDyne's laboratory work for two reasons, 1) to eliminate possible poor quality materials before use in the test facilities and 2) to obtain data which can be correlated to performance of spinel castable materials and eventually used in developing the material specifications.

Similar procedures will be developed for other materials over the course of the HTAH development program.

3.1.5 Materials Analyses

Materials analysis work completed during the reporting period included analysis of pristine and exposed materials and deposits from tests run under Contract DE-AC01-78ET10814 as well as analysis of material from VTF Test 3 and collection of samples for analysis from MTF Heat 203.

Analyses from Earlier Tests

Three spinel-based materials were analyzed in their pristine forms as used in VTF Tests 1 and 2 and in MTF Heat 202 under the earlier contract (Ref 6). The results of these analyses are shown in Table 11. Norton LS-812 and Taylor X-13337 are stoichiometric spinel castables used as the test valve insulation for VTF Tests 1 and 2. The LS-812 performed well in these tests and the X-13337 performed poorly. Corhart X-317 is the fused cast magnesia-spinel material used to form the cored brick matrix for MTF Heat 202 and the bulk of the matrix for Heat 203 as discussed in Section 3.1.1.

A startling result is the absence of phosphate in the Taylor material which has been called a "phosphate bonded" castable. The analyzed sample was removed from the test valve by the valve manufacturer prior to testing. The absence of phosphate could well explain the lack of green strength and subsequent poor performance of this material as opposed to more favorable test results which had been obtained using samples of this material in the MTF. The "corundum" in this material may well have been calcium hexaluminate which probably acted as the bonding agent for casting in the valve. Both of the castables differed slightly from the actual stoichiometric ratio of 28% MgO to 71% Al_2O_3.

Analysis of material deposited in the matrix flow passages during Heat 202 is shown in Table 12. It had been postulated earlier that these deposits consisted of degradation products from the X-317 hot liner in the hot gas supply duct, which had deteriorated badly and flowed into the matrix. The analyses in Table 12 verify this assumption. As in the case of deposits from Heat 201, presented in previous reports, the magnesia content of the deposits (37-47%) is far greater than that of Rosebud ash (20%) in the deposits near the top of the matrix. Calcia and iron oxide are also present in the deposits, but at levels (1-4%) greatly reduced from coal ash (15% and 7%, respectively). Thus the deposits are seen to consist of reaction products of the hot gas supply duct liner and the injected coal ash. The character of the deposits varied with position in the matrix, the alumina content decreasing and the magnesia and silica increasing as the deposits flowed toward the bottom of the matrix.

Analyses of test valve refractories and deposits removed after Valve Test 2 are shown in Table 13. A number of results can be observed. The gate area, which is shielded from the gas stream during the gas phase, showed minimal chemical change to the refractory insulation. The other areas of the valve, such as the body and the follwer ring, which were exposed to the gas stream all exhibited a decrease in alumina and often showed formation of potassium aluminum silicate ($KAlSiO_4$). This may be due to reaction of K_2O with Al_2O_3 from the bond phase, since even in the Taylor castable alumina apparently plays a part in the bonding. The iron content is probably due to the presence of steel reinforcing fibers in the valve insulation. Little unreacted ash is seen, even in deposits on the floor of the gate cavity. These deposits are seen to be degraded refractory, having reacted with both seed and ash, and are thought to be the cause of scratches on the valve seats (see Section 3.2.2).

Analyses from Current Contract Tests

As discussed in Section 3.1.1, calcium aluminate bonded spinel castable (Norton LS-812) was used in a portion of the hot gas supply duct of the VTF. This material degraded badly, in contrast to excellent performance as a matrix hot liner in a previous MTF test. Analysis of a sample of the degraded castable was obtained from the manufacturer during the reporting period. The manufacturer's report is summarized in the following:

> "The evaluation from a ceramic point of view evolves around the material's microstructure and the phase composition changes occurring at the reacting surface. X-ray diffraction and petrographic microscopy of the cross-sections were employed in this determination.

"The microstructure of the sample submitted is a high density, low porosity spinel refractory. Porosity and spinel grain size do not appear to have changed in the unreacted area (see Fig 7) and at the reacted zone (see Fig 8). Likewise, the amount of glassy phase between the grains does not appear to change between the unreacted zone and the hot face of the specimen.

"The phase composition of the hot face indicated the presence of major spinel, moderate amounts of forsterite ($2MgO.SiO_2$) and enstatite ($MgO.SiO_2$) and trace amounts of alumina. The unreacted area of the refractory had major spinel and minor amounts of alumina present.

"The mode of failure was characterized by attrition of the refractory during 55 hours of exposure as evidenced by the increase of inner diameter at the combustion zone. The failure mode thus appears to be due to the reaction of silica in the coal ash with the refractory lining in the combustion chamber. This reaction is indicated by the presence of enstatite ($MgSiO_3$) and forsterite (Mg_2SiO_4) in the hot face sample. Since enstatite melts well below the temperature in the combustion chamber, liquid (glass) would be expected to be found at the hot face. Fig 8 a photomicrograph taken at the hot face, and Fig 7, taken in the unreacted refractory about 1.5 cm in the hot face, show equal amounts of glass in both zones. The reason glass is not observed is that when it forms at the spinel grain and refractory surface, it is swept from boundaries the refractory face by the turbulence generated in the combustion chamber. Therefore, there was a constant attrition of the exposed refractory during the test. This reaction is more rapid where a smaller grain size is present at the hot face (Fig 9).

"The reaction that occurs at the hot face can best be illustrated by the ternary phase diagram (Fig 10) of MgO-Al_2O_3-SiO_2. Assuming the overall composition of the refractory is at the spinel composition on the MgO-Al_2O_3 binary juncture at the base line, the composition moves toward the SiO_2 apex. The bulk composition at the hot face becomes more silica rich and spinel reacts with the liquid at 1800 C about half way through the spinel stability field to form corundum, forsterite and liquid. With further melting, the more siliceous enstatite is stabilized. It appears that this is the reaction occurring along the hot face of the refractory.

"The reaction is much more complex than this as there are other components present such as CaO, Fe_2O_3, K_2O, etc., which would depress the melting point further. The above mechanism is felt to be the principal reaction leading to erosion and eventual failure of the refractory."

Thus it appears that an ash reaction is the primary cause of failure of the spinel castable material. It appears that in the region of the hot gas supply duct where the seed has not yet vaporized the spinel material does not resist the ash corrosion whereas in other test regions, including potassium vapor, this material has performed well. As discussed in 3.1.1, rebonded fused grain magnesia chrome (Corhart RFG) has performed well in the regions of the hot gas supply ducts near the combustors of the MTF and VTF.

Samples of the exposed materials used in MTF Heat 203 have been collected, including fused cast magnesia-spinel (Corhart X-317) fused cast chromia (Carborundum Monofrax E), sintered spinel (Norton SX-471), and spinel castable (Norton LS-812). Analyses of the samples will be achieved primarily through the Montana laboratories, although some work will also be done at FluiDyne and through other laboratories as appropriate.

3.2 Task 2 - Operability, Performance, and Materials Testing

3.2.1 Matrix Test Facility (MTF)

During the reporting period, the MTF hot gas supply duct was redesigned and tested, the MTF was reassembled, Heat 203 was run, and the MTF was dissassembled for inspection.

Earlier tests of the MTF (Heats 201 and 202) were complicated by degradation of the refractory materials in the hot gas supply duct. The refractory duct lining reacted with the seed/ash laden gas stream and combined with the coal ash. This ash-refractory combination was then carried into the matrix and formed deposits in the matrix flow passages. The presence of this ash-refractory material made it impossible to determine whether the ash by itself would have accumulated in the flow passages over a long term test. Making this determination was a major objective of the matrix tests.

In order to eliminate the refractory degradation problem, the hot gas supply duct was redesigned. As discussed in Section 3.1.1, Corhart RFG was determined to be the best material for the inner liner in the hot gas supply duct. In addition, it was determined that the supply duct as used for Heats 201 and 202 had been too small in inner diameter. Thus, the duct was rebuilt with an inner diameter of 0.28 m (11 in.) rather than the previous 0.15 m (6 in.), primarily in order to provide a larger volume for expansion of the flame from the combustor and to reduce the severity of flame and particle impingement on the refractory surface. The redesigned duct configuration is illustrated in Fig 11. From this figure, it can be seen that three sections of the duct were modified; the third section downstream of the main burner included a transition from the 0.28 m (11 in.) diameter to the previously used 0.15 m (6 in.) diameter. The fourth section

was used in the condition it was following Heat 202; this section had a 0.15 m (6 in) inner diameter and a duct lining of Corhart X-317.

The hot gas supply duct was tested during the week of July 21, prior to attaching the cored brick matrix, in order to confirm that the redesign had successfully resolved the refractory degradation problem. The conditions for the test were selected to match the planned operating conditions during the gas phase for Heat 203, the next test of the MTF. The duct was tested for 60 hours of continuous operation with a mass flow rate of 0.13 kg/sec (1000 lbm/hr) and a duct exit gas temperature of approximately 1922 K (3000 F). A gas temperature of 1978 K (3100 F) was the desired level, but heat loss in the duct was greater than anticipated, resulting in the slightly reduced temperature. The solids injection rate was controlled to produce a gas composition including 1% by weight potassium (2.3% potassium sulfate) and 0.1% by weight Montana Rosebud ash.

The test duration of 60 hours at test conditions was selected so that the test could be completed in one work week, including time required to reach operating conditions and to shut down after completing the test, while still having a long enough duration to assess the duct liner materials performance. The test duration represented 30% of the time that the hot gas supply duct would be operated with seed/ash injection during the 300 hour matrix test (Heat 203).

The results of the test indicated that the redesigned hot gas supply duct would not cause a recurrence of the earlier experimental problems over the course of running Heat 203. The duct walls remained intact, with no significant degradation of the magnesia chrome (Corhart RFG) material. In addition, no significant amount of seed/ash material was deposited in the duct.

Reassembly of the MTF was completed following the duct test. The matrix was assembled using the materials delineated in Section 3.1.1. The uppermost 5% of the 5.2 m (17 ft) cored brick matrix was constructed from fused cast chromia (Carborundum Monofrax E). The next 45% of the matrix was constructed from magnesia-spinel (Corhart X-317) bricks which had previously been used in the matrix during Heat 201, which had a duration of 420 hours, and Heat 202, which had a duration of 750 hours. Pristine magnesia-spinel was used for the next 40% of the matrix. The lowermost 10% of the matrix was constructed from sintered spinel bricks (Norton SX-471). The matrix support was made from calcium aluminate bonded spinel castable (Norton LS-812) as described in Section 3.1.1.

The objectives of Heat 203 were as follows:

1. Operation of the MTF for 300 hours without accumulation of deposits in the matrix flow passages,

2. accumulation of additional testing time on the magnesia-spinel bricks previously tested for 1170 hours,

3. evaluation of the fused cast chromia material for use at the top of the matrix,

4. evaluation of the sintered spinel material for use at the bottom of the matrix,

5. evaluation of the castable matrix support,

6. emissions and chemical composition measurements as discussed in Sections 3.2.3 and 3.2.5, and

7. evaluation of several high temperature instruments for use as diagnostic and/or control instrumentation in future test work and full-scale HTAH systems.

Heat 203 was run during the month of October. The total duration of the test was 446 hours, including startup and shutdown of the facility. Of this total duration, the MTF operated at test conditions, operating cyclically with seed/ash injection during the gas phase, for 303 hours. As in previous test work under the HTAH development program, the seed/ash injection rate was controlled to produce reheat gas composition including 1% by weight potassium (2.3% potassium sulfate) and 0.1% by weight Montana Rosebud ash.

Some of the test data from Heat 203 is presented in Figs 12 through 19. The mass flow rates through the cored brick matrix on gas and air phases is shown in Figs 12 and 13. The solid temperatures at the top and bottom of the matrix, as measured with disappearing filament type optical pyrometers, are shown in Figs. 14 through 17. The friction factor, or dimensionless pressure loss, across the cored brick matrix at the end of gas and air phases is shown in Figs 18 and 19.

The initial test plan called for operation with a flow rate of 0.13 kg/s (1000 lbm/hr). However, due to the increased heat loss in the gas supply duct discussed above, the temperature of the gas delivered to the matrix was somewhat lower than desired. In order to overcome this heat loss, the mass flow was increased to 0.16 kg/s (1275 lbm/hr). (The combustor flame temperature was also increased slightly, but a fuel-to-air ratio of 0.06 and the corresponding flame temperature were chosen as maximum limits to avoid damage to the gas supply duct refractory lining.) Operating in this manner, top of matrix solid temperatures averaging 1920 K (3000 F) were obtained at the end of gas phase, as seen in Fig 14.

Observation of the top matrix brick showed that it was being severely depleted under these operating conditions. Therefore, after 160 hours of operation with seed/ash injection the mass flow was reduced to approximately the original planned level (see Fig 12) and the flame temperature reduced slightly in order to lower the temperature of the top matrix brick. As seen in Fig 14, the top of matrix temperature was reduced to approximately 1860 K (2885 F) under the adjusted conditions. However, this proved to have no discernible effect on the severe attrition of the top matrix brick. The seed and ash injection rates were adjusted to maintain the proportions of seed and ash when the mass flow adjustments were made.

The only other departure from the planned test procedure of operating cyclically for 300 hours under constant conditions was due to a laboratory power failure which occurred after 374 hours total elapsed time. The power failure resulted in shutdown of the MTF fans and burners for 17 minutes. The seed/ash injection was halted for roughly 3.5 hours, however, to allow the system to regain some of the temperature lost during the brief power outage.

Following the completion of Heat 203, the MTF was disassembled for inspection. Samples of refractory materials and deposits were collected for analysis. A discussion of the degree to which the test objectives delineated above were met is given in the following, based on review of the test data and on preliminary observations of the disassembled facility. Further interpretation of the results will be presented after results of the deposit analyses are obtained.

The MTF was operated for 300 hours with no attempt to remove any accumulated deposit by operating in a "cleanout" mode. However, accumulation of deposits did occur, as evidenced by the friction factor, seen in Figs 18 and 19. The friction factor increased steadily throughout the test. The rate of increase increased sharply after the mass flow was reduced in order to lower the top of matrix temperature. The friction factor decreased very rapidly when seed/ash injection was stopped due to the power failure, and continued to decrease for roughly 8 hours after seed/ash injection was resumed. The friction factor then began to increase again and continued to do so until the test was concluded.

Deposits were evident in the matrix flow passages when the MTF was disassembled. The nature of the deposits must be determined through analysis, but it appears that the refractory lining of the hot gas supply duct did not contribute to the formation of deposits in the matrix. Although the RFG liner had degraded to some degree (as opposed to its excellent condition following the hot gas supply duct test), depleted refractory material appears to have accumulated in the bottom of the duct and not carried into the matrix flow passages. The degradation of the RFG duct liner may have been due to the slightly higher temperature and significantly higher velocity during Heat 203 relative to the earlier duct-only test resulting from the mass flow adjustments discussed above.

It should be noted that due to the relatively large heat losses in the MTF, the mass flow per unit area of the matrix flow passages is significantly greater than would be the case in a full-scale HTAH. The MTF has been operated in this manner in order to overcome these heat losses and to achieve the desired solid temperatures. Since the seed/ash loading is maintained proportional to the mass flow, this also results in a

significantly larger amount of seed/ash material supplied per unit area. For example, at the two flow rates used during Heat 203, the seed/ash loading per matrix flow area exceeded expected full-scale HTAH values by factors of about 1.4 and 1.8. Thus the rates of deposition observed in the MTF would also be expected to exceed rates of deposition in a full-scale system under similar operating conditions.

The X-317 material was exposed to an additional 300 hours under simulated HTAH service conditions, bringing the total for the reused X-317 bricks to 1470 hours. Visual inspection of the material indicates continued good resistance to the HTAH environment except for the bricks immediately below the Monofrax E material, which were significantly altered. This may be due to the poor performance of the Monofrax E matrix bricks.

The Monofrax E bricks at the top of the bed were severely depleted in the 300 hour test. However, Monofrax E showed excellent performance as the "target" for deflecting the reheat gas flow from the hot gas supply duct vertically downward into the matrix. A possible explanation for this disparity in performance may be that the chromia is lost by vaporization; since the matrix material has a high surface to volume ratio it could have been rapidly depleted, whereas the target material embedded in a sidewall has a low surface to volume ratio. Analysis of the exposed Monofrax E material may help to clarify this situation.

The sintered spinel (Norton SX-471) bricks and the spinel castable (Norton LS-812) matrix support survived the test satisfactorily. Analysis of the degree of attack is also needed to assess the performance of these materials.

The emissions and chemical composition measurements were successfully completed during the course of the test. Results of these measurements are discussed in Sections 3.2.3 and 3.2.5.

Several high temperature instruments were tested for measuring gas and solid temperatures automatically. An infrared gas temperature instrument (Ircon Series Q) was deemed unsuitable for use in the MTF environment; measured gas temperatures generally were several hundred degrees lower than expected. The instrument could only give reasonable readings by artificially reducing the emittance setting. Discussions with the manufacturer indicated that the need to view the gas in a hot cavity resulted in the poor performance. A fiber optic type infrared sensor (Vanzetti TM-1) and an infrared solid pyrometer (Ircon Series 2000) both gave results which correlated well with the disappearing filament type pyrometer. One or more of these instruments may be purchased for use in future tests.

Plans for future work include modification of the facility to improve the degree to which the MTF simulates an actual directly-fired HTAH and additional tests of HTAH materials and operating conditions. The test objectives and conditions will be coordinated with experimental work at Montana State University so that test work at FluiDyne and at MSU will be complementary and will provide useful information for the HTAH development program.

Modifications to the MTF will include enlarging the flow area and incorporating a refractory dome type matrix support. Selection of materials and operating conditions will include consideration of the observed accumulation of deposits during Heat 203 as well as information from the next HTAH matrix test at MSU.

3.2.2 Valve Test Facility (VTF)

During the reporting period, the VTF was reassembled and Valve Test 3 was run. Several operational problems were encountered with the VTF hot gas supply and Test 3 was interrupted twice for modifications to the VTF. The facility was operated for a total of 592 hours during three operating periods (denoted Tests 3A, 3B, and 3C) including startups and shutdowns. During this total operating period, the VTF was operated in its test cycle including opening and closing the test valve, pressurizing and depressurizing for 375 cycles. Seed and ash were injected into the gas stream to produce a simulated radiant boiler exhaust including 1% by weight potassium (2.3% potassium sulfate) and 0.1% by weight Montana Rosebud ash for 154 hours and 282 valve cycles during Test 3. The problems causing shutdown of the VTF were not related to performance of the test valve.

Following Valve Tests 1 and 2 (completed under Contract DE-AC01-78ET10814, see Ref 6), several modifications were made to the VTF. The castable insulation in the test valve was completely removed and replaced with a new lining of calcium aluminate bonded spinel castable (Norton LS-812). The valve seats were not resurfaced, however.

The hot gas supply duct was also modified as indicated in Fig 20. The inner diameter of a portion of the duct was expanded to 0.28 m (11 in) to overcome a problem of instability of the main burner which had limited the achievable mass flow during Tests 1 and 2. The LS-812 castable was used as the duct liner in this expanded diameter portion. A transition to the previously existing 0.15 m (6 in) inner diameter duct lined with rebonded fused grain magnesia chrome (Corhart RFG) was made by cutting the RFG bricks adjacent to the new LS-812 liner as indicated in Fig 20.

The storage heater was also modified slightly. Flange rings were made to better seal the pressure vessel around supports which are needed for the internal heat storage tubes; this change was made to alleviate leakage problems encountered during Tests 1 and 2. A damaged stainless steel liner in the hot pressurization line from the storage heater to the upper sections of the VTF was also replaced.

Once these modifications were completed, Test 3 was begun. The objective of Test 3 was to extend the operating time of the VTF for a longer duration and continue the evaluation of HTAH gas inlet valve operability and materials, valve leakage and heat loss, and performance of vessel insulation refractories in response to pressurization/depressurization cycles.

Valve Test 3 was started on February 25. The full design flow rate was readily achieved with the hot gas supply duct modification described above. However, after 55 hours of operation with seed/ash injection, the flow rate had decayed to approximately 70% of the design flow and become very erratic, accompanied by recurrence of a vibration problem encountered at high flow rates during Tests 1 and 2. The facility was shut down for inspection at this point, and it was found that the main burner opening had become partially blocked by a thin slag-like layer and that the LS-812 castable has deteriorated and eroded substantially. This first operating period was denoted Test 3A.

Modifications were then made to the hot gas supply duct, as shown in Fig 21. The LS-812 was replaced with an RFG liner, as discussed in Section 3.1.1. Five test samples were also included in the sidewall of the hot gas duct of various materials as discussed in Section 3.1.1 (see Fig 21) to investigate the performance of these materials in the hot gas duct application. These materials were fused cast stoichiometric spinel (Carborundum Monofrax LS) and eutectic spinel (Carborundum Monofrax LE), fused cast magnesia-spinel (Corhart X-317), alumina chrome ramming mix (A.P. Green Jade Ram), and the LS-812 castable coated with an alumina chrome mortar (A.P. Green Jade Set). In addition, a cylindrical insert was added to the burner outlet, extending the burner throat by 0.15 m (6 in.) and providing an area for accumulation of slag without restricting the burner opening as shown in Fig 21. LS-812 castable coated with Jade set mortar was used for this insert.

Test 3B was started on March 24. However, after 50 hours of operating with seed/ash injection, the RFG hot liner in the transition section from the 0.28 m (11 in) combustion chamber to the 0.15 m (6 in) duct cracked and failed. The liner bricks had been cut to form the transition and were too thin at the lower edge to provide sufficient strength. As a result, the backup insulation material was attacked by the hot, seed/ash laden gas stream. Insulating firebrick flowed into the gas supply duct, filling the slag accumulation region around the cylindrical insert at the bottom of the test channel and depositing on the walls of the gas supply duct and the test valve cavity and seats.

This insulation failure caused a second shutdown of the facility. All sections of the VTF gas supply upstream of (below) the test valve were removed, and the refractory was replaced. The test valve gate was also removed for cleaning and removal of the firebrick deposits; the valve seats were still not resurfaced.

The slag tap was removed from the VTF at this point. The slag tap had been incorporated in the orginal design to remove slag which may have deposited on the walls of the water cooled test valve and flowed down the sidewalls of the hot gas supply duct. However, no material was collected in the tap in any of the tests to this point. The source of operational difficulty was that some of the injected slag had become disentrained from the gas stream below the slag tap and thus could not be removed. Since the slag tap had been ineffective, and since the hot gas supply duct now had to be repaired, the slag tap was eliminated.

The new configuration of the VTF hot gas supply duct is shown in Fig 22. The channel was expanded to the 0.28 m (11 in) inner diameter for a large distance, and the transition to the 0.15 m (6 in.) size upstream of the test valve was made with a sufficiently thick layer of RFG material. The "45° lateral" piece formerly used for the slag tap opening was moved to the lowermost position in the duct; this was done in order to prepare for a possible future modification in which the main burner would be moved to fire through the 45° leg. The slag accumulation insert was made from a magnesia-chrome ramming mix (Corhart K-29).

Having made this second set of modifications, Test 3C was started on June 15. The slag insert cracked and thus failed to remedy the problem of accumulation of material in the main burner, and Test 3C was stopped after 49 hours of operation with seed/ash injection. Due to budget limitations, Test 3 was concluded at this point.

The test objective of extending the operating time of the VTF to continue evaluation of the HTAH gas inlet valve and of refractory response to pressurization cycles was achieved. Original plans had called for a target of 300 hours of operation with seed/ash injection; however, the additional costs incurred due to the required modifications resulted in termination of the test after 154 hours with seed/ash injection.

The data from Test 3 has been analyzed in terms of leakage through the test valve. The procedure used to reduce the leakage data is discussed in the following.

During each pressurization phase, air phase, and depressurization phase, strip chart recordings were made of the pressure in the high pressure portion of the VTF and of the air temperature in the upper spray chamber (see Fig 23). From the strip chart recordings, the leakage through the test valve can be reduced from the rates of decay of the system pressure and temperature. The leakage mass flow is given by:

$$\dot{m} = \frac{V}{RT}\left[\frac{dp}{dt} - \frac{p}{T}\left(\frac{dT}{dt}\right)\right] \qquad (1)$$

where $\dot{m}$ = leakage mass flow
p = pressure
T = bulk average temperature
V = pressurized volume
R = gas constant for air

Determination of the bulk average temperature, however, is extremely difficult since the pressurized volume includes air at temperatures ranging from ambient at the pressurization valve to about 1922 K (3000 F) in the hottest temperature regions, including temperature gradients along the storage heater and through the porous insulating refractories (Fig 23). Therefore, the method chosen for determining the test valve leakage was to monitor the temperature at a single point in the system where measurement could be accurately and reliably achieved over the course of an entire test and relate the measured temperature to the bulk average temperature through empirical constants. This gives the leakage computation in the form:

$$\dot{m} = \alpha \frac{V}{RT_m} \left[\frac{dp}{dt} - \beta \frac{p}{T_m} \left(\frac{dT_m}{dt} \right) \right] \qquad (2)$$

where T_m = measured temperature

The factors α and β then relate the bulk average temperature and temperature decay rate to the measured values by:

$$\alpha = \frac{Tm}{T} \qquad (3)$$

$$\beta = \alpha \frac{dT/dt}{dTm/dt} \qquad (4)$$

The values of α and β are not constant in time. The temperature measured in the spray chamber will initially have a lower value and a greater rate of decay than the bulk average temperature, since the spray chamber has water cooled metal walls with no insulation (spray quench water is not introduced to the spray chamber during the pressurization, air, and repressurization phases). As the air phase continues, however, the decay rate of the measured temperatures will eventually become smaller than that of the bulk average temperature.

If the VTF operates in a state of cyclic equilibrium, and if measurements of pressure, temperature, and decay rates are always made at the same point in the VTF cycle, the values of α and β can be considered constant for that point in the cycle. This assumption was made in order to compute the leakage mass flow through the valve during operation of the VTF from the raw measured data.

In order to determine the values of α and β, leakage data measured in so-called "cold flow" tests was compared with the strip chart recordings from Valve Test 1, in which the VTF was operated cyclically with clean flow (i.e., no seed/ash injection). The cold flow tests were conducted with the VTF at ambient temperature, and the pressurizing air was unheated. In these tests, the measured temperature closely approximated the bulk average temperature, so α and β were assumed to be unity. This allowed a straightforward calculation of the leakage mass flow from the strip chart recordings.

A heat transfer analysis showed that, for leakage flow rates less than about 0.01 kg/sec (0.022 lbm/sec), the air actually reaching the valve seats did not differ in absolute temperature by more than 10% from the temperatures in the cold flow tests regardless of the temperature level entering the main valve cavity. This is due to heat loss by the air to the water cooled valve body and stems. Furthermore, calculations of mass flow through a channel of abritrary dimension including the effects of friction and heat transfer indicated that variations of air temperature of even greater magnitude had virtually no effect on the leakage rate due to the high rate of heat loss to the cooled valve seats. Since the leakage rate during the initial cold flow tests was only about 0.0015 kg/sec (0.0033 lbm/sec), it was concluded that the leakage flow during operation of the VTF at elevated temperature would not differ from the cold flow measurements during the early operation of the facility before any changes in the valve sealing surfaces could occur.

The values of α and β were then empirically determined by selecting values which provided a good match between the initial cold flow measurements and the early measurements during the first test of the VTF. The values thus determined were:

$$\alpha = 0.5 \qquad (5)$$

$$\beta = 0.16 \qquad (6)$$

These values are also supported by estimates of the bulk average temperature which established an allowable range into which the empirically determined values fit.

The leakage mass flow results are shown in Fig 24. Results from Valve Tests 1, 2, and 3 are shown in this figure, with the leakage plotted vs. number of valve cycles since the test valve was received from the manufacturer. The cold flow measurements made at various times during the conducting of the valve tests are shown as well as the leakage measurements during actual operation of the VTF including periods with and without injection of seed and ash into the hot gas stream.

A number of results are evident from the test valve leakage data shown in Fig 24. During operation with clean flow in Test 1, the leakage flow rate was quite stable. When seed/ash injection was begun in Test 2, the leakage increased slightly. The sharp increase in leakage after 385 cycles was caused by degradation of phosphate bonded spinel castable insulation, which caused scoring of the valve seats. As was shown in Section 3.1.5, this castable material was lacking in the phosphate bond phase and never attained sufficient green strength. This

condition accelerated the degradation in the presence of seed and ash. The calcium aluminate bonded spinel castable insulation was installed in the test valve at this point before Test 3 was begun. The scored valve seats were not resurfaced.

The cold flow leakage measurements made immdediately after Test 2 and immediately before Test 3 indicate that the leakage was reduced considerably after the valve was reassembled with the new insulation. This was perhaps due to slight misalignment of the scratches on the body and gate seats during reassembly. The leakage quickly increased to the Post-Test 2 level when Test 3 was begun. At the point when seed/ash injection was begun during Test 3, a dramatic reduction in leakage was observed. The seed material apparently deposited on the seats and helped to fill in the leakage gaps caused by earlier scoring of the seats and allowed the valve to effect a better seal.

The leakage level fluctuated about a much reduced level for about 75 cycles. The fluctuations may be due to buildup and subsequent "washing out" of the seed deposits in the leakage scratches. Operational difficulties resulted in a stoppage of the seed/ash injection and the leakage rapidly increased to the highest value yet observed. This may have been due to abrasive action of wall deposits on the seats which were no longer protected by the powdery seed material. The leakage again declined dramatically when the seed was restarted, but the range of fluctuations in leakage over the next 50 cycles was much greater.

The VTF was shut down at this point due to slag accumulation in the main burner, as discussed above. Test 3 was restarted after some modifications were made to the hot gas supply duct. Again the leakage decreased dramatically when seed/ash injection was begun, but over the next 90 cycles, the

leakage steadily increased. The VTF was again shut down at this point when it was discovered that a severe insulation failure had occurred in the hot gas supply duct, as discussed above. Insulating firebrick and slag were found to have deposited on the valve seats, preventing good contact of the sealing surfaces. The cold flow measurements made after this shutdown indicated an increase in leakage of a factor of 2.2 over the cold flow measurement made 100 cycles earlier. The valve gate was removed from the valve and the slag/firebrick deposits removed from the valve body and gate, and the hot gas supply duct was repaired. The valve insulation refractory was not repaired or replaced.

When Test 3 was restarted for this test segment, the leakage level had returned to roughly the same value as before the duct insulation failure. Again the leakage decreased when seed/ash injection was begun, and the leakage remained roughly the same at an average value of about 0.005 kg/sec (0.011 lbm/sec) for the remaining 90 valve cycles.

Despite the considerable operational difficulties encountered with the VTF hot gas supply duct, the test valve leakage has not shown a large increase during normal operation of the facility after a total of 780 valve cycles, including approximately 410 cycles with seed/ash injection. The peak value in leakage during the last operating period was 0.011 kg/sec (0.024 lbm/sec) compared to the initial value of 0.0015 kg/sec (0.0033 lbm/sec) when the valve was received, a factor of 10 increase. The increase in leakage was caused by failure of the initial valve insulation, which was shown to be defective, by operation of the VTF without seed/ash injection during a segment of Test 3, and by failure of the refractory insulation in the VTF hot gas supply duct. Despite these severe operational

problems, the final peak value of the leakage represented only 33% of the value which was allowed for leakage of the gas inlet valve at 827 kPa (120 psia) in the model used in full-scale studies, when corrected to the dimensions of the test valve. At no time during operation of the VTF did the test valve leakage exceed the predicted value from the full-scale studies model. Further information on valve leakage in a full-scale HTAH is shown in Section 3.3.1.

The valve test results to date indicate that use of a gate-type gas inlet valve for HTAH systems will be technically feasible. Long term service life results must yet be obtained, but the leakage measurements during Valve Tests 1, 2, and 3 indicate that even if substantial damage to the valve seats occurs, the valve can effect an adequate seal due to the presence of seed in the gas stream which condenses on the cooled seats. However, the presence of seed and slag has not inhibited the operation of the test valve due to buildup of material on the valve seats. Some material has accumulated in the valve body during each of Tests 2 and 3, but not enough to inhibit valve operation.

Analysis of the test data also showed that the measured thermal conductivity of the refractory material in the pressurized sections has not changed significantly over the course of operation to date. This indicates that the materials have not been affected by pressure cycling. A final determination of the pressure cycling effects can not be made until the refractories are removed at some future date, however.

A concept was developed for eliminating the problem of accumulation of material in the VTF main burner. The concept will require redesign and modification of the lower sections of the facility. This design work and the resulting laboratory modifications will be done during the next quarterly reporting period. Valve Test 4 will be started upon completion of the modifications. The goal of Test 4 will again be to extend the operating period of the VTF with the present test valve and pressurized area refractory materials. The target duration for Test 4 will be 1000 hrs/2000 valve cycles.

3.2.3 Emissions Measurements

Emissions measurements were made during Heat 203 in the MTF. The intent of the measurements was to determine whether or not the matrix in the MTF had any catalytic effect on NO_x in the reheat gas stream. The measurements were made by extracting samples of the gas with the water cooled probe shown in Figs 25, 26, and 27 and analyzing the samples with flue gas analysis instruments. In particular, NO_x measurements were made with a DuPont Photometric Analyzer. Results of the measurements also included O_2, CO_2, and CO concentrations.

Measurements of the NO_x concentration were made in the simulated radiant boiler exhaust gas at the entrance to the matrix and at the exit from the matrix during periods of operation before and after seed/ash injection was started. Comparison of the NO_x levels entering and leaving the matrix showed a 15% increase in NO_x concentration across the matrix with no seed/ash present and a 5% increase with seed/ash present. All values exceeded the level at the entrance to the matrix measured during Heat 202 (Ref 6). No effort was made to explain this discrepancy.

While it is unlikely that the NO_x level actually increased as the gas passed through the cored brick matrix, it was concluded that no catalytic effect for NO_x reduction was present. The slight observed increases may have been due to temporal variations, since the measurements could not be made at the same time due to the availability of only one probe, or to measurement differences caused by the different temperature levels of the sampled gas stream.

This subtask has been eliminated from the Statement of Work for continuation of efforts under this contract, and no further effort will be made concerning NO_x measurements in the MTF.

3.2.4 Creep Testing Apparatus

Design of a dilatometer for making creep measurements in the HTAH service environment was completed during the reporting period. Construction and testing of the dilatometer have not been authorized under this Contract but are anticipated at some future date.

In order to be able to design high temperature air heaters for MHD power plants, creep data will be needed for the various matrix, hot liner, and insulation materials at the service temperatures. At present, creep data for most refractories in unavailable at the high temperatures required. High temperature creep measurements are underway at Montana Tech for a number of HTAH candidate materials. Such measurements can only be made in heated air, however. The question of how the seed/ash laden MHD gas affects the creep resistance refractories can be addressed in such tests only by making measurements on samples which have

been exposed to the HTAH service environment. In order to confirm that this procedure correctly predicts the results of seed/ash exposure on materials under load, it will be important to make some creep tests in the HTAH service environment. For this reason, a creep test apparatus was designed which can be used to test materials under load while being subjected to the simulated HTAH service environment of the MTF.

The dilatometer design is shown in Fig 28. A brief description is given in the following.

Adaptation To Matrix Test Facility

The dilatometer has been designed for installation in the hot gas duct of the Matrix Test Facility. The dilatometer duct I.D. is 0.15 m (6 in). End flanges are provided to mate a nominal 0.76 m (30 in) diameter pipe. This adaptation is to allow creep tests to be performed as piggy-back tests during other MTF tests, thus reducing the costs of the creep tests. The dilatometer may be mounted as a part of the MTF hot gas duct through which the entire hot gas flow is passed. However, erosion due to liquid ash particles may be a problem in this configuration. Thus, the dilatometer will most likely be mounted as a bypass leg or as a right-angle extension of the MTF hot gas supply when creep tests are performed.

Horizontal Configuration

The dilatometer is designed with the hot gas duct oriented horizontally and the the refractory test sample held transverse to the gas flow and also in a horizontal position. This configuration will keep the sample and the measurement components of the dilatometer from being exposed to liquid seed and/or slag which may be present in the bottom of the duct.

Measurement Symmetry

The function of the dilatometer is to measure the change in length of a sample subjected to a compressive load. The load is also measured. Perhaps the most unique feature of the design is measurement symmetry, i.e., all components involved in the measurement of the change in length of the sample are identical at both ends of the sample. They are geometrically identical as well as being similar in terms of their thermal environment. This symmetry should greatly reduce the need for complex calibrations prevalent in most existing dilatometers where at least one of the rods translating the displacement of the sample to a transducer is located in the test gas stream or the test cavity of a furnace.

Access To Sample and Viewport

The upper portion of the dilatometer duct is a removable section for access to the test sample. This section of the duct also contains an air-cooled viewport for observing the test sample throughout the test.

Cooling Systems

The design has two primary cooling systems, one with air cooling and one with water cooling.

The air cooling system has two inlets located near each of the displacement transducers. The purpose of the air cooling is two-fold. First, the air cooling keeps the transducers cool and, secondly, it provides air to purge the gaps around the measurement rods and the rams to prevent contamination by seed or ash in the hot gas stream. The cooling air is discharged to the hot gas stream.

The water cooling system cools the jacket of the dilatometer duct including the access cover and the duct support frame. The water cooling on the duct minimizes the amount of duct insulation required and reduces thermal expansion of all metal parts. The water cooling in the support frame reduces thermal expansion in that component. The two water cooling systems (duct including cover and support frame) may be supplied in series at a flow rate of 0.015 m^3/hr (4 GPH). The estimated water temperature rise at this flow rate is less than 5.6 K (10 F).

Measurement Range and Samples

The dilatometer was designed for the capacity to make creep measurements at stress levels up to the maximum encountered in full-scale MHD HTAH studies. The maximum stress levels reached in various heater concepts was approximately 1 MPa (150 psi). The design can apply up to 890 N (200 lbs) on a refractory sample having any diameter up to a maximum of 38 mm (1.5 in) along the centerline with less than 0.08 mm (0.003 in) displacement of the centerline from rest. Each transducer core has a translation range of $\pm$ 5.08 mm (0.200 in). The transducer are Schaevitz Type E-200 whose maximum operating temperature is 367 K (200 F). The load cell is a standard 1.8 kN (400 lb) FluiDyne load cell, Drawing No. 020342A.

Consumables

In the event of a fracture of a sample, it is probable that the sapphire measurement rods and the ram end caps will be damaged or broken. These same components could also be damaged by chemical attack by the hot gas stream. These

consumables would cost up to $10000 for a complete test set based on a single order price. Quantity order (5 to 10 sets) could reduce the price by nearly 50%. These prices are based on sapphire measurement rods approximately 152 mm (6 in) long. The design provides for the shortening of these rods by replacing the cool end with interchangeable metal extensions.

3.2.5 Effluent Air Stream

Measurements of the potassium content of the effluent air stream from the MTF were made during Heat 203. The interest in these measurements lies in determining the level of potassium which is picked up by the air stream as it passes through the cored brick matrix. This information bears on the electrical isolation problem in a HTAH.

The measurements were performed by extracting samples of the effluent air stream from the top of the matrix with the water cooled probe (as shown in Fig 27) and bubbling the samples through impingers filled with distilled water. The probe was then washed after completion of the sample extraction. The impinger contents and the probe washings were then analyzed for potassium content. Samples were extracted over several segments of air phases to investigate the time dependence of the measurements.

The results are presented in Fig 29. The measured data are represented fairly well by an exponential time decay whereby:

$$\text{wt \% K} = 0.25\ e^{-t/4\ \text{min}} \qquad (7)$$

The measured potassium content represents the average concentration over the time during which a particular measurement is made. The average value for each of the time periods that measurements were made was calculated by integrating Eq 7 over the time period and dividing by the time interval. A comparison of the measured values with averages calculated from Eq 7 is shown in Table 14. All of the data points agree well with this equation except for the measurements made over 12 minute intervals. Therefore, Eq 7 is felt to be a reasonable representation of the carryover of potassium to the effluent air stream during Heat 203.

This information may be used to estimate the potassium carryover in a full-scale HTAH for the purpose of estimating the electrical conductivity of the air stream leaving the HTAH system. The estimates are needed in order to evaluate electrical isolation techniques for the directly-fired HTAH.

This subtask has been eliminated from the Statement of Work for continuation of efforts under this contract, and no further effort will be made to measure potassium in the effluent air stream in the MTF.

3.3 Task 3 - Full-Scale Design Concepts

3.3.1 Size/Cost Analysis and Parametric Studies

During the reporting period, the size/cost computer code was used to conduct a parametric study of the directly-fired HTAH for a 1000 MW_e power plant in order to assess the implications of various design constraints, and an example HTAH system was defined as a focal point for the

full-scale studies. The cost effectiveness of various insulation and manifold schemes was then examined for this basic example HTAH. Several performance parameters of an individual heater in the example HTAH were then studied with the STRHEX computer code. In addition to these basic heater size, cost, and performance studies, engineering studies of the effects of HTAH valve reliability and leakage were made to assess the impact of these concerns on the MHD plant. In addition, an evaluation was made of the effect of particulate matter in the MHD gas stream on radiation heat loss in the HTAH system.

Parametric Study and Example HTAH

Flow rates and allowable pressure losses for a directly-fired HTAH for a 1000 MW_e power plant were taken from work done by STD Engineering Corporation under subcontract to FluiDyne under Contract DE-AC01-78ET15602 (Ref. 6). The temperature of the inlet air to the HTAH was reduced to 922 K (1200 F) from the value of 1000 K (1340 F) used in the STD work, however, to represent more reasonable expected performance of the low temperature air heater.

The air inlet temperature and the gas inlet temperature represent major operating constraints on the HTAH. Another major constraint results from the requirement that seed and slag be allowed to drain from the heater during each gas phase; this requirement translates into a lower limit on the maximum bottom of matrix solid temperature, i.e., the temperature of the bottom of the matrix at the end of the gas phase. The allowable thermal stress in the webs between heater flow passages is another operating constraint on the system since high thermal stresses could damage the ceramic heat storage medium.

Results of the parametric study are shown in Figs 30-32. The constraints used were that the air inlet temperature was 922 K (1200 F), the maximum bottom of matrix solid temperature must reach 1400 K (2060 F), and the maximum allowable thermal stress was 25.5 MPa (3700 psi) as calculated by the size/cost computer code. The results are presented in terms of air temperature delivered to the combustor vs. required bed height for various radiant boiler outlet gas temperatures and three different heat exchanger flow passage diameters. The cost relative to the selected example HTAH discussed in the following) and heat exchanger effectiveness are also indicated.

As seen in Figs 30-32, for a given air temperature delivered to the combustor, requiring a lower gas temperature from the radiant boiler (as would be required if materials having insufficient temperature service limits were used) results in an increase in required bed height and cost. Thus, ceramic materials capable of withstanding the highest possible temperature are of great importance to the HTAH development program. A radiant boiler outlet temperature of 1994 K (3130 F) and a heater system gas inlet temperature of 1978 K (3100 F) are considered the maximum achievable with commercially available materials. Another limitation of the exit temperature from the radiant boiler is NO_x decomposition. If a lower temperature is required, the heater bed length must be increased and delivered air temperature decreased. Figs 30-32 enable estimates of this trade-off to be made.

Another result seen in Figs 30-32 is that the effect of requiring large flow passage diameters is significant at delivered air temperatures greater than about 1550 K (2300 F). The percentage increase in bed height and cost required for larger hole diameter is roughly the same for all temperature

levels; as the bed height and cost become larger for the higher delivered air temperatures, the penalty due to larger hole diameters becomes large. At present, 25.4 mm (1 in) holes are considered the smallest feasible flow passages. If slag fluxing additives or operating techniques are developed to allow the use of smaller holes without fouling of the flow passages, higher air outlet temperatures will be achievable for the same bed height.

The matrix support is an item of major importance in the HTAH development program. The matrix support must be capable of withstanding temperatures up to 1400 K (2060 F) to accommodate removal of seed and slag from the directly-fired heaters, as discussed above. In addition, the matrix support must have sufficient corrosion/erosion resistance and the support structure must withstand the cyclic thermal stress imposed by regenerative air heater service. Commercial experience in the area of secondary ammonia reformers has demonstrated the feasibility of perforated ceramic dome type supports which operate at temperatures in the range of 1280 K (1850 F) to 1310 K (1900 F) and at loads of about 200 kPa (30 psi). These supports have been limited to about 4 m (13 ft) in diameter.

The HTAH matrix support represents an extension of state-of-the-art technology with respect to both seed/slag removal and thermal cycling. A further extension of the technology in the form of increased diameter would add to the risk. The major implication of limiting the diameter of the individual heater beds is that a large number of heaters will be required for large system flow rate requirements. For example, a HTAH for a 1000 MW_e power plant would require 28 active heaters plus one each for periods of pressurization and depressurization or a total of 30 heaters if the individual heater beds are restricted to a diameter of 4.3 m (14 ft).

The use of such a large number of heaters initially may seem to imply reduced reliability due to the large number of flow sequencing valves required in the HTAH system. However, the use of a large number of heaters results in the diameter of the valves being reduced if single valves are used for each heater duct. Restricting the size of valves to approximately the present level of blast furnace valve technology will very likely result in increased valve reliability over the much larger valves required if fewer heaters were used. If more than one valve is used for each heater duct due to valve size limitations, the number of valves and thus, the overall valve reliability is not affected by the number of heaters. Should larger diameter matrix support concepts and valves be developed and reliability demonstrated, a reduction in the total number of heaters in the HTAH should be considered.

Based on the above considerations, a HTAH gas inlet temperature of 1978 K (3100 F), corresponding to a radiant boiler outlet temperature of 1994 K (3130 F), and a total of 30 heaters were chosen as inputs for the example HTAH. With these inputs, as well as the constraints of 922 K (1200 F) air inlet temperature and 1400 K (2060 F) maximum botton of matrix solid temperature, the parametric curves shown in Figs 33-37 were constructed. In these figures, bed diameter, bed height, thermal stress, cycle time, and cost relative to the example case are shown. The example case was defined by requiring that the bed diameter not exceed 4.3 m (14 ft) and the bed height not exceed 6.7 m (22 ft) as implied by the matrix support limitations discussed above, and that the total cycle time be at least 30 min to limit the number of cycles/year required of the sequencing valves. A flow passage diameter of 25.4 mm (1 in) was also selected based on expectations of seed/slag fouling prevention requirements. Specifics of the example HTAH are given in Table 15.

The results are shown in Figs 33-37 as functions of heat exchanger effectiveness, where

$$\text{EFFECTIVENESS (Air Side)} = \frac{T_{\text{AIR OUT}} - T_{\text{AIR IN}}}{T_{\text{GAS IN}} - T_{\text{AIR IN}}} \qquad (8)$$

It can be seen that the bed height, cycle time, and cost increase sharply over the example case values if the air outlet temperature is increased above about 1750 K (2690 F) while the bed diameter is relatively insensitive to air temperature. The increase in bed diameter with hole diameter is due to decreased geometric porosity achievable with larger holes and to the need to balance heat transfer and pressure drop considerations. The thermal stress decreases with increasing air temperature because the thermal stress is the limiting design criterion at air temperatures less than a particular value for a given hole diameter, i.e., 1756 K (2700 F) for 19 mm (0.75 in) holes, 1833 K (2840 F) for 25.4 mm (1 in.) holes, and 1878 K (2920 F) for 31.8 mm (1.25 in) holes. Bed diameter and cost do not decrease significantly for air outlet temperature less than the example case value of 1788 K (2758 F) but the bed height and cycle time show significant decreases. Based on the results of the parametric study, the example HTAH as selected represents a reasonable vehicle to use for cost, performance, and control studies in order to identify HTAH development needs and define goals for the development program.

Comparison of the cost of an HTAH having the performance and size requirements defined for the example case, but with various insulation schemes, are shown in Table 16. These comparisons demonstrate the importance of the insulation scheme to the total HTAH cost and the need for development of insulation materials to achieve the lowest potential cost.

The first column, lowest risk brick, represents an insulation system in which all material layers are constructed of bricks having ample thicknesses for structural integrity. In addition, high density, seed resistant materials are specified for use in all areas where the temperature is greater than 1289 K (1860 F) as an assurance against attack by potassium containing vapors. This system therefore has the lowest risk of failure and correspondingly, the highest cost of the systems considered.

The second column in Table 16 represents a system in which the brick thicknesses are reduced and the potassium vapor problem is not considered beyond the so-called "hot liner" surrounding the heat storage matrix. A large cost reduction is realized, along with a corresponding greater risk due to the uncertainty of structural integrity and the possibility of alkali vapor corrosion.

An even greater cost reduction is seen in the third system, in which monolithic or castable insulating refractories are used. This insulation system also has greater risk than the most conservative brick scheme due to questions of structural integrity, anchoring requirements, and alkali corrosion resistance. A scheme utilizing brick and castable combinations, as shown in the fourth column, also represents a cost reduction over the lowest risk brick system, although not as great as for the higher risk brick or monolithic insulation schemes.

The final column in Table 16 represents the insulation materials selection discussed in Section 3.1.1, in which four layers of insulation were proposed, including an insulating spinel brick and a high strength insulation brick capable of withstanding the temperature and alkali corrosion resistance requirements of the HTAH. Again, a significant cost reduction is seen over the lowest risk brick insulation scheme, but not as great as for the other reduced cost schemes.

These cost comparisons show the importance to the overall HTAH development program of developing insulation materials and construction techniques which will allow the use of improved insulation schemes and result in reduced cost of the HTAH. Thus, a primary goal of the work under Task 1, Materials Selection, Development and Evaluation is to select materials for testing and property determination which will meet the criteria posed by the most cost-effective schemes illustrated in Table 16. Testing and evaluation of castable materials and high strength insulating brick have the highest priority for insulation materials. It must be emphasized however, that even the lowest risk brick insulation scheme would require subscale and large scale testing under HTAH conditions to verify performance.

Another cost comparison is shown in Table 17, in which reducing the size of the HTAH system manifolds is considered as a potential cost reducing method. The magnitude of cost reduction is on the same order as that obtained by using the four layer insulation scheme. In the case of manifold size reduction, the benefits of decreased cost must be balanced against effects on total system performance (see Section 3.2.2) and possible duct erosion due to higher velocity.

Idealized Performance of Individual Heater

A computer code denoted as STRHEX was developed in earlier HTAH work to make calculations of the performance of individual heaters in a system of regenerative heat exchangers. The code is upgraded from time to time to add the capacity needed for examining particular concerns of the HTAH development program. The code now has the capability to handle 2-dimensional (axial and radial) temperature fields, temperature dependent transport properties, arbitrary time functions of the inlet air and gas stream flow rate and temperature and arbitrary specifications of material properties in the axial dimension. It was used to calculate the performance of a single heater in the example HTAH described above, under the assumption that the flow rates through and the performance of all heaters is identical.

The sequence of events through which an individual heater in the example HTAH would pass is shown in Table 18. The flow rate through an individual heater based on this sequence is shown in Fig 38. The ideal temperature history for an individual heater is shown in Fig 39. The inlet gas and air temperatures and flow rates include effects due to heat loss in the ducts and manifolds and mass loss due to valve leakage and pressurization/depressurization. The ideal performance curves shown in Figs 38 and 39 were used to assess the degree of variability in individual heater performance determined from the dynamic system performance model (see Section 3.3.2). Many computer runs have been made with the STRHEX model; the result of these studies has been to verify that individual heater performance can be scaled by heat exchanger effectiveness in the same manner as indicated in Figs 30-37.

Calculations of the thermal stress at inner surfaces of the heater matrix flow passages are shown in Fig 40. The cored brick material is stressed in tension during the air phase and in compression during the gas phase. The most severe thermal stress occurs at the bottom of the matrix dring the first 40% of the air phase. This condition results from the need to raise the bottom of matrix solid temperature to a level of 1400 K (2060 F), at the end of the gas phase to promote drainage of seed/slag from the matrix flow passages. The low temperature, 922 K (1200 F), air which is introduced at the bottom of the matrix then results in very high stress levels, which decay as the solid temperature decreases. The thermal stress levels are much lower at the middle and top of the matrix.

The thermal stress calculations are based on the assumption that the bricks are a continuous, elastic medium. Thus, the calculated stresses are indications of the maximum levels that could exist with idealized materials. Porous refractory materials can withstand potentially high stress conditions, however, due to the presence of gaps in the material microstructure - microcracks form which prevent the high stresses from developing. Highly dense materials, however, more closely approximate the continuous medium. The calculations emphasize the need for thermal stress resistant materials, particularly in the bottom region of the matrix where the variation in stress level over the course of a heater cycle is very large. The fused cast magnesia-spinel, discussed earlier, has demonstrated the ability to withstand thermal cycling due to its particular microstructure in spite of its high density.

Calculations of the radial temperature profile across the cored brick matrix at the end of the gas phase are shown in Fig 41. The three curves were computed using different models for the thermal resistance of the flow passages; models 1 and 2 represent upper and lower limits on the thermal resistance of the flow passages while model 3 falls between these extreme values.

As can be seen from these profiles, for the example HTAH conditions, a temperature variation on the order of 19 K (35 F) can exist in the matrix. This is especially important to consider in HTAH design at the bottom of the matrix, where a minimum temperature of 1400 K (2060 F) is specified at the end of the gas phase for effective seed/slag drainage. To assure that the seed/slag material drains effectively at the outer edges of the matrix, a temperature as high as 1419 K (2095 F) may be required in the center of the matrix.

HTAH Valve Reliability

A study of MHD plant reliability (Refs 7, 8, and 9) was reviewed with respect to reliability of the HTAH. In particular, the question of valve life was considered, and it was shown that using different assumptions for valve life dramatically reduces the number of spare heater modules required in an HTAH system to achieve a given HTAH unavailability requirement. Changing the failure rates for individual valves, but following the same method outlined in Ref 8 for determining HTAH unavailability, resulted in a decrease from 8 spare modules required to only 1 spare required in order to achieve a 2% unavailability.

In the study, summarized in Ref 7, the unavailability of the MHD plant was computed from unavailability or "effective forced outage rate" due to the various system components. The HTAH unavailability was dominated by forced outage due to valves. The valve failure rates assumed in the study were based on early estimates of life in steel plant blast furnace stoves. More recent experience has shown much longer valve life. Also, the analysis of Ref 7 assumed the same failure rate (equal to the worst) for each valve in the HTAH system. There are six valves for each heater and their service requirements vary widely. The influence of longer valve life and individual valve conditions on HTAH availability were studied using the methods of Ref 7.

The approach taken in Ref 7 was to assume a mean valve life based on early steel industry experience with hot blast valves and to compute from this a failure rate, λ_v, for individual valves in an indirectly-fired HTAH. This failure rate was used for each of the six valves associated with each heater vessel giving a total failure rate of $\lambda = 6\lambda_v$ for each heater module. The failure rate was arbitrarily doubled for directly-fired HTAH systems because of the presumably more severe service environment.

The mean life assumed in Ref 7 for steel industry hot blast valves was 2.2 years, based on an estimated range of 1-5 years. This gave a failure rate for the indirectly-fired HTAH calculations of $\lambda_v = 0.5$ (each valve every 2 years). The method used in determining this value is summarized in Table 19.

However, recent information on improved blast furnace valve designs has indicated that valve life of up to 10 years has been achieved (Ref 10). The general blast furnace

valve literature and discussions with blast furnace valve manufacturers indicate that the primary causes of valve failures in the steel industry are warping and cracking of cooled metal parts; this is generally due to fouling of the water cooling passages which results in a non-uniform temperature distribution. Impurities and particulate matter in the cooling water are the causes of the trouble, since untreated river water is generally used as the coolant. The 10 year life quoted above resulted from the use of treated cooling water. Since treated, boiler quality water will be used in an MHD electric power plant, it is reasonable to assume that clean water will be available for valve cooling.

The HTAH hot gas inlet valve will have the most severe conditions of the temperature and pressure (and gas stream composition for the directly-fired case). The pressure and temperature are somewhat higher than for blast furnace hot valves. Therefore, an estimated mean life of 5 years seems reasonable. This results in a failure rate of $\lambda_v = 0.22$ for a gas inlet valve in the indirectly-fired HTAH availability analysis when the value of λ_v from Table 19 is ratioed by 2.2 years/5 years.

As noted earlier, it was assumed in Ref 7 that all valves have the same failure rate. Since the severity of service for some of the valves is much lower than that of the gas inlet valve, lower failure rates should be used for these valves. For example, the air inlet valve will have a service temperature of only 922 K (1200 F) with clean air passing through it in its open position. Based on the value of 0.22 for the hot gas inlet valve, failure rates were estimated for the various valves in an indirectly-fired heater. The estimated failure rates are shown in Table 20.

If the rate is doubled for the severity factor arbitrarily assigned to the directly-fired heater, a rate of $\lambda = 2 \times 0.69 = 1.38\ yr^{-1}$ is obtained rather than the value of $\lambda = 2 \times 6\lambda_v = 6\ yr^{-1}$ from Table 19. The value of 1.38 for the failure rate results in a significant reduction in HTAH unavailability as shown in Fig 42. Time between MHD plant shutdowns was assumed in Ref 7 to be exponentially distributed about a mean period which was established on the basis of data from coal fired base load power plants and on an assumed overall MHD plant forced outage rate requirement of 16%. All failed valves would be replaced during these plant shutdowns for other problems in the MHD plant. Plant shutdown would not be made in the event of HTAH valve failure; a heater module including a failed valve would be off-loaded and a spare heater module with all associated valves would be brought on line until one of these repair opportunities would arise due to shutdown for other plant problems. Valve failures were also assumed to be exponentially distributed about the mean values.

A value of 2% HTAH unavailability was postulated as a requirement. In order to meet this requirement, 8 spare heater modules with all associated valves would be required in a HTAH system having 14 active heaters according to Ref 8. However, if the value of $\lambda = 1.38$ is used, only 1 spare module would be required to meet the 2% unavailability objective.

The effect of the assumed severity factor is shown in Fig 43. A severity factor of 2 may in fact not be justified in light of the valve test results reported in Section 3.2.2. These results indicate that the presence of seed material in the gas stream compensates for damage to the

valve sealing surfaces. This may actually result in an enhancement of valve life (severity factor < 1) as compared to the steel industry experience. This situation will become clearer as long term valve tests become available. As can be seen in Fig 43, a moderate enhancement in the assumed mean valve life (severity factor = 0.84) results in reducing the required number of spare heaters to achieve 2% unavailability to zero, while an increase in the factor to as much as 3 results in a requirement of only 2 spare heaters.

The availability analysis of Ref 7 requires that spare heaters be brought on line immediately in the case of valve failures; if all spares are already in use, the HTAH is operated at reduced capacity if a module must be off-loaded. Maintaining a large number of spare heaters in a state of readiness and bringing new heaters on line represent potentially complex problems in the operation of a HTAH. Thus a minimum number of required spare heaters is desirable from a HTAH operation standpoint as well as from the obvious capital cost penalty viewpoint. However, as shown above, using different estimates for HTAH valve failure rates in the analysis results in a requirement of only 1 or 2 spare heaters at worst and shows that a 2% unavailability requirement may be achievable without the use of any spare heaters in a HTAH system.

Effect of Leakage and Pressurization/Depressurization Losses

The effects of mass loss due to valve leakage and pressurization/depressurization losses on the overall MHD plant was studied. Valve leakage results in a loss of pressurized combustion air; this leakage flow bypasses the combustor, channel, and radiant boiler and passes directly

to the components downstream of the HTAH. Pressurized air is also lost to the downstream components when the individual heaters are depressruized after each air phase by discharging air to the gas outlet manifolds. In addition, a residual inventory of low pressure channel exhaust gas is mixed with the pressurized combustion air after each gas phase as the heater is pressurized.

The effect of this overall mass loss on the overall plant is minimal. No penalty is incurred in the downstream components; the air mass lost from the HTAH can be compensated for by reducing the secondary combustion air which is added upstream of the bottoming plant. Since combustion air to the MHD combustor is lost, however, additional pressurized air must be supplied to the HTAH in order to maintain the required total channel flow and temperature. This additional air imposes a penalty in the form of power required to compress the air which will be lost by leakage and pressurization/depressurization.

The additional compressor power required may be estimated by the following equation.

$$P \simeq \frac{\dot{m} \quad Cp \quad T_1}{\eta_m \quad \eta_c} \left[\left(\frac{P_2}{P_1} \right)^{(\gamma-1)/\gamma} - 1 \right] \qquad (9)$$

where: $\dot{m}$ is the additional mass flow required to compensate for valve leakage and pressurization/depressurization losses

C_p is the specific heat of air

T_1 is the compressor inlet temperature

η_c is the compressor efficiency

η_m is the efficiency of a compressor drive motor

P_2/P_1 is the pressure ratio

γ is the ratio of specific heats for air

The following assumed values were used:

$P_2/P_1 = 9$

$T_1 = 288$ K (519 R, 59 F)

$\eta_c = 0.87$ (no intercooling)

$\eta_m = 0.98$

A small power recovery is realized by the bottoming plant since the compressor outlet temperature will be greater than the stack temperature of the bottoming plant. This recovered power can be estimated by:

$$P_R \simeq \dot{m}\, C_p\, (T_2 - T_{stack})\, \eta_\beta \qquad (10)$$

where: T_2 is the compressor outlet temperature

T_{stack} is the bottoming plant stack temp.

η_β is the bottoming plant conversion efficiency

The following assumed values were used

$$T_2 = 578 \text{ K } (1040 \text{ R}, \ 580 \text{ F})$$

$$T_{stack} = 422 \text{ K } (760 \text{ R}, \ 300 \text{ F})$$

$$\eta_\beta = 0.33$$

The net additional power required to compensate for valve leakage and pressurization/depressurization losses is thus given by

$$P_{net} = P - P_R \qquad (11)$$

The effect of this additional power requirement on the overall plant efficiency is shown in Fig 44 for a 1000 MW_e power plant. Calculations were made for two cases, a plant having an overall efficiency of 45% and a plant having an overall efficiency of 50% (computed without accounting for the additional power required to compensate for mass loss due to valve leakage and pressurization/depressurization losses).

The loss in efficiency is plotted vs. the time averaged mass loss in Fig 44. Three values of the mass loss are indicated. First, a value is shown which represents a calculation of the net mass exchange due to pressurization/depressurization for the example HTAH discussed above. The second value adds to this pressurization/depressurization loss a total valve leakage mass loss estimated on the basis of results of valve tests reported in Section 3.2.2. The third value includes total valve leakage as computed by the size/cost computer code for the example HTAH in addition to

the pressurization/depressurization loss. It should be noted that these calculations of mass loss are all based on the example HTAH which has 30 individual heaters. A HTAH having a smaller number of heaters would have a smaller total mass loss.

The effect on total plant efficiency is seen to be quite small. For example a plant having an efficiency of 50% when disregarding mass loss in the HTAH has an efficiency of 49.66% when the additional power requirement due to mass loss is accounted for, based on estimates from the valve testing results. Even when the more pessimistic size/cost computer code calculations are used, the efficiency is reduced to only 49.91%. Corresponding reduced efficiencies for a plant having 45% efficiency with no mass loss are 44.96% and 44.93%. The use of a directly-fired HTAH can raise the overall plant efficiency by 5 or more percentage points over a system with oxygen enrichment and moderate preheat. Thus, efficiency reductions on the order of 0.04% to 0.09% are insignificant when compared to the overall efficiency advantage realized through use of the directly-fired HTAH.

Effect of Particulate Radiation

Due to the recent availability of material on particle size and distribution and heat transfer in the MHD channel, diffuser, and radiant boiler (Refs 11-13), the radiative heat exchange model used in the size/cost computer code and other HTAH computational models was revie ed. The contribution to the total heat transfer due to radiation exchange between particulate matter in the gas stream and duct or flow passage walls has been estimated in previous work from assumed particulate concentrations and size distributions. This contribution has been recalculated using information given in Refs 11-13 for use in future full-scale studies work.

The results of these calculations are shown in Fig 45. As can be seen in this figure, the magnitude of particle radiation is fairly small for small passage diameters, such as the heat exchange matrix flow passages. The magnitude of the particle radiation term increases toward a maximum value as the passage diameter increases, for example in the large manifolds carrying the radiant boiler exhaust gas to the HTAH. Incorporation of the improved particulate radiation term as shown in Fig 45 will improve the HTAH simulation in future full-scale studies.

3.3.2,5 Dynamic System Performance Simulation (SCAMP) and Control Systems

The SCAMP computer code was used during the reporting period to make calculations of the dynamic performance of the example HTAH for a 1000 MW_e power plant under various conditions. A total of four runs of the SCAMP code were made, in which the performance of the example HTAH was calculated for the following conditions:

1. Large manifolds - gas and air inlet and outlet manifolds sized to allow a velocity no greater than 30 m/sec (100 ft/sec); 2000 sec gas phase and 800 sec air phase for each individual heater.

2. Step change in gas temperature - the transient response of the system with large manifolds to a step change of 111 K (200 F) in the inlet gas temperature.

3. Small manifolds - manifolds reduced in diameter by $\sqrt{2}$ to give maximum velocity of 60 m/sec (200 ft/sec); 2000 sec gas phase and 800 sec air phase for each individual heater.

4. Small manifolds with control - air and gas phase durations fixed individually for individual heaters to control maximum bottom of matrix solid temperature.

A brief summary of the results of these four runs is given in the following. Further details will be presented in a topical report on the performance and control studies of the 1000 MW_e plant example HTAH.

The sequencing of the example heater system for the performance calculations is summarized in Tables 18, 21, and 22. The events through which an individual heater is cycled and the time scale are shown in Table 18. The example system as described in Table 15 has 30 individual small diameter heaters. The layout of the heaters (see Section 3.3.3) is symmetric such that it consists of two identical groups of 15 heaters with the attendant manifolds, ducts, and valves. The heater sequence selected for the performance and control studies consists of a particular pattern which is identical for each of the 15 heater groups, but offset by half of an individual heater cycle. Each 15 heater group receives half the total gas flow and delivers half the total air flow. This allows the SCAMP code to be run for only a 15 heater system at greatly reduced computer cost compared to a 30 heater system, and the total system output is determined by adding together two output curves skewed by half a cycle.

Details of the sequence for each 15 heater group are given in Table 21. This sequence is repeated for each of the 15 heaters. A summary of the total cycle for the 30 heater system is shown in Table 22. This cycle is similar to the individual 15 heater group cycles except that

pressurization or depressurization may be occurring in 2 heaters at the same time in the 30 heater cycle. Fig 46 identifies the heaters and the sequence for one 15 heater group. The ideal flow rates through an individual heater based on this heater sequence were shown in Fig 38; this situation would result if all heaters participated equally in the flow distribution.

The temperature of the outlet air from the 30 heater system with large manifolds is shown in Fig 47. The temperature exhibits a short term ripple of about 15 K (27 F) with a period of about 1.5 min due to the droop in outlet air temperature from each individual heater. This ripple is superimposed on a longer term oscillation with a period of about 15 min due to the location of the individual heaters relative to the air and gas manifolds. The resulting temperature variations amount to roughly 2% of the average delivered air from a 30 heater system cycle.

The total system gas outlet temperature is shown in Fig 48. The outlet gas temperature also shows the short term ripple and longer term oscillation, and a total variation in temperature of less than 2%. Similar results were observed in an earlier example case with 10 heaters; the periods of oscillation were longer and the total temperature variations were somewhat larger.

The outlet air temperature shown in Fig 47 represents the discharge of the HTAH air manifold. The duct needed to carry this air to the combustor will act to further damp the oscillation in delivered air temperature. Definition of the air duct requirements and definition of allowable air temperature fluctuations at the combustor will be needed in order to establish the HTAH control needs and to assess the effectiveness of control schemes studied.

The long term oscillation in the system outlet temperatures is due to the fact that each individual heater in the system does not receive the ideal flow rates as shown in Fig 38 and thus does not exhibit the ideal performance shown in Fig 39. Unequal distribution of flows results from pressure losses due to the required branching and manifolding as illustrated schematically in Fig 46. For example, a heater which is far from the inlet gas manifold will tend to receive lower than the ideal gas flow; if the heater is also near the inlet air manifold, it may receive higher than the ideal air flow. The result will be a lower than ideal outlet air temperature from this particular heater.

In addition to the overall system outputs as shown in Figs 47 and 48, the SCAMP code can be used to study the performance of the individual heaters. For example, the performance of a typical heater (Heater 14) is illustrated in Figs 49-52. The solid temperatures at the top and bottom of the matrix are shown in Figs 49 and 50, and the outlet air and gas temperatures are shown in Fig. 51. These temperatures can be compared with the ideal temperatures shown in Fig 38 to assess the degree of variation of each heater from the ideal case. Similarly, the air and gas flow rates through each individual heater (illustrated for Heater 14 in Fig 52) can be compared with the ideal flow rates in Fig 38.

The HTAH system pressure losses are shown in Figs 53 and 54. The system inlet air pressure is 867 kPa (125.81 psia) and the gas inlet pressure is 107 kPa (15.58 psia). The air pressure loss shows a number of spikes which are due to pressurization/depressurization of the various heaters. These spikes represent changes in the pressure loss on the order of 20% of the average pressure

loss of 27.6 kPa (4 psi) or pressure surges of about 0.7% of the system air pressure. Similar spikes are seen in the gas side pressure loss on the order of 11% of the average 4.1 kPa (0.6 psi) loss or surges of 0.4% of the system gas pressure. In addition to these sharp spikes, an oscillation of much smaller amplitude is also seen in the air and gas pressure losses. Again, definition of the pressure requirements at the combustor will be needed to establish control needs and assess effectiveness of control methods. Figs 49-52 illustrate the type of performance calculations which can be made with the SCAMP code in order to screen and define control systems and operating methods.

In the second computer run, the HTAH gas inlet temperature was subjected to a step change of 111 K (200 F), being reduced from 1963 K (3075 F) to 1852 K (2875 F). The purpose of this run was to study the system response to a variation in temperature, such as might occur due to a load change or an upset in MHD plant operating conditions.

The HTAH system response to the step change in gas inlet temperature is shown in Fig 55. The results are presented in the form of transfer functions η for the outlet air and gas temperatures where

$$\eta = \frac{T - T_{FINAL}}{T_{INITIAL} - T_{FINAL}} \qquad (12)$$

T = temperature at time t

$T_{INITIAL}$ = temperature before step change

T_{FINAL} = temperature system will reach after transient period following step change

The values of T_{FINAL} for both the outlet air and gas temperatures were computed by assuming that the heat exchanger effectiveness on the air and gas sides remained constant, i.e.,

$$\left(\frac{T_{G\ in} - T_{G\ out}}{T_{G\ in} - T_{A\ in}}\right)_{INITIAL} = \left(\frac{T_{G\ in} - T_{G\ out}}{T_{G\ in} - T_{A\ in}}\right)_{FINAL} \quad (13)$$

$$\left(\frac{T_{A\ out} - T_{A\ in}}{T_{G\ in} - T_{A\ in}}\right)_{INITIAL} = \left(\frac{T_{A\ out} - T_{A\ in}}{T_{G\ in} - T_{A\ in}}\right)_{FINAL} \quad (14)$$

As can be seen in Fig 55, the outlet air and gas temperature response can be approximated by an exponential decay from the initial state to the final state. The outlet air temperature response is much faster than the outlet gas temperature response. The transfer functions have been reduced to less than half of the initial values within 2 cycles for the air temperature and 3 cycles for the gas temperature. To reduce the system output transfer functions to 10% of the initial values would require a total of approximately 5 cycles for the air temperature and 12 cycles for the gas temperature.

The transfer functions shown in Fig 55 may now be used to estimate HTAH system response to step changes in fluid inlet temperatures without requiring a run of the SCAMP code.

The HTAH outlet air temperature for the two small manifold cases is shown in Figs 56 and 57. Results from the three steady state computer runs are summarized in Table 23.

The air outlet temperature variation with large manifolds is 24 K (44 F) and the gas outlet temperature variation is 16 K (29 F). With small manifolds, the air outlet temperature variation increases to 50 K (90 F) and the gas outlet temperature variation increases to 31 K (56 F). Thus the reduction in manifold size, which reduces the HTAH cost by 9% (Table 17), doubles the air and gas outlet temperature variations.

The increase in outlet temperature variation with decrease in manifold size arises from the resulting degree of variation in flow through the individual heaters in the system. Comparing Figs 47 and 56, it is evident that the short term ($\sim$ 1.5 minute) variations in air outlet temperature, which arise from the temperature droop in the individual heaters, are essentially unchanged in the small manifold case. However, the longer term ($\sim$ 10 min) variation in outlet temperatures is greater. This longer term variation is due to the fact that the location of each individual heater relative to the air and gas manifolds affects the amount of flow it receives, since the pressure loss in the manifolds is not insignificant relative to the pressure loss in the heater flow passages. Heater-to-heater differences in the flow rate produce heater-to-heater differences in performance; thus different heaters produce different <u>levels</u> of air outlet temperature even through the <u>droop</u> in temperature remains nearly the same. When the manifold size is decreased, the pressure loss in the manifolds becomes even more significant and differences in flow rate are increased. The longer term variations in system outlet temperature are then increased.

In order to effectively drain seed/slag from the heaters during normal operation of the HTAH, the bottom of matrix solid temperatures must exceed the melting point of seed (1342 K or 1956 F for potassium sulfate) for a sufficient period of time during each gas phase. In order to assure that this condition is realized, 1400 K (2060 F) has been selected for the criterion which the maximum bottom of matrix temperature of each individual heater should meet or exceed. Neither the large or small manifold system, operating with all heater cycles having the same gas and air phase durations, meet this criterion (Table 23, third column). Some individual heaters have maximum bottom of matrix temperatures as low as 1336 K (1944 F) for the large manifold case and 1279 K (1843 F) for the small manifold case. This is because of the variation in flow rates, and thus heater performance, due to location of the individual heaters relative to the manifolds as discussed above.

For this reason, a control system was implemented in the SCAMP model to determine whether the bottom of matrix temperature criterion could be achieved. The concept was to allow those individual heaters which did not achieve the temperature criterion to operate with a lengthened gas phase and a shortened air phase, maintaining the same total heater cycle time so that the heater sequence is not affected.

The method used to select the changes in gas and air phase durations was as follows. Several runs were made with the STRHEX code, modeling an individual heater in the example HTAH. The phase durations were systematically varied to produce duce the curve shown in Fig 58, which indicates the amount that the phase duration should be modified to achieve a corresponding change in maximum bottom of matrix temperature. The results showed that the temperature would vary as a linear function of

the change in phase duration. The durations of the air and gas phases for several heaters in the 30 heater system were then altered to achieve the desired result. Secondary effects due to changes in phase duration of other heaters in the system were ignored for the first attempt at implementing the control concept.

As seen in Table 23, when this concept was used with the SCAMP code for the small manifold HTAH, the maximum bottom of matrix temperature criterion for all heaters was nearly achieved. A new choice of phase durations for the individual heaters including the secondary effects could have been made in order to improve the bottom of matrix temperatures further, but since the capability of the control concept had been demonstrated, another SCAMP run was not made in consideration of budget constraints.

The air outlet temperature for the small manifold HTAH with control system is shown in Fig 57. The total variation in air outlet temperature is the same as for the small manifold case without control, although the form of the outlet temperature over time is different. This result demonstrates the capability to operate a HTAH in such a manner as to control a particular parameter, in this case as required for heater operability, while maintaining the overall HTAH performance.

This control concept could be readily used in an actual HTAH system. Sensing of a temperature which is too low or a pressure drop which is too high would result in an adjustment of the phase times by the HTAH controller. Study of the system response with regard to those parameters which affect the overall MHD plant performance will be required in order to evaluate the possible use of this or other control concepts. Analysis of the SCAMP data from the runs made to date and of future SCAMP data will be directed toward this objective.

3.3.3 System Layouts

The objective of this subtask is to prepare HTAH system layouts for the purpose of integrating individual component modeling or design studies. The level of effort for the layouts is consistent with that needed to identify development needs which should be addressed in the HTAH development program.

During the reporting period, a layout for the example HTAH for a 1000 MW_e plant was conceived and a concept for providing for thermal expansion of the HTAH was developed. The overall layout was arrived at through consideration of overall insulation requirements; compactness of the overall HTAH system; valve orientation, insulation, and installation requirements; manifold and duct design considerations; individual heater vessel plenums, matrix support and arrangement of flow passages; and problems related to the intersections of large diameter, refractory lined ducts and manifolds.

The development of a thermal expansion concept for the HTAH is complicated primarily by the operating methods and the large physical size of components. Thermal expansion accommodation must be provided during startup and shutdown when very large thermal growth occurs, but the system later stabilizes at operating conditions. At operating temperature, smaller displacements between components occur due to differences in temperature level. The second consideration is the impracticality of locating expansion joints in very large pipes and especially those whose cross-sections are not circular or those which carry a relatively high pressure.

The overall system layout for the example HTAH is shown in Fig 59. The size, shape, and operating pressure for the major piping components are listed in Table 24. The equivalent outer diameter given is the nominal pipe shell diameter. All of the piping is insulated internally and externally such that the pipe shell temperature is nominally 533 K (500 F) at operating conditions.

The thermal expansion design concept proposed here is guided by the following precepts:

1. Provide a set of fixed points in the gas mains located at the intersection of the centerline of the gas mains and the intersection of each gas manifold.

2. Provide a rigid connection between the gas-in manifold and the heater and allowing the heater to move horizontally along the direction of a heater run on a system of support rails.

3. Avoid expansion joints in the gas-in and gas-out manifolds due to their catenary shape and avoid expansion joints in the large, high-pressure air-out manifold.

4. Relocate the air mains near the HTAH centerline (between the gas mains) so that the location of their interface point with other MHD components does not have large lateral movements during startup and shutdown.

5. Assume that all pipe shells at any given time differ in temperature by no more than $\pm$ 28 K (50 F), i.e., a relative difference not to exceed 56 K (100 F).

A schematic diagram of the thermal expansion design concept applying these guidelines is shown in Fig 60. Expansion joints are located in the gas mains, the gas-out ducts and the air-out ducts.

From a fixed point in the gas-in main, the gas-in manifold, the adjacent heater row, and the air-out manifold move as a rigid unit as thermal expansion occurs. It will be important to the design to maintain only a small relative temperature difference between the shell of the gas-in manifold and the air-out manifold. The total thermal growth of these two manifolds is approximately 102 mm (4 in) from 288 K (60 F) to the operating temperature of 533 K (500 F) during startup. A relative temperature difference of 56 K (100 F) between these two manifolds would result in approximately 6 mm (0.25 in) difference in thermal growth between each heater in a given row.

The gas-out and air-in manifolds are isolated from the heaters by expansion joints located in the ducts. These expansion joints are selected to accommodate lateral movement due to relative differences in shell temperature. It is not necessary to accommodate the overall growth during startup since all four manifolds are parallel and expand equal amounts. A list of the required expansion joints is given in Table 25.

In summary, it is shown that a concept to accommodate the thermal expansion of the HTAH can be developed utilizing conventional engineering practices. However, without details of the actual methods of supporting the major piping elements and the heaters, some difficult engineering problems remain. The major remaining concerns are the accommodation of thermal growth in the vertical direction, particularly of the individual heaters, the restraint of piping where large pressure-area forces or thrusts are developed, and the compatibility of the expansion of the refractory insulation within the piping system.

3.3.4 Cost Estimates

During the reporting period, the algorithms used to compute the HTAH cost in the size/cost program were reviewed. In particular, the cost model for intersections of ducts and manifolds was upgraded and incorporated in the size/cost code. A complete, separate cost estimate of the example HTAH originally planned was not completed. Since the primary interest in cost estimates at the present time is in relative costs for various HTAH concepts, verification of the level of costs from the size/cost code to a great degree of accuracy is not considered important.

3.3.6 Matrix Support Test Facility

The support for a full-scale HTAH cored brick matrix presents certain unique development problems. The matrix support structure must withstand the corrosive HTAH service conditions and must be capable of supporting the weight of the cored brick matrix while being subjected to high operating temperatures and large stresses induced by thermal cycling. Tests in subscale test facilities can provide information concerning the corrosion resistance of potential matrix support materials and the ability to prevent accumulation of seed/slag material in the matrix support structure.

In order to study the capability of a support structure to withstand the dead load and thermal cycling loads to be encountered in a full-scale system, however, the support structure must be tested at a sufficiently large scale to simulate the actual conditions to be encountered.

Cored brick matrix diameters on the order of 4.3 m (14 ft) are anticipated for full-scale HTAH systems. Larger diameters are anticipated to be difficult to achieve due to the matrix support requirements. Thus, tests of matrix support structure concepts at approximately this size level will be required in order to verify that a matrix support will be suitable for use in a full-scale HTAH.

The objective of work under this subtask is to identify a concept for a test facility which can be used to obtain the needed information as part of the HTAH development program. Such a concept was identified during the reporting period, and the test facility was defined in terms of one matrix support concept, a perforated ceramic dome. Other matrix support concepts could also be tested in the facility. The facility design effort was limited to a conceptual level due to budget constraints.

The concept developed for the matrix support test facility is to construct a support structure which is loaded from above to simulate the dead load of the cored brick matrix. This structure is then alternately heated and cooled by a heated gas stream which flows vertically upward through the matrix support to simulate the material temperatures and the thermal stresses to which an actual matrix support would be exposed. The gas stream would be clean, since the intent of the tests is not to evaluate the corrosion resistance of the material, but rather to study the mechanical integrity of the structure. The use of clean gas will significantly reduce the cost of the test facility. Methods to simulate the loading of the matrix support in the most inexpensive manner were also sought in developing the facility concept.

Two different methods of loading the support structure were considered. The first loading method utilizes a hydraulic load system while the second method employs a static load. These loading methods are illustrated in Figs 61 and 62.

The concept of the ceramic dome support was developed in earlier work (Ref 6). The concept has been applied in a subscale preheater through a design furnished by FluiDyne to the General Electric Company (Ref 15). The objective of the support concept is to control the thermal expansion in the outer metal ring in such a way that its movement compensates for the thermal expansion and contraction of the refractory arch due to the cyclic temperature variations to which the arch is exposed.

The basis of the matrix support test facility is to test matrix support concepts with a limited facility which is less costly than constructing and testing an entire full-scale air heater module. The designs shown in Figures 61 and 62 have retained only the elements required to meet the test objectives. In both design cases, the hot gas which flows through the support arch is always directed upward and temperature cycling is accomplished through varying the inlet gas flow rate and temperature. Flow rates and temperatures are indicated in Figs 61 and 62.

The load on the ring and arch which represents the weight and load distribution of the full-scale HTAH matrix is simulated in the first case by placing a short stack of refractory bricks on top of the arch, then placing a layer of refractory pebbles (spheres) above the bricks and finally

applying controlled hydraulic loads to the pebbles. The layer of pebbles is necessary so that the load surfaces of the hydraulic cylinders do not block the flow passages in the cored brick stack. The cored bricks and pebbles may be made of inexpensive materials since corrosion resistance is not required.

Further evaluation of this loading technique will be required. It is possible that individual pebbles may block the cored brick flow holes. It is also possible that some weaker pebbles could fracture under the loading.

The static load case is similar to an actual air heater in the sense that the load is applied by an actual column of bricks. Again, inexpensive materials would be used for the column of bricks. This case is better than the hydraulic load case in terms of simulation of actual load, and is simpler in concept. However, the static load case does not have the testing flexibility of the hydraulic load case. Desired changes in the test load would require significant time and effort. A further consideration is that in the event of failure of the matrix support assembly being tested, major facility repairs would be necessary.

Preliminary cost estimates for construction of both facility concepts indicated that the cost of a column of bricks would be roughly comparable to the cost of a hydraulic load system and its attendant cooling system.

This subtask has been eliminated from the Statement of Work for continuation of efforts under the contract. Therefore, no further efforts will be expended on design of a matrix support test facility at this time. Design of a facility following the concept developed should be undertaken at a future time in the HTAH development program in order to ensure that a matrix support concept suitable for use in a full-scale HTAH can be developed.

3.3.7 Alternative Heater Systems

The objective of work under this subtask is to identify design concepts for full-scale MHD air heaters which may serve as alternatives to the regenerative heater concept being pursued as the basis of the HTAH development program. Those concepts which show promise may be considered for future full-scale designs should certain aspects of the HTAH as conceptualized in the development program prove to be technically or economically unfeasible.

Three alternative heater concepts, all of the ceramic, regenerative type, were examined during the reporting period. These concepts were: (1) an intermediate temperature air heater (ITAH) for preheat of air or oxygen enriched air to 1200 K (1700 F), (2) a HTAH incorporating upflow of the radiant boiler exhaust gas for heating air from compressor discharge temperature to a level in the range of 1400-1500 K (2060 - 2250 F), and (3) an integrated ITAH and HTAH system for heating air from compressor discharge temperature to 1788 K (2758 F).

Concepts were first identified which would provide alternative solutions to certain HTAH development problems. Modifications were then made to the size/cost computer code in order to treat these concepts, and the code was used to make a preliminary examination of each case. The actual computer runs were made after the directive was received from DOE to focus the full-scale studies on heater systems for a 600 MW_e plant. Thus, the alternative heater systems were nominally sized for a 600 MW_e plant.

For comparison purposes, an example HTAH for a 600 MW_e plant was first defined following the same basic criteria used to define the example HTAH for a 1000 MW_e plant as described in Section 3.3.1. System studies of MHD plants were not used in order to size the HTAH; the flow rates used for the 1000 MW_e plant example were simply scaled by 60%. The parameters of the example HTAH for a 600 MW_e plant are shown in the first column of Table 26. Identical flow rates were used for size/cost studies of the alternative heater systems. System studies would be required of course, in order to realistically define flow rates for these alternate systems since the levels of preheat are different and since oxygen enriched air would probably be used in certain of the concepts. However, for the preliminary examination desired, the level of effort required to obtain such studies was not justified.

ITAH for 1200 K (1700 F) Preheat

This type of heater would be applicable to MHD demonstration facilities, such as the ETF, or first generation MHD power plants, in which oxygen enriched air will be used to fire the combustor. A ceramic, regenerative heater of this type could find application at an early stage in the MHD program since development needs are minimal, as opposed to the directly-fired HTAH. The ITAH would be fired directly with the exhaust from the heat and seed recovery boiler (HSR or HRSR). The temperature of the reheat gas would thus be low enough so that seed and ash remaining in the gas stream would be in the form of dry, solid particles.

The parameters of the system as conceived in this study are shown in the second column of Table 26. A temperature of 1289 K (1860 F) was chosen for the heat and seed recovery boiler exhaust and the inlet gas temperature to the ITAH.

The temperature of the oxygen enriched air entering the ITAH was assumed to be equal to a compressor discharge temperature of 589 K (600 F). Low cost material was chosen for the cored brick heat storage matrix, since resistance to alkali vapor and liquid coal ash are not required in this system. A metallic matrix support was used due to the modest bottom of matrix temperature. Insulation materials as specified in Section 3.1.1 were also used.

As seen in Table 27, when compared to a HTAH, the ceramic heater cost is reduced by 77% if the ITAH is used. This does not represent a total plant cost reduction, however. A plant incorporating the ITAH would have corresponding cost increases since the radiant boiler would be replaced by a larger HRSR boiler and an oxygen plant would also be required. The ITAH would have advantages over the HTAH, disregarding these differences in the remainder of the plant, due to this reduced heater cost and due to the lack of need for extensive development. Experimental evaluation of erosion of inexpensive cored brick materials by solid seed and ash particles and choice of appropriate material represents the only technology development need for the ITAH.

Several distinct advantages of the ceramic ITAH over a metallic ITAH are evident. A significantly higher preheat temperature will be achievable from the ceramic heater. A limit of 922 K (1200 F) is generally considered the maximum achievable from a metallic ITAH. The increased preheat temperature, in this case 278 K (500 F) would significantly reduce the required level of oxygen enrichment and thus the cost of the oxygen plant. Reduced size of the oxygen plant will also result in increased power plant efficiency. The higher allowable HRSR boiler exhaust temperature for the ceramic heater would also allow reduced cost of the HRSR boiler.

Upflow HTAH

The concept of passing the radiant boiler exhaust gas vertically downward through the HTAH cored brick matrix was chosen earlier in the HTAH development program as the basic HTAH configuration which would be addressed through full-scale studies and subscale tests. This choice was based primarily on the requirements for support of the cored brick matrix. A ceramic or cooled metallic matrix support must have sufficient strength at the operating temperature to support the matrix without undergoing excessive deformation. The likelihood of developing materials with sufficient strength and creep resistance at temperatures approaching 1978 K (3100 F) and also capable of withstanding the corrosive HTAH environment was perceived to be small. Thus it was decided to concentrate on the downflow concept, in which the highest material temperatures are experienced in the region of minimum load and lowest temperatures in the region of maximum load.

A HTAH incorporating upward flow of the radiant boiler gas, reduced to a lower temperature than for the downflow HTAH, was considered under the alternative heater studies. This system offers an advantage over the downflow heater concerning the requirement to operate the HTAH without accumulation of seed/slag material in the cored brick matrix flow passages. In order to meet this requirement, the downflow HTAH must be operated in such a manner that the bottom of the matrix exceeds the seed freezing temperature for some portion of each cycle, as discussed earlier in this report. Additional requirements may also be identified through ongoing experimental work.

In the case of the upflow HTAH, however, the thermal gradient and the gravitational gradient in the heater act in the same direction. Thus if seed/ash material is deposited on the flow passage walls it will flow in a direction such that its viscosity is continually reduced. This may allow the heater to be operated without accumulation of deposits more easily since deposits will tend to be more free flowing. Furthermore, drainage of material from the flow passages will be able to occur at all times throughout the operation of the HTAH.

The choice of a ceramic dome type matrix support was made for this alternative heater concept. Results presented in Section 3.1.2 indicate that fused cast magnesia-spinel has sufficient creep resistance to be used as a matrix support material at temperatures as high as about 1750 K (2700 F). The upper temperature limit may be even higher than this; measurements at temperatures of up to 1923 K (300 F) showed excellent creep resistance at low stress levels, but more data at higher stress levels is needed to clarify the situation.

Two cases were studied for the upflow HTAH. In the two cases reheat gas inlet temperatures of 1700 K (2600 F) and 1589 K (2400 F) were chosen. In both cases the air inlet temperature was chosen to be 589 K (600 F); the combustion air is fed directly from the compressor outlet to the top of the air heaters. Parameters of these systems are shown in columns 3 and 4 of Table 26. The matrix and insulation materials were the same as used for the reference HTAH system. Air preheat temperatures of 1508 K (2255 F) and 1411 K (2080 F) were found for the two upflow HTAH cases. As seen in Table 27, the cost of these systems was reduced by 22-23% over the cost of the reference HTAH, primarily due

to the overall lower temperature and resulting decrease in required insulation, both in ducts and manifolds and in the heater vessels.

The upflow system thus is seen to have advantages over the downflow HTAH. The cost of the heater itself is reduced significantly. Furthermore, the need for a low temperature heater is eliminated, resulting in a further MHD plant cost reduction. The level of preheat, while not as high as proposed for the downflow HTAH, is high enough that oxygen enrichment would not add to the plant efficiency (Ref 14) and thus an oxygen plant would not be required. Some offsetting penalty would be caused by the requirement to reduce the radiant boiler exhaust temperature, thus increasing the cost of the radiant boiler. The overall plant efficiency would also be reduced due to the lower preheat temperature. If fused cast magnesia-spinel or another material is shown to have sufficient creep strength to allow reheat gas inlet temperatures as high as achievable for the downflow HTAH, however, these two penalties would not be applicable.

The development needs for an upflow HTAH are similar to those for the downflow HTAH with regard to materials and operability. Should it become evident that operation of a downflow HTAH without accumulation of deposits presents too difficult a problem, or that the presently anticipated temperature level for air preheat with a downflow HTAH can not be achieved due to material temperature limits, the upflow HTAH should be considered an option for further design studies and for subscale testing.

Integrated ITAH and HTAH

The third alternative heater concept involves combining the ceramic, regenerative ITAH with a HTAH in order to take advantage of the ceramic ITAH features. In this integrated heater system, the ITAH heats combustion air from compressor discharge temperature to 1172 K (1650 F) and the HTAH further heats the air to 1778 K (2742 F). The higher temperature of the inlet air to the HTAH simplifies the operation of the heater, lessening the impact of the requirement to raise the bottom of matrix temperature to 1400 K (2060 F) to prevent accumulation of deposits. A second advantage of the integrated design is that the arrangement significantly reduces the total number of valves required for the heater system, affecting a large cost reduction.

A flow schematic is shown in Fig 63 and the heater arrangement is illustrated in Fig 64. A quench gas flow is provided to quench the exhaust gas from the HTAH to 1283 K (1850 F), thus providing a gas stream containing only dry particulate as was assumed in the earlier discussion of the ceramic ITAH. The HTAH and quench gas thus serve to perform part of the contribution to gas conditioning which the HRSR boiler would perform in a plant with oxygen enrichment. The reheat gas bypass flow serves to reduce the flow through the heater system as required in order to balance the heater system energy. This flow could be modulated in order to add heat to the HTAH system if required to remove seed/slag deposits. Mixing details for these flow loops have not been considered in this cursory study.

System parameters are shown in Table 28. Modest diameter constraints for the HTAH vessel, related to matrix support considerations and system valves, were imposed in the system

sizing. Relative cost information was developed only for the heater vessels, since the novel layout envisioned for the integrated system made an assessment of the manifold and other costs beyond the scope of the study. It can be seen from Table 28 that the integrated system, which eliminates the need for a metallic low temperature heater while providing the maximum envisioned preheat level, had a total cost of the individual heaters only 57% greater than for the individual heaters in a HTAH alone. Furthermore, the total number of valves required is reduced from 96 for a single 16 heater HTAH system to only 40 for the integrated ITAH/HTAH system, (see Table 29) which would result in a significant valve cost reduction.

Conclusions from Alternative Heater Studies

This subtask has been eliminated from the Statement of Work for continuation of efforts under this contract. Therefore, development of additional alternative heater concepts will be discontinued. However, certain advantages of the system concepts developed during the reporting period have been demonstrated and are worthy of further consideration in the heater development program.

In view of the need for a decision to be made concerning the use of a metallic or ceramic ITAH to be used for demonstration facilities with oxygen enrichment, further study of the ceramic ITAH will be conducted. The ceramic ITAH will be considered one of the design options for consideration under the subtask described in Section 3.1.1.

In addition, if experimental work conducted under Task 2 and at Montana State University indicates that prevention of accumulation of deposits in the downflow HTAH will be economically unfeasible, or that the reheat gas temperature will have to be

limited to a lower level than presently anticipated, or if property measurements show that potential matrix and matrix support materials have sufficient creep resistance at temperatures greater than presently anticipated, the upflow HTAH will be considered for further study and experimental evaluation.

The integrated ITAH/HTAH system is presented for possible study by systems analysts, and further work on this concept is not anticipated at this time. Should such a system be shown to be advantageous to the overall MHD program, further study will be considered.

3.3.8 Electrical Isolation

The objective of work under this subtask is to identify development needs concerning electrical isolation of the HTAH from the MHD combustor. Since the combustor will in all likelihood be maintained at the same electrical potential as the upstream end of the MHD channel, and the HTAH will probably be at ground potential, the duct carrying the heated air from the HTAH to the combustor will have a large potential difference from one end to the other. Efforts were undertaken to determine whether the presence of seed carryover to the air stream from the heater matrix poses any special problems requiring technology development before an electrical isolation system for the directly-fired HTAH can be designed.

Two considerations were investigated in this context. Information was obtained on the electrical conductivity of potassium-containing air and of refractory material which could be used for lining the duct carrying heated air from the HTAH to the combustor.

Electrical conductivity of air at various temperatures and with various degrees of potassium contamination was determined with assistance from Dr. R.H. Eustis at Stanford University. Results are shown in Table 30. Using the test data reported in Section 3.2.5 and assuming that the average delivered air temperature would be 1755 K (2700 F) and that all heaters would have a 15 minute air phase, a rough interpolation from Table 30 shows that the conductivity of the air stream would be on the order of 1.6×10^{-3} mho/m.

Calculations of the electrical conductivity of typical hot liner refractories at air outlet manifold temperatures were also made. These calculations showed that the innermost refractory materials are conductive enough to present an isolation problem if the isolation section is very short. Thus, a gap in the refractory insulation will probably be required for electrical isolation if a short isolation section is required. If a moderately long length of duct is acceptable, however, the refractory conductivity does not present a concern. Several concepts for avoiding arc formation in the duct were also discussed with Dr. Eustis.

This subtask has been eliminated from the Statement of Work for continuation of efforts under this contract, and further efforts will not be made at this time to study electrical isolation concepts for the directly-fired HTAH. In view of the moderate level of conductivity anticipated for the air stream and duct refractories as shown in the studies during the reporting period, extensive development in the electrical isolation area is not expected to be necessary before design of an actual directly-fired HTAH can be accomplished. Further analysis and testing of isolation concepts may be required at some future date, however.

4.0 CONCLUSIONS

Tests in the Valve Test Facility have indicated that a refractory lined, water cooled, gate-type valve will prove to be suitable for use as the gas inlet valve for the directly-fired HTAH. Results to date indicate that valve leakage is minimal and that the presence of seed material in the gas flow decreases leakage. Operation of the test valve has not been inhibited by exposure to simulated seed/ash bearing radiant boiler exhaust gas. Longer term tests will be required and are planned in future work to clarify these observations; the test valve has been operated for a total of 780 cycles to date.

Studies of full-scale HTAH systems also have shown that at most 1 spare heater module with associated valves would be required in a system of 14 active heaters in order to assure a 2% HTAH unavailability rate, if reasonable assumptions for valve life are made. Also, mass loss in a full-scale HTAH due to valve leakage and pressurization/depressurization losses was shown to result in a reduction of MHD plant efficiency of less than 0.1%. When compared to the gain in efficiency resulting from use of a HTAH, this penalty is negligible.

Cored bricks of fused cast magnesia-spinel (Corhart X-317) have continued to demonstrate good resistance to the directly-fired HTAH service conditions in tests of the Matrix Test Facility. In addition, measurements at Montana Tech have shown that this material has sufficient creep resistance to withstand HTAH design loads with no significant deformation.

Material property data is being collected in a formal materials data base. Cooperation of outside organizations such as Montana Tech, MSU, and MERDI in performing measurements

according to test requirements established by FluiDyne has proved to be extremely useful in assembling this information and will be needed in the future to insure that the data base requirements are achieved. Liaison with refractory manufacturers has been effective, resulting in several programs for development of HTAH materials and fabrication techniques.

A potential cost-saving method for construction of a full-scale matrix support was identified through selection of a castable material for the matrix support in the MTF and development of a technique for installing it. Size/cost computer code studies have shown that the selection of an insulation scheme for a full-scale HTAH is a major factor in determining HTAH cost. A four-layer insulation scheme selected for full-scale studies was shown to result in a cost lower than the lowest risk insulation scheme but greater than schemes using castable insulation materials.

Analysis of HTAH system and individual heater performance has demonstrated the capability to control HTAH performance parameters using a concept under which the lengths of time that individual heaters are on gas and air phases are varied as required while a constant total cycle time is maintained.

Design of a dilatometer for making measurements of refractory creep in the directly-fired HTAH service environment has been completed. Construction and testing of this device at a future time in the HTAH development program will allow confirmation of creep information inferred from the conventional creep tests (at Montana Tech) of pristine material samples and samples which have been exposed to the HTAH environment. A concept for a test facility to test matrix support concepts at large scale has also been developed.

Construction and testing at a future time will provide needed information on the requirements for and capabilities of high temperature matrix support concepts.

Preliminary studies of alternative heater concepts have identified possible advantages in the use of a ceramic, regenerative intermediate temperature air heater (ITAH) for early MHD plants with oxygen enrichment. The ITAH will be considered further in full-scale studies. The upflow HTAH may be considered for further study and for experimental evaluation at a future time in the heater development program.

Measurements made in the MTF during the reporting period indicated that the cored brick matrix did not have a catalytic effect on NO_x in the reheat gas stream. Thus, a reduction of NO_x due to contact of the MHD channel exhaust gas with the directly-fired HTAH cored bricks should not be considered in computing NO_x emissions from a MHD power plant.

REFERENCES

1. Youngblood, G.E., Montana Energy and MHD Research and Development Institute, private communication.

2. Kitto, K.L., Montana College of Mineral Science and Technology, private communication.

3. Jackson, D., Corhart Refractories Company, private communication.

4. Trostel, L. J., Norton Company, private communication.

5. Johns-Manville Refractory Production Information, Section 150, Part 10.

6. FluiDyne Engineering Corporation, "MHD Air Heater Development Technology," Final Report for Contract DE-AC01-78ET10814; March 1981.

7. Lippert, T.E., et al, "MHD Systems Evaluation and Requirements," Proceedings of the Seventh International Conference on MHD Electrical Power Generation, Massachusetts Institute of Technology, Cambridge, Massachusetts, June 16-20, 1980.

8. McCutchan, D.A., et al, "Operational Analysis of MHD," Progress Status Report, Period Covering April-June, 1978, EPRI Contract No. RP-639-1.

9. McCutchan, D.A., et al, "Operational Analysis of MHD," Progress Status Report, Period Covering July-September, 1978, EPRI Contract No. RP-639-1.

10. Kuckertz, W., "High-Duty Valves for Blast Furnaces and High-Temperature Stoves," Iron and Steel Engineer, December 1979, p. 53.

11. Ahluwalia, R.K., and Im, K.H., "Heat Transfer Scaling Laws for MHD Channels and Diffuser," Proceedings of Seventh International Conference on MHD Electrical Power Generation, Massachusetts Institute of Technology, Cambridge, Massachusetts, June 16-20 1980, pp. 187-194.

12. Im, K.H., and Ahluwalia, R.K., "Heat Transfer Scaling Laws for MHD Radiant Boilers," Proceedings of Seventh International Conference on MHD Electrical Power Generation, Massachusetts Institute of Technology, Cambridge, Massachusetts, June 16-20 1980, pp. 329-336.

13. Ariesson, P.C., Eustis, R.H., and Self, S.A., Measurements of the Size and Concentration of Ash Droplets in Coal-fired MHD Plasmas," Proceedings of Seventh International Conference on MHD Electrical Power Generation, Massachusetts Institute of Technology, Cambridge, Massachusetts, June 16-20 1980, pp. 807-814.

14. Pian, C.C.P., Staiger, P.J., and Seikel, G.R., MHD Performance Calculations with Oxygen Enrichment, DOE/NASA/2674-79/4, NASA TM-79140, June 1979.

15. Omori, S., et al, "A Direct Coal Fired Wet Bottom Ceramic Regenerative Heat EXchanger for Closed Cycle MHD," Proceedings Of Seventh Conference on MHD Electrical Power Generation, Massachusetts Institute of Technology, Cambridge, Massachusetts, June 16-20 1980, pp. 807-814.

TABLES

TABLE 1

SUMMARY OF MATERIALS SELECTION FOR FULL-SCALE HTAH

	Area	Gas Temp. K (F)	Diameter m (ft)	Heat Flux W/m^2	Heat Flux (Btu/hr-ft^2)	Cost* $/m^2	Cost* ($/ft^2)	Layers Inside Shell
1.	Gas Inlet Duct	1963 (3075)	2.18 (7.2)	1051	333	2614	243	4
2.	Gas Outlet Duct	1333 (1940)	1.83 (6.0)	1011	321	1171	109	2
3.	Air Inlet Duct	920 (1200)	0.79 (2.6)	402	127	85	8	1
4.	Air Outlet Duct	1787 (2760)	1.07 (3.5)	904	287	1994	185	4
5.	Pressurization Duct	920 (1200)	0.36 (1.2)	381	121	85	8	1
6.	Depressurization Duct	1333 (1940)	0.41 (1.3)	1018	323	1165	108	2
7.	Vessel Center	1875 (2915)	4.27 (14.0)	1009	320	2673	248	4
8.	Upper Plenum (Master)	1875 (2915)	4.27 (14.0)	1009	320	2673	248	4
9.	Upper Plenum (Max. Nozzle)	1875 (2915)	2.18 (7.2)	992	315	2295	213	4
10.	Upper Plenum (Min. Nozzle)	1875 (2915)	1.07 (3.9)	905	287	2295	213	4
11.	Lower Plenum (Master)	1333 (1940)	2.74 (9.0)	834	264	2271	211	3
12.	Lower Plenum (Max. Nozzle)	1333 (1940)	1.83 (6.0)	1011	321	1171	109	2
13.	Lower Plenum (Min. Nozzle)	920 (1200)	0.79 (2.6)	453	144	1171	109	2
14.	Gas Inlet Manifold Small End	1963 (3075)	3.10 (10.2)	1053	334	3003	279	4
15.	Gas Outlet Manifold Small End	1333 (1940)	2.59 (8.5)	1010	320	1548	144	2
16.	Air Inlet Manifold Small End	920 (1200)	1.12 (3.7)	490	155	85	8	1
17.	Air Outlet Manifold, Small End	1787 (2760)	1.52 (5.0)	968	307	2299	214	4
18.	Gas Inlet Manifold Large End	1963 (3075)	6.20 (20.3)	1120	355	3011	280	4

* 1980 Dollars/Shell Surface Area

TABLE 1 (Continued)

SUMMARY OF MATERIALS SELECTION FOR FULL-SCALE HTAH

	Area	Gas Temp. K (F)	Diameter m (ft)	Heat Flux W/m^2	Heat Flux ($Btu/hr-ft^2$)	Cost* $\$/m^2$	Cost* ($\$/ft^2$)	Layers Inside Shell
19.	Gas Outlet Manifold Large End	1333 (1940)	5.18 (17.0)	933	296	1543	143	2
20.	Air Inlet Manifold Large End	920 (1200)	1.57 (5.1)	464	147	85	8	1
21.	Air Outlet Manifold, Large End	1787 (2760)	2.13 (7.0)	1032	327	2299	214	4

* 1980 Dollars/Shell Surface Area

TABLE 2

HTAH GAS INLET DUCT - REFRACTORY LAYUP CONCEPT

Description: 2.18 m (86 inch) Inside Diameter Vertical Duct Carrying MHD Exhaust Gas from Manifold to Heater

Interface Temperature		Material	Diameter		Thermal Conductivity	
K	(F)		m	(in)	W/m-K	(Btu-in/hr-ft^2-F)
1963	(3075)		2.18	(86)		
		Dense Spinel Brick			1.76	(12.2)
1860	(2888)		2.41	(95)		
		Insulating Spinel Brick			1.35	(9.4)
1554	(2338)		3.02	(119)		
		High Strength Insulation Brick			0.50	(3.5)
1286	(1855)		3.25	(128)		
		Block Insulation			0.14	(1.0)
577	(578)		3.43	(135)		
		Shell			0.14	(1.0)
			3.48	(137)		
		External Coating			0.07	(0.5)
			3.51	(138)		

$Q = 1051\ W/m^2$ (333 Btu/ft^2 hr)

Cost = \$2614/m^2 (\$243/ft^2) + Labor

TABLE 3

Insulation Schemes for ITAH
(Based on Plane Wall)

Interface Temperature K (F)	Material	Thickness m (in.)	
1311 (1900)			
	Norton LS-812 (Spinel Castable)	0.15 (6)	Gas Inlet Manifold/Ducts $Q = 918\ W/m^2$ (291 Btu/hr-ft^2)
1230 (1754)			
	Sauerisen No. 72 (acid resistant cement)	0.30 (12)	
367 (200)			
	Shell		
1311 (1900)			
	A.P. Green Lo Abrade (Castable)	0.15 (6)	Air Outlet Manifolds/Ducts $Q = 931\ W/m^2$ (295 Btu/hr-ft^2)
1106 (1530)			
	A.P. Green Castable No. 20 (Fireclay)	0.23 (9)	
367 (200)			
	Shell		
755 (900)			
	Sauereisen No. 72 (acid resistant cement)	0.13 (5)	Air Inlet and Gas Outlet Manifolds/Ducts $Q = 994\ W/m^2$ (315 Btu/hr-ft^2)
367 (200)			
	Shell		

TABLE 4

MATERIALS DATA BASE INFORMATION FOR CORHART X-317

Generic Designation: Fusion Cast Magnesia 35% Alumina **ASTM Designation:** None

Method of Fabrication: Fusion Cast from Arc Furnace into Steel or Graphite Molds Annealed and Diamond Sawed

Manufacturers Name and Address: Corhart Refractories Co., 1600 West Lee St., Louisville, KY 40210, (502)778-3311

Application: Direct-Fired MHD Air Heater Matrix and Liner

MHD/UTAH Experience: 1100 Hours MTF Heat 201, 202

Composition: 64% Magnesia, 34% Alumina, 1% Silica, 1% Other

Mixing/Curing Instructions (castables):

Data Source and Validity: Measurements, Manufacturer's Data, and FluiDyne Estimates
Creep Data is Valid only for 500 psi, 2600°F.

Density: 2963 kg/m^3 (185 lbm/ft^3) **Porosity:** 15.0 Volume %

Data Valid from 294 K (70 F) to 2033 K (3200 F)

Property	Temperature, K (F)							
	294 (70)	811 (1000)	1033 (1400)	1256 (1800)	1478 (2200)	1700 (2600)	1922 (3000)	2033 (3200)
Modulus of Elasticity, GPa (psi)	172 (25×10^6)	172 (25×10^6)	172 (25×10^6)	172 (25×10^6)	166 (24×10^6)	159 (23×10^6)	145 (21×10^6)	124 (18.0×10^6)
Poisson's Ratio	.29	.29	.30	.32	.35	.38	.40	.42
Thermal Conductivity[1] W/m·K (Btu/hr-ft-F)	10.44 (6.03)	7.49 (4.33)	6.20 (3.58)	5.19 (3.00)	4.59 (2.65)	4.07 (2.35)	3.63 (2.10)	3.41 (1.97)
Specific Heat[1] J/kg·K (Btu/lbm·F)	921.0 (.220)	1214.1 (.290)	1256.0 (.300)	1297.8 (.310)	1360.6 (.325)	1381.5 (.330)	1402.5 (.335)	1423.4 (.340)
Thermal Stress Limit MPa (psi)	31.0 (4500)	31.0 (4500)	31.0 (4500)	31.0 (4500)	31.0 (4500)	30.4 (4400)	29.7 (4300)	27.6 (4000)
Thermal Expansion Coeff. K^{-1} (F^{-1})	9.54×10^{-6} (5.3×10^{-6})	9.54×10^{-6} (5.3×10^{-6})	9.54×10^{-6} (5.3×10^{-6})	9.54×10^{-6} (5.3×10^{-6})	9.90×10^{-6} (5.5×10^{-6})	10.26×10^{-6} (5.7×10^{-6})	10.80×10^{-6} (6.0×10^{-6})	11.34×10^{-6} (6.3×10^{-6})
Modulus of Rupture[3] MPa (psi)	31.0 (4500)	31.0 (4500)	31.0 (4500)	31.0 (4500)	31.0 (4500)	30.4 (4400)	29.7 (4300)	27.6 (4000)
Compressive Strength[2] MPa (psi)	138 (20,000)	138 (20,000)	138 (20,000)	124.2 (18,000)	103.5 (15,000)	82.8 (12,000)	55.2 (8,000)	41.4 (6,000)
Critical Stress Intensity Factor[3] $MPa \cdot m^{1/2}$ ($psi \cdot in^{1/2}$)	.00462 (4.2)	.00462 (4.2)	.00462 (4.2)	.00462 (4.2)	.00462 (4.2)	.00451 (4.1)	.00440 (4.0)	.00418 (3.8)
Creep Rate Under Load, %/hr[2]								
@ 0.2 MPa (25 psi)	1.0×10^{-14}	1.0×10^{-13}	1.0×10^{-12}	1.0×10^{-11}	1.0×10^{-10}	1.0×10^{-9}	1.0×10^{-8}	1.0×10^{-7}
@ 0.7 MPa (100 psi)	1.0×10^{-13}	1.0×10^{-12}	1.0×10^{-11}	1.0×10^{-10}	1.0×10^{-9}	1.0×10^{-8}	1.0×10^{-7}	1.0×10^{-6}
@ 3.4 MPa (500 psi)	1.0×10^{-12}	1.0×10^{-11}	1.0×10^{-10}	1.0×10^{-9}	1.0×10^{-8}	1.0×10^{-7}	1.0×10^{-6}	1.0×10^{-5}
@ 6.9 MPa (1000 psi)	1.0×10^{-11}	1.0×10^{-10}	1.0×10^{-9}	1.0×10^{-8}	1.0×10^{-7}	1.0×10^{-6}	1.0×10^{-5}	1.0×10^{-4}

1. Superscripted Numbers Refer to References at End of Text.

TABLE 5

MATERIALS DATA BASE INFORMATION FOR NORTON LS-812

Generic Designation: Spinel Castable **ASTM Designation:** None

Method of Fabrication: Fused Spinel Grains are Mixed with Calcium Aluminate Cement

Manufacturers Name and Address: Norton Co., 1 New Bond Street, Worcester, MA 01606, (617) 853-1000 (Louis Trostel)

Application: Direct-Fired MHD Hot Liner, Do Not Use for Matrix Above 2400°F

MHD/HTAH Experience: MTF Heat 202 Hot Liner Six-Inch ZJ Valve

Composition: 73% Alumina, 24% Magnesia, 2.4% Calcia, 1% Silica

Mixing/Curing Instructions (castables): Nine Pints Water Per 100 lbs, Use Paddle Mixer, see Norton Bulletin S-AP-G1

Data Source and Validity: Measurements and FluiDyne Estimates

Data is for Material Fired to 2500°F

Density: 2499/m^3 (156 lbm/ft^3) **Porosity:** 30.0 Volume %

Data Valid from 294K (70 F) to 2033 K (3200 F)

Property	Temperature, K (F)							
	294 (70)	811 (1000)	1033 (1400)	1256 (1800)	1478 (2200)	1700 (2600)	1922 (3000)	2033 (3200)
Modulus of Elasticity, GPa (psi)	104 (15×10^6)	104 (15×10^6)	104 (15×10^6)	97 (14×10^6)	90 (13×10^6)	83 (12×10^6)	76 (11×10^6)	69 (10×10^6)
Poisson's Ratio	.29	.29	.30	.32	.35	.38	.40	.42
Thermal Conductivity[1] W/m·k (Btu/hr-ft-F)	5.76 (3.33)	3.55 (2.05)	3.06 (1.77)	2.68 (1.55)	2.34 (1.35)	2.08 (1.20)	1.73 (1.0)	1.60 (.925)
Specific Heat[1] J/kg·K (Btu/lbm·F)	921.0 (.220)	1214.1 (.290)	1256.0 (.300)	1297.8 (.310)	1360.6 (.325)	1381.5 (.330)	1402.5 (.335)	1423.4 (.340)
Thermal Stress Limit MPa (psi)	13.5 (1950)	13.5 (1950)	13.5 (1950)	12.4 (1800)	10.4 (1500)	8.3 (1200)	6.9 (1000)	4.8 (700)
Thermal Expansion Coeff. K^{-1} (F^{-1})	9.0×10^{-6} (5.0×10^{-6})	9.0×10^{-6} (5.0×10^{-6})	9.0×10^{-6} (5.0×10^{-6})	9.0×10^{-6} (5.0×10^{-6})	9.0×10^{-6} (5.0×10^{-6})	9.0×10^{-6} (5.0×10^{-6})	9.0×10^{-6} (5.0×10^{-6})	9.0×10^{-6} (5.0×10^{-6})
Modulus of Rupture MPa (psi)	13.5 (1950)	13.5 (1950)	13.5 (1950)	12.4 (1800)	10.4 (1500)	8.3 (1200)	6.9 (1000)	4.8 (700)
Compressive Strength[2] MPa (psi)	41.4 (6000)	41.4 (6000)	27.6 (4000)	20.7 (3000)	17.9 (2600)	13.8 (2000)	10.4 (1500)	6.9 (1000)
Critical Stress Intensity Factor $MPa \cdot m^{1/2}$ ($psi \cdot in^{1/2}$)								
Creep Rate Under Load, %/hr								
@ 0.2 MPa (25 psi)								
@ 0.7 MPa (100 psi)								
@ 3.4 MPa (500 psi)								
@ 6.9 MPa (1000 psi)								

1. Superscripted Numbers Refer to References at End of Text.

TABLE 6

MATERIALS DATA BASE INFORMATION FOR JOHNS MANVILLE YUMA

Generic Designation: High Strength Insulating Firebrick

ASTM Designation: None

Method of Fabrication: Sintered with Fugitive Organic Filler

Manufacturers Name and Address: Johns Manville, Inc., Ken Caryl Ranch, Denver, CO 80217, (303) 979-1000

Application: Backup, Do Not Expose to MHD Gas

MHD/HTAH Experience: None

Composition: 39.3% Alumina, 56.3% Silica, 1.6% Ferric Oxide, 1.6% TIO_2, .27% CAO, 31% MGO, .53% Alkali

Mixing/Curing Instructions (castables):

Data Source and Validity: Manufacturer's Data (not verified) and FluiDyne Estimates

Density: 977 kg/m^3 (61 lbm/ft^3) Porosity: 60. Volume %

Data Valid from 294 K (70 F) to 1644 K (2500 F)

Property	Temperature, K (F)							
	294 (70)	533 (500)	811 (1000)	1089 (1500)	1367 (2000)	1478 (2200)	1589 (2400)	1644 (2500)
Modulus of Elasticity, GPa (psi)	34.5 (5.0×10^6)	34.5 (5.0×10^6)	34.5 (5.0×10^6)	27.6 (4.0×10^6)	20.7 (3.0×10^6)	13.8 (2.0×10^6)	6.9 (1.0×10^6)	3.5 (5.0×10^5)
Poisson's Ratio	.20	.20	.20	.20	.20	.20	.20	.20
Thermal Conductivity[5] W/m·k (Btu/hr-ft-F)	-	.405 (.2342)	.424 (.2450)	.453 (.2617)	.488 (.2817)	.519 (.300)	.536 (.310)	.554 (.320)
Specific Heat J/kg·K (Btu/lbm·F)	1256.0 (.30)	1256.0 (.30)	1256.0 (.30)	1256.0 (.30)	1256.0 (.30)	1256.0 (.30)	1256.0 (.30)	1256.0 (.30)
Thermal Stress Limit MPa (psi)	2.07 (300)	2.07 (300)	2.07 (300)	2.07 (300)	1.73 (250)	1.38 (200)	1.04 (150)	.69 (100)
Thermal Expansion Coeff. K^{-1} (F^{-1})	9.0×10^{-6} (5.0×10^{-6})	9.0×10^{-6} (5.0×10^{-6})	9.0×10^{-6} (5.0×10^{-6})	9.0×10^{-6} (5.0×10^{-6})	9.0×10^{-6} (5.0×10^{-6})	9.0×10^{-6} (5.0×10^{-6})	9.0×10^{-6} (5.0×10^{-6})	9.0×10^{-6} (5.0×10^{-6})
Modulus of Rupture[5] MPa (psi)	2.07 (300)	2.07 (300)	2.07 (300)	2.07 (300)	1.73 (250)	1.38 (200)	1.04 (150)	.69 (100)
Compressive Strength[5] MPa (psi)	3.80 (550)	3.80 (550)	3.80 (550)	3.80 (550)	3.11 (450)	2.42 (350)	2.07 (300)	1.38 (200)
Critical Stress Intensity Factor $MPa \cdot m^{1/2}$ ($psi \cdot in^{1/2}$)	.00011 (.1)	.00011 (.1)	.00011 (.1)	.00011 (.1)	.00011 (.1)	.00011 (.1)	.00011 (.1)	.00011 (.1)
Creep Rate Under Load, %/hr								
@ 0.2 MPa (25 psi)								
@ 0.7 MPa (100 psi)								
@ 3.4 MPa (500 psi)								
@ 6.9 MPa (1000 psi)								

1. Superscripted Numbers Refer to References at End of Text.

TABLE 7

MATERIALS DATA BASE INFORMATION FOR JOHNS MANVILLE C-22Z

Generic Designation: High Strength Insulating Brick ASTM Designation: None

Method of Fabrication: Sintered with Fugitive Organic Binder

Manufacturers Name and Address: Johns Manville, Inc., Ken Caryl Ranch, Denver, CO 80217, (303) 979-1000

Application: Back-up Only, Do Not Expose to Combustion Gas

MID/HTAH Experience: None

Composition: 34.1% Al_2O_3, 59.4% SiO_2, .8% Fe_2O_3, 1.2% TIO_2, 3.4% CAO, .2% MGO, 1.0% Alkali

Mixing/Curing Instructions (castables):

Data Source and Validity: Manufacturer's Data (not verified) and FluiDyne Estimates

Density: 753 kg/m^3 (47 lbm/ft^3) Porosity: 65 Volume %

Data Valid from 294 K (70 F) to 1367 K (2000 F)

Property	Temperature, K (F)							
	294 (70)	533 (500)	811 (1000)	922 (1200)	1033 (1400)	1144 (1600)	1256 (1800)	1367 (2000)
Modulus of Elasticity, GPa (psi)	34.5 (5.0×10^6)	34.5 (5.0×10^6)	34.5 (5.0×10^6)	27.6 (4.0×10^6)	20.7 (3.0×10^6)	13.8 (2.0×10^6)	6.9 (1.0×10^6)	3.5 (5.0×10^5)
Poisson's Ratio	.20	.20	.20	.20	.20	.20	.20	.20
Thermal Conductivity[5] W/m·k (Btu/hr-ft-F)	2.51 (1.45)	2.80 (1.62)	3.55 (2.05)	-	-	-	-	-
Specific Heat J/kg·K (Btu/lbm·F)	1256.0 (.30)	1256.0 (.30)	1256.0 (.30)	1256.0 (.30)	1256.0 (.30)	1256.0 (.30)	1256.0 (.30)	1256.0 (.30)
Thermal Stress Limit MPa (psi)	1.45 (210)	1.45 (210)	1.45 (210)	1.38 (200)	1.24 (180)	1.04 (150.3)	.76 (110.0)	.41 (60.0)
Thermal Expansion Coeff.[5] K^{-1} (F^{-1})	9.0×10^{-6} (5.0×10^{-6})	9.0×10^{-6} (5.0×10^{-6})	9.0×10^{-6} (5.0×10^{-6})	9.0×10^{-6} (5.0×10^{-6})	9.0×10^{-6} (5.0×10^{-6})	9.0×10^{-6} (5.0×10^{-6})	9.0×10^{-6} (5.0×10^{-6})	9.0×10^{-6} (5.0×10^{-6})
Modulus of Rupture[5] MPa (psi)	1.45 (210)	1.45 (210)	1.45 (210)	1.38 (200)	1.24 (180)	1.04 (150)	.76 (110)	.41 (60)
Compressive Strength[5] MPa (psi)	2.28 (330)	2.28 (330)	2.28 (330)	2.21 (320)	2.07 (300)	1.86 (270)	1.59 (230)	1.24 (180)
Critical Stress Intensity Factor MPa·$m^{1/2}$ (psi·$in^{1/2}$)	.00011 (.1)	.00011 (.1)	.00011 (.1)	.00011 (.1)	.00011 (.1)	.00011 (.1)	.00011 (.1)	.00011 (.1)
Creep Rate Under Load, %/hr								
@ 0.2 MPa (25 psi)								
@ 0.7 MPa (100 psi)								
@ 3.4 MPa (500 psi)								
@ 6.9 MPa (1000 psi)								

1. Superscripted Numbers Refer to References at End of Text.

TABLE 8

MATERIALS DATA BASE INFORMATION FOR JOHNS MANVILLE SUPEREX 2000

Generic Designation: 2000°F Block Insulation ASTM Designation: None

Method of Fabrication: Sintered

Manufacturers Name and Address: Johns Manville, Inc. , Ken Caryl Ranch, Denver CO 80217, (303) 979-1000

Application: Backup Only

MHD/HTAH Experience: None

Composition: 74.8% SiO_2, 4.3% Al_2O_3, 6.0% CAO, 2.0% Fe_2O_3, .3% TIO_2, .8% MCO, 2.7% Alkali

Mixing/Curing Instructions (castables):

Data Source and Validity: Manufacturer's Data (not verified) and FluiDyne Estimates

Density: 384 kg/m^3 (24.0 lbm/ft^3) Porosity: 85.0 Volume %

Data Valid from 294K (70 F) to 1367 K (2000 F)

Property	Temperature, K (F)							
	294 (70)	367 (200)	478 (400)	589 (600)	700 (800)	811 (1000)	1089 (1500)	1367 (2000)
Modulus of Elasticity, GPa (psi)	6.9 (1.0×10^6)	6.9 (1.0×10^6)	6.9 (1.0×10^6)	6.9 (1.0×10^6)	6.9 (1.0×10^6)	.69 (1.0×10^5)	.069 (1.0×10^4)	.0069 (1.0×10^3)
Poisson's Ratio	.20	.20	.20	.20	.20	.20	.20	.20
Thermal Conductivity[5] W/m.K (Btu/hr-ft-F)	.0678 (.0392)	.0722 (.0417)	.0779 (.0450)	.0851 (.0492)	.0922 (.0533)	.0995 (.0575)	.1168 (.0675)	.1341 (.0775)
Specific Heat J/kg·K (Btu/lbm·F)	1256.0 (.30)	1256.0 (.30)	1256.0 (.30)	1256.0 (.30)	1256.0 (.30)	1256.0 (.30)	1256.0 (.30)	1256.0 (.30)
Thermal Stress Limit MPa (psi)	.311 (45.0)	.311 (45.0)	.311 (45.0)	.311 (45.0)	.311 (45.0)	.276 (40)	.207 (30)	.069 (10)
Thermal Expansion Coeff. k^{-1} (F^{-1})	9.0×10^{-6} (5.0×10^{-6})	9.0×10^{-6} (5.0×10^{-6})	9.0×10^{-6} (5.0×10^{-6})	9.0×10^{-6} (5.0×10^{-6})	9.0×10^{-6} (5.0×10^{-6})	9.0×10^{-6} (5.0×10^{-6})	9.0×10^{-6} (5.0×10^{-6})	9.0×10^{-6} (5.0×10^{-6})
Modulus of Rupture[5] MPa (psi)	.311 (45.0)	.311 (45.0)	.311 (45.0)	.311 (45.0)	.311 (45.0)	.276 (40)	.207 (30)	.069 (10)
Compressive Strength[5] MPa (psi)	.897 (130)	.897 (130)	.897 (130)	.897 (130)	.897 (130)	.828 (120)	.690 (100)	.345 (50)
Critical Stress Intensity Factor $MPa \cdot m^{1/2}$ ($psi \cdot in^{1/2}$)								
Creep Rate Under Load, %/hr								
@ 0.2 MPa (25 psi)								
@ 0.7 MPa (100 psi)								
@ 3.4 MPa (500 psi)								
@ 6.9 MPa (1000 psi)								

1. Superscripted Numbers Refer to References at End of Text.

Need Date	Material	Bulk Density	Porosity	Elastic Modulus	Poisson's Ratio	Thermal Conductivity	Specific Heat	Thermal Stress Limit	Thermal Expansion	Electrical Resistivity	Thermal Emissivity	Rupture Modulus	Fracture Parameter	Compressive Strength	Creep	Creep in HTAH Environment	Corrosion Resistance
	Matrix	1	1	1	1	1	1	1	1		1	1	1	1	1		1
FY 82	Hot Liner	1	1			1	1		1	1		1		1	1		1
	Insulation	1	1			1									1		1
	Matrix	2, 3	2, 3	2, 3	2, 3	2, 3	2, 3	2, 3	2, 3		2, 3	2, 3	2	2, 3	2, 3		2, 3
FY 83	Hot Liner	2, 3	2, 3			2, 3	2, 3		2, 3	2, 3		2		2, 3	2, 3		2, 3
	Insulation	2, 3	2, 3			2, 3	3								2, 3		2, 3
	Matrix	3	3	3	3	3	3	3	3		3	3	3	3	3	3	3
FY 84	Hot Liner	3	3			3	3			3					3		3
	Insulation	3	3			3									3		
FY 85	Matrix	3, 4	3, 4	3, 4	3, 4	3, 4	3, 4	3, 4	3, 4		3, 4	3, 4	3, 4	3, 4	3, 4	4	3
	Hot Liner	3, 4	3, 4	3	3	3, 4	3, 4	3	3, 4	3, 4		3, 4		3, 4	3, 4		3
	Insulation	3, 4	3, 4			3, 4								3, 4	3, 4		
FY 86	Matrix	5	5	5	5	5	5	5	5		5	5	5	5	5	5	5
	Hot Liner	5	5	5	5	5	5	5	5	5	5	5	5	5	5	5	5
	Insulation	5	5			5	5		5	5		5		5	5		

CODE:

1 - Preliminary Data for Subscale Tests and Design Studies
2 - Data for 5 MW Technology Development Unit
3 - Updated Data for Design Studies
4 - Data for Final Long Duration Subscale Test
5 - Data Base for Design at Increased Scale

TABLE 9 PRIORITY SYSTEM FOR MATERIAL PROPERTY DETERMINATION

TABLE 10

Test Program
For Spinel Castables

Item	Type of Test	Possible Diagnostic Uses	ASTM No.
1.	Sieve analysis	Affects bulk density, strength, dimensional changes after firing. Gross differences may indicate improper cement: aggregate ratio	C 371
2.	Water used to cast (i.e., to attain proper ball-in-hand consistency)	Influenced by amount and quality of cement and, to a lesser extent, by aggregate size distribution. Also influenced by care and skill used to prepare test pieces.	C 860
3.	Linear dimensional change after drying	Relatively insensitive to minor quality variations.	C 134
4.	Bulk density of test bars after drying	Relatively insensitive to minor quality variations.	C 134
5.	Strength after drying (preferrably M.Ø.R.)	Affected by amount and quality of cement in mix and, to lesser extent, aggregate size distribution.	C 133
6.	Linear dimensional change after firing to 2900°F w/5 hour soak	Affected by factors listed under Item 5 plus chemical purity.	C 134
7.	Strength (preferably M.Ø.R.) after firing to 2900°F w/5 hour soak	Same as Item No. 6, but M.Ø.R. test is more sensitive to quality changes	C 133
8.	Chemical analysis (CaO, MgO, Fe_2O_3, SiO_2, and alkalis)	Very important influence on performance at the highest temperature	Various

TABLE 11

COMPARISON OF CALCIUM ALUMINATE BONDED SPINEL CASTABLE (NORTON LS-812), PHOSPHATE BONDED SPINEL CASTABLE (TAYLOR X-13337) AND FUSION CAST SPINEL (CORHART X-317)

Oxide		Method	Norton	Taylor	Corhart
Al_2O_3		Wet	73.9%	65.2%	18.5%
CaO		Wet	3.0	0.9	0.4
Fe_2O_3		Wet	0.1	0.2	0.2
MgO		Wet	22.3	32.0	79.3
P_2O_5		Wet	N.D.	N.D.*	N.D.
SiO_2		Wet	0.40	0.52	0.1
$MgAl_2O_4$	Spinel	XRD	65%	65%	30%
	Corundum	XRD	30%	15	-
MgO	Periclase	XRD	5%	-	55
	Amorphous	XRD	-	-	15

N.D. Below Detection Limits of 0.3% and *0.01%

TABLE 12

ANALYSIS OF MATRIX CORE DEPOSITS FROM HEAT 202

Oxide		Method	Melting Point	Distance from Top of Matrix (m)		
			K	0.4	1.4	4.1
Al_2O_3		Wet	2323	52.2	38.4	17.7
CaO		Wet	2853	1.7	3.1	3.6
Fe_2O_3		Wet	1838	0.9	1.9	1.4
MgO		Wet	3075	36.6	45.6	47.1
SiO_2		Wet	~2000	7.7	10.7	30.0
K_2O		Flame	-	0.02	0.3	0.03
$MgAl_2O_4$	Spinel	XRD	2378	65	55	40
MgO	Periclase	XRD	3075	20	35	40
Mg_2SiO_4	Forsterite	XRD	2163	15	-	5
$CaMgSiO_4$	Montecellite	XRD	1923	-	10	-

TABLE 13

ANALYSIS OF REFRACTORIES AND DEPOSITS FROM TEST VALVE AFTER TESTS 1 AND 2

	Oxide	Method	Valve Body				Sliding Gate (T)				
							Follower		Gate		Follower Ring Throat (Inner Surface)
			Lower Throat Lining (T) (Inner Surface)	Lower Throat Lining (T) (Interior)	Gate Cavity Deposits	Upper Throat Lining (N) (Inner Surface)	Upper Surface	Lower Surface	Upper Surface	Lower Surface	
	Al_2O_3	Wet	30.9	49.2	39.3	43.1	58.5	30.7	61.9	64.1	38.4
	CaO	Wet	5.5	4.2	2.0	4.2	0.8	6.0	0.8	0.8	2.7
	Fe_2O_3	Wet	4.6	5.4	3.3	3.4	0.3	4.1	2.7	0.3	4.6
	MgO	Wet	26.5	11.0	20.9	25.0	37.6*	29.8	32.3*	33.2	33.8
	P_2O_5	Wet	0.3	0.4	0.15	0.4	N.D.	0.4	N.D.	N.D.	0.3
	SiO_2	Wet	23.4	21.9	7.8	15.6	0.7	23.8	0.6	0.6	11.6
	K_2O	Flame	8.9	7.3	15.0	8.0	2.1	5.3	1.7	1.0	5.3
$MgAl_2O_4$	Spinel	XRD	15	35	15	40	70	30	80	80	30
MgO	Periclase	XRD	15	10	30	30	30	5	10	20	7
$KAlSiO_4$	Kalsilite	XRD	20	-	-	15	-	10	-	-	10
Mg_2SiO_4	Forsterite	XRD	-	15	-	-	-	-	-	-	-
$CaMgSiO_4$	Montecellite	XRD	30	15	-	-	-	-	-	-	20
K_2SO_4	Arcanite	XRD	-	-	15	-	-	-	-	-	-

*, By Difference

T, Taylor Spinel

N, Norton Spinel

TABLE 14

WT % POTASSIUM IN EFFLUENT AIR STREAM, MTF - HEAT 203

Time Period	Calculated Avg. from Wt % = $0.25\ e^{-t/4}$	Measured Wt %
0-5 min.	.143%	.148%
0-6 min.	.129%	.123%
4-9 min.	.052%	.048%
7-12 min.	.025%	.026%
6-12 min.	.029%	.029%
0-12 min.	.079%	.050%
0-12 min.	.079%	.053%

TABLE 15

DESCRIPTION OF EXAMPLE DIRECTLY-FIRED HTAH FOR 1000 MW_e PLANT

Item	MHD Gas	Air	Units
Flow in	836 (1844)	683 (1506)	kg/sec (lbm/sec)
Flow Out	849 (1872)	670 (1478)	kg/sec (lbm/sec)
T_{in}	1978 (3100)	919 (1200)	K (F)
T_{out}	1326 (1926)	1788 (2748)	K (F)
P	869 (126)	108 (15.6)	kPa (psi)
ΔP	4.5 (0.65)	17.2 (2.5)	kPa (psid)
Vessels	20	8	Heaters
Flow Duration	2000	800	Seconds
Heat Duty	706 (6.7×10^5)		MW (Btu/sec)
Bed Diamater	4.3 (14)		m (ft)
Bed Height	6.7 (22)		m (ft)
Thermal Stress	25.5 (3700)		MPa (psi)
Hole Size/Web	25/14 (1.0/0.55)		mm (inches)
P/DP Units	2		Vessels
Inlet Valve Diameter	2.2 (86)	0.8 (31)	m (inches)
Outlet Valve Diameter	1.8 (72)	1.1 (42)	m (inches)
Heat Loss	6		Percent

TABLE 16

HTAH Cost Comparisons for
Various Insulation Schemes

HTAH Component	Insulation Scheme: Lowest Risk Brick	Higher Risk Brick	Monolithic	Combined Brick/ Castable	4-Layer Insulation (Ref. 4)
Heater Vessels (Including Matrix)	.44	.35	.31	.39	.42
Manifolds	.31	.14	.09	.16	.25
Support Structure	.08	.05	.05	.07	.06
Other	.17	.16	.16	.17	.17
Total Relative Cst.	1.00	.70	.61	.79	.90

Does not include collector manifold(s) from radiant boiler

TABLE 17

HTAH Cost Comparison for Large and Small Manifold Design, Lowest Risk Brick Insulation

HTAH Component	Large Manifold System	Small Manifold System
Heater Vessels (Including Matrix)	0.44	0.44
Manifolds	0.31	0.23
Support Structure	0.08	0.07
Other	0.17	0.17
Total	1.00	0.91

Does not include collector manifolds(s) from radiant boiler

TABLE 18

CYCLE EVENTS FOR EXAMPLE HTAH - INDIVIDUAL HEATER

Event	Running Time, Sec.	Delta Time, Seconds
"On Air"	0	800
Air Valve Full Open	7	7 /14
Air Valve Starts to Close	800	14
Air Valve Closed	814	-
Depressurization Valve Starts to Open	814	6
Depressurization Valve Full Open	820	61
Depressurization Valve Starts to Close	881	6
Depressurization Valve Full Closed	887	0
Gas Valve Starts to Open	887	13 /26
"On Gas"	900	2000
Gas Valve Full Open	913	13 /22
Gas Valve Starts to Close	2900	26
Gas Valve Full Closed	2926	0
Pressurization Valve Starts to Open	2926	6
Pressurization Valve Full Open	2932	55
Pressurization Valve Starts to Close	2987	6
Pressurization Valve Full Closed	2993	0
Air Valve Starts to Open	2993	7 /14
"On Air" - End of Cycle	3000	0

Table 19

BASIS OF AIR HEATER UNAVAILABILITY DUE TO VALVE FAILURES

(Extracted from Reference 8)

A. Failure Rate Assumptions

- Steel Industry Experience

  Quoted life of blast valves = 1 - 5 years

  Average duty = 6000 cycles/year

  Geometric mean life = $\sqrt{5}$ = 2.2 years or 13,400 cycles

- Separately-Fired Heater Assumptions

  Assumed mean life = 2.2 years = 13,400 cycles

  Expected duty = 8760 (0.75) = 6,570 cycles/operating year

  Mean life m = 13400/6570 = 2.0 operating years

  λ_V = 1/m = 0.5 failure/year

  Module failure rate = $6\lambda_V$ = 3.0/years

  Range = 1 - 5 year^{-1}

- Direct-Fired Heater Assumptions

  Assumed "environmental severity factor" (reduction in life) = 2

  Mean valve life m = 1.0 operating years

  λ_V = 1.0/year failures/year

  Module failure rate = $6\lambda_V$ = 6.0 failures/year

  Range = 2 - 10 year^{-1}

TABLE 20

ESTIMATED VALVE FAILURE RATES FOR SEPARATELY-FIRED HTAH

VALVE	FAILURE RATE, YR^{-1} REF 5	CURRENT
Gas Inlet	.5	.22
Air Outlet	.5	.11
Gas Outlet	.5	.11
Depressurization	.5	.11
Air Inlet	.5	.07
Pressurization	.5	.07
Total For 1 Heater	$\lambda = 3\ yr^{-1}$	$\lambda = 0.69\ yr^{-1}$

TABLE 21

DETAIL OF EVENTS FOR EXAMPLE HTAH - 15 HTR GROUP (1/2 FLOW)

Event	Number of Heaters On Air	Number of Heaters On Gas	Time, sec.	
Air Valve starts to open - HTR A	4.0	10.0	-7.0	Start of Air Valve Overlap
Air Valve 1/4 Open - HTR A	4.25	10.0	-3.5	
HTR A Air Valve 1/2 Open				End of Press/Valving Sequence - HTR A
HTR B Air Valve starts to Close	4.5	10.0	0.0	Start of Depress/Valving Sequence - HTR B
HTR A Air Valve 3/4 Open				
HTR B Air Valve 1/4 Closed	4.5	10.0	3.5	
HTR A Air Valve Full Open				
HTR B Air Valve 1/2 Closed	4.5	10.0	7.0	
HTR B Air Valve 3/4 Closed	4.25	10.0	10.5	
HTR B Air Valve Full Closed	4.0	10.0	14.0	End of Air Valve Overlap
HTR B Depress. Valve Opens	4.0	10.0	14.0	
HTR B Depress. Valve Full Open	4.0	10.0	20.0	Start of HTR B Depress.
HTR B Depress. Valve Closes	4.0	10.0	81.0	End of HTR B Depress.
HTR B Depress. Valve Closed	4.0	10.0	87.0	
HTR B Gas Valve Opens	4.0	10.0	87.0	Start of Gas Valve Overlap
HTR B Gas Valve 1/4 Open	4.0	10.25	93.5	
HTR C Gas Valve Closes				Start of Press/Valving Sequence - HTR C
HTR B Gas Valve 1/2 Open	4.0	10.50	100.0	End of Depress/Valving Sequence - HTR B
HTR C Gas Valve 1/4 Closed				
HTR B Gas Valve 3/4 Open	4.0	10.50	106.5	

TABLE 21 (Continued)

DETAIL OF EVENTS FOR EXAMPLE HTAH - 15 HTR GROUP (1/2 FLOW)

Event	Number of Heaters On Air	Number of Heaters On Gas	Time, sec.	
HTR C Gas Valve 1/2 Closed				
HTR B Gas Valve Full Open	4.0	10.4	113.0	
HTR C Gas Valve 3/4 Closed	4.0	10.25	119.5	
HTR C Gas Valve Full Closed	4.0	10.0	126.0	End of Gas Valve Overlap
HTR C Press. Valve Opens	4.0	10.0	126.0	
HTR C Press. Valve Full Open	4.0	10.0	132.0	Start of HTR C Press.
HTR C Press. Valve Closes	4.0	10.0	187.0	End of HTR C Press.
HTR C Press. Valve Closed	4.0	10.0	193.0	
HTR C Air Valve Opens	4.0	10.0	193.0	Start of Air Valve Overlap
HTR C Air Valve 1/4 Open	4.25	10.0	196.5	
HTR D Air Valve Closes				Start of Depress/Valving Sequence - HTR D
HTR C Air Valve 1/2 Open	4.5	10.0	200.0	End of Press/Valving Sequence - HTR C
HTR D Air Valve 1/4 Closed				
HTR C Air Valve 3/4 Open	4.5	10.0	203.5	
HTR D Air Valve 1/2 Closed				
HTR C Air Valve Closes	4.5	10.0	207.0	
HTR D Air Valve 3/4 Closed	4.25	10.0	210.5	
HTR D Air Valve Closed	4.0	10.0	214	End of Gas Valve Overlap

(Sequence repeats through 15 heaters.)

TABLE 22

SUMMARY OF TOTAL CYCLE FOR 30 HTR CONFIGURATION - EXAMPLE HTAH FOR 1000 MW_e PLANT

Time, Sec	Number of Heaters on Air	Number of Heaters on Gas
0.0	8.5	20.5
3.5	8.5	20.5
6.5	8.5	20.5
7.0	8.5	20.5
10.5	8.25	20.5
13.0		20.5
14.0	8.0	
19.5	8.0	20.25
20.0	8.0	
26	8.0	20.0
32	8.0	20.0
81	8.0	20.0
87	8.0	20.0
93.0	8.0	
93.5		20.25
96.5	8.25	
100.0	8.5	20.5

TABLE 23

Outlet Fluid Temperature Variation and Maximum Bottom of Matrix Solid Temperatures from SCAMP Computer Code Runs

	Total Variation in Outlet Air Temperature K (F)	Total Variation in Outlet Gas Temperature K (F)	Range of Individual Heater Maximum Bottom of Matrix Solid Temperature * K (F)
Large Manifolds	24 (44)	16 (29)	1336-1393 (1944-2047)
Small Manifolds	50 (90)	31 (56)	1279-1446 (1843-2143)
Small Manifolds with control by Air/Gas Phase Duration	51 (92)	21 (38)	1379-1451 (2023-2152)

*Maximum Bottom of Matrix Temperature of at least 1400 K (2060 F) is desired for each individual heater to promote effective seed/slag drainage

TABLE 24 MAJOR FACILITY PIPING

		Equivalent O.D., m (ft)	Cross-Sectional Shape	Max. Operating Pressure, kPa (psia)
Mains	Gas-In	15.2 (50)	Double Arch	110 (16)
	Gas-Out	12.2 (40)	Double Arch	110 (16)
	Air-In	1.5-3 (5-10)	Round	869 (126)
	Air-Out	2.6-4.6 (8.5-16)	Round/Catenary	869 (126)
Manifolds	Gas-In	4.6-7.6 (15-25)	Catenary	110 (16)
	Gas-Out	3.0-5.8 (10-19)	Catenary	110 (16)
	Air-In	1.5-2.0 (5-6.5)	Round	869 (126)
	Air-Out	2.6-3.2 (8.5-10.5)	Round	869 (126)
Ducts	Gas-In	3.5 (11.5)	Round	110 (16)
	Gas-Out	2.3 (7.5)	Round	110 (16)
	Air-In	1.1 (3.5)	Round	869 (126)
	Air-Out	2.1 (7)	Round	869 (126)

TABLE 25. EXPANSION JOINT REQUIREMENTS

		No. Req'd	Location	Type	Axial Movement* mm (in)	Lateral Movement* mm (in)
Main	Gas-In	2	Between Heater Rows	Flexspan-Series 500 (12 in. face-to-face)	89 (3.5)	64 (2.5)
Main	Gas-Out	2	Between Heater Rows	Flexspan-Series 500 (12 in. face-to-face)	89 (3.5)	64 (2.5)
Duct	Gas-Out	30	Between Valve & Gas-Out Manifold	Metal (12 Convolutions)	136.4 (5.37)	10.7 (0.42)
Duct	Air-In	30	Between Valve & Air-In Manifold	Metal (16 Convolutions)	72.1 (2.84)	8.1 (0.32)

* Expansion Joint Limit

TABLE 26

Comparison of Alternative Heater Concepts
for 600 MW_e Plant

	Reference HTAH		ITAH		Upflow HTAH 1		Upflow HTAH 2		Units	
Reheat Gas Flow	504	(1112)	504	(1112)	504	(1112)	504	(1112)	kg/sec	(lbm/sec)
Air/Oxidizer Flow	408	(900)	408	(900)	408	(900)	408	(900)	kg/sec	(lbm/sec)
Gas Inlet Temp	1972	(3089)	1289	(1860)	1700	(2600)	1589	(2400)	K	(F)
Gas Outlet Temp	1349	(1969)	840	(1053)	1034	(1401)	992	(1327)	K	(F)
Air/Oxidizer Inlet Temp	922	(1200)	589	(600)	589	(600)	589	(600)	K	(F)
Air/Oxidizer Outlet Temp	1788	(2758)	1200	(1700)	1508	(2255)	1411	(2080)	K	(F)
Total Number of Heaters	16		6		16		16			
Heaters on Gas	11		4		11		11			
Heaters on Air/Oxidizer	4		1		4		4			
Heat Duty	422	(1442)	279	(953)	431	(1473)	383	(1307)	MW	(10^6 Btu/hr)
Bed Diameter	4.4	(14.6)	7.5	(24.5)	4.3	(14.0)	4.2	(13.8)	m	(ft)
Bed Height	6.5	(21.4)	8.1	(26.7)	6.8	(22.2)	6.8	(22.2)	m	(ft)

TABLE 27

RELATIVE COSTS OF ALTERNATIVE HEATER CONCEPTS FOR 600 MW_e PLANT

	Reference HTAH	ITAH	Upflow HTAH 1	Upflow HTAH 2
Heater Vessels (Including Matrix)	0.45	0.14	0.38	0.37
Manifolds	0.26	0.06	0.14	0.10
Support Structure	0.07	0.04	0.16	0.16
Valves	0.17	0.06	0.05	0.05
Other	0.05	0.03	0.04	0.04
Total Relative Cost	1.00	0.33	0.78	0.72

TABLE 28

Comparison of Reference HTAH and
Integrated ITAH/HTAH for 600 MW_e Plant

Item	Reference HTAH	Integrated ITAH/HTAH: ITAH Section	Integrated ITAH/HTAH: HTAH Section	Units
Reheat Gas Flow	504 (1112)	400 (882)	365 (805)	kg/sec (lbm/sec)
Air Flow	408 (900)	408 (900)	408 (900)	kg/sec (lbm/sec)
Gas Inlet Temperature	1972 (3089)	1366 (1998)	1978 (3100)	K (F)
Gas Outlet Temperature	1349 (1969)	734 (862)	1366 (1998)	K (F)
Air Inlet Temperature	922 (1200)	589 (600)	1172 (1650)	K (F)
Air Outlet Temperature	1788 (2758)	1172 (1650)	1778 (2740)	K (F)
Total Number of Heaters	16	5	15	
Bed Diameter	4.4 (14.6)	8.1 (26.6)	4.4 (14.3)	m (ft)
Bed Height	6.5 (21.4)	10.4 (34.0)	7.7 (25.4)	m (ft)
Relative Cost of Heater Vessels (Including Matrix)	1.0	1.19	0.38	
		(1.57 for Integrated System)		

TABLE 29

Valves Required for Integrated
ITAH/HTAH System for 600 MW_e Plant

Type of Valve	ITAH Only			HTAH Only			Integrated ITAH/HTAH		
	No.	Temperature		No.	Temperature		No.	Temperature	
		K	(F)		K	(F)		K	(F)
Gas Inlet	15	1978	(3100)	5	1283	(1850)	15	1978	(3100)
Gas Outlet	15	1367	(2000)	5	733	(860)	5	733	(860)
Air Inlet	15	1172	(1650)	5	589	(600)	5	589	(600)
Air Outlet	15	1778	(2740)	5	1172	(1650)	5	1778	(2740)
Pressurization	15	1172	(1650)	5	589	(600)	5	589	(600)
Depressurization	15	1172	(1650)	5	589	(600)	5	589	(600)
TOTAL	90			30			40		

TABLE 30

Electrical Conductivity of Air Stream with Various Levels of Potassium Contamination

Air Stream Temperature	wt % K			
	0.001%	0.01%	0.1%	1.0%
1550 K	$\mu_e = .146$ $n_e = 7.88 \times 10^{14}$ $\sigma = 1.84 \times 10^{-5}$	$\mu_e = .146$ $n_e = 2.43 \times 10^{15}$ $\sigma = 5.68 \times 10^{-5}$	$\mu_e = .138$ $n_e = 7.78 \times 10^{15}$ $\sigma = 1.72 \times 10^{4}$	$\mu_e = .104$ $n_e = 2.91 \times 10^{16}$ $\sigma = 4.85 \times 10^{-4}$
1700 K	$\mu_e = .151$ $n_e = 5.62 \times 10^{15}$ $\sigma = 1.36 \times 10^{-4}$	$\mu_e = .150$ $n_e = 1.76 \times 10^{16}$ $\sigma = 4.24 \times 10^{-4}$	$\mu_e = .145$ $n_e = 5.65 \times 10^{16}$ $\sigma = 1.31 \times 10^{-3}$	$\mu_e = .111$ $n_e = 2.13 \times 10^{17}$ $\sigma = 3.79 \times 10^{-3}$
1850 K	$\mu_e = .156$ $n_e = 3.14 \times 10^{16}$ $\sigma = 7.84 \times 10^{-4}$	$\mu_e = .155$ $n_e = 9.90 \times 10^{16}$ $\sigma = 2.46 \times 10^{-3}$	$\mu_e = .152$ $n_e = 3.17 \times 10^{17}$ $\sigma = 7.72 \times 10^{-3}$	$\mu_e = .117$ $n_e = 1.19 \times 10^{18}$ $\sigma = 2.22 \times 10^{-2}$
2000 K	$\mu_e = .162$ $n_e = 1.40 \times 10^{17}$ $\sigma = 3.64 \times 10^{-3}$	$\mu_e = .161$ $n_e = 4.43 \times 10^{17}$ $\sigma = 1.14 \times 10^{-2}$	$\mu_e = .156$ $n_e = 1.42 \times 10^{18}$ $\sigma = 3.54 \times 10^{-2}$	$\mu_e = .123$ $n_e = 5.22 \times 10^{18}$ $\sigma = 1.03 \times 10^{-1}$

Stream Saturated with K_2SO_4

Pressure = 10 atm

	1550 K	1700 K	1850 K	2000 K
Max. wt % K in gas:	0.0078%	0.050%	0.23%	0.77%

Interpolated values for maximum σ at each temperature:

	1550 K	1700 K	1850 K	2000 K
Max. σ =	5.03×10^{-5}	9.33×10^{-4}	1.13×10^{-2}	9.12×10^{-2}

NOTE: Electrical mobility μ_e in m^2/weber
Number density n_e in m^{-3}
Electrical conductivity σ in mho/m

FIGURES

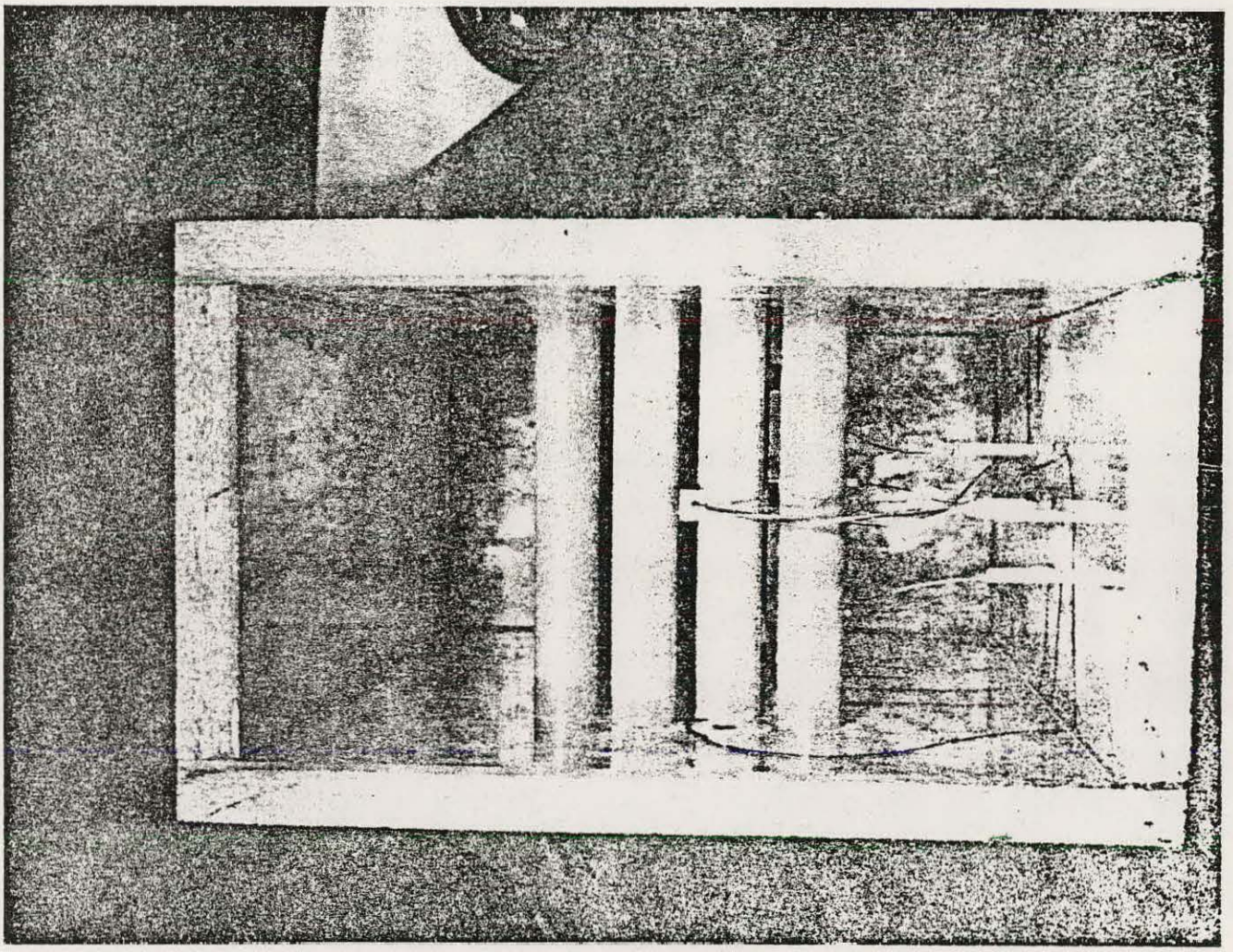

FIGURE 1 MOLD FOR CASTING MATRIX SUPPORT FOR MTF

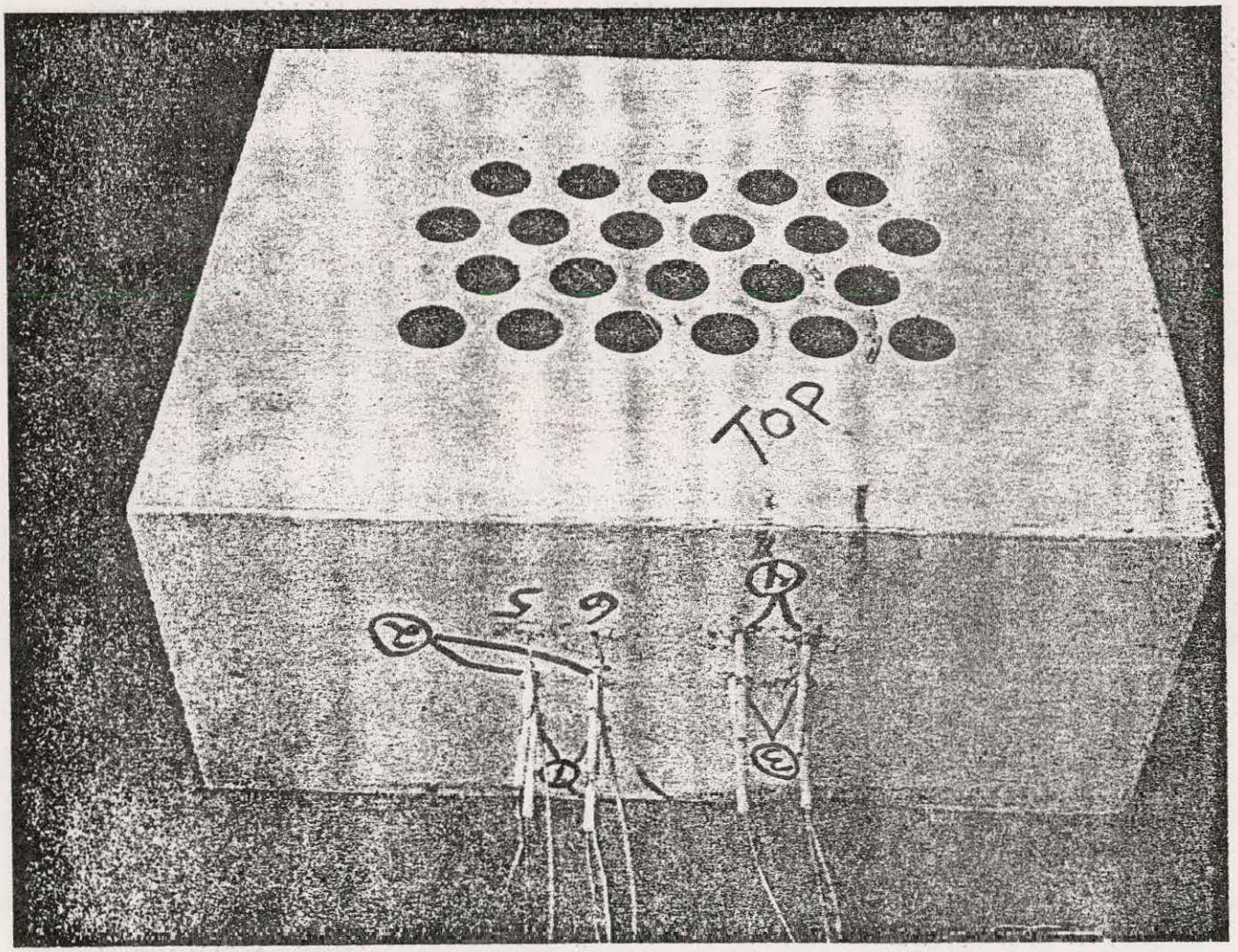

FIGURE 2 CASTABLE SPINEL MATRIX SUPPORT BRICK FOR MTF

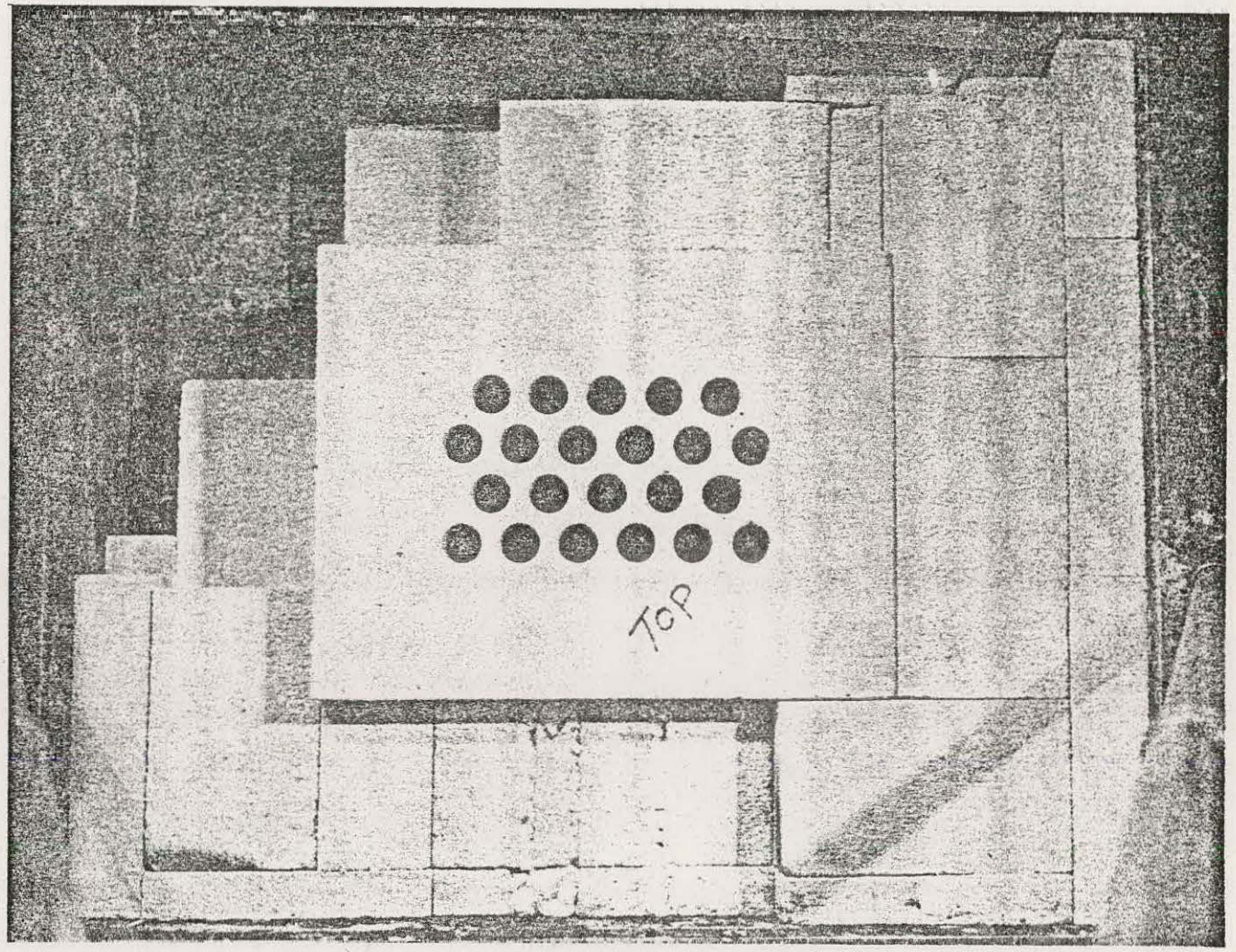

FIGURE 3 MATRIX SUPPORT BRICK BEING INSTALLED IN MTF

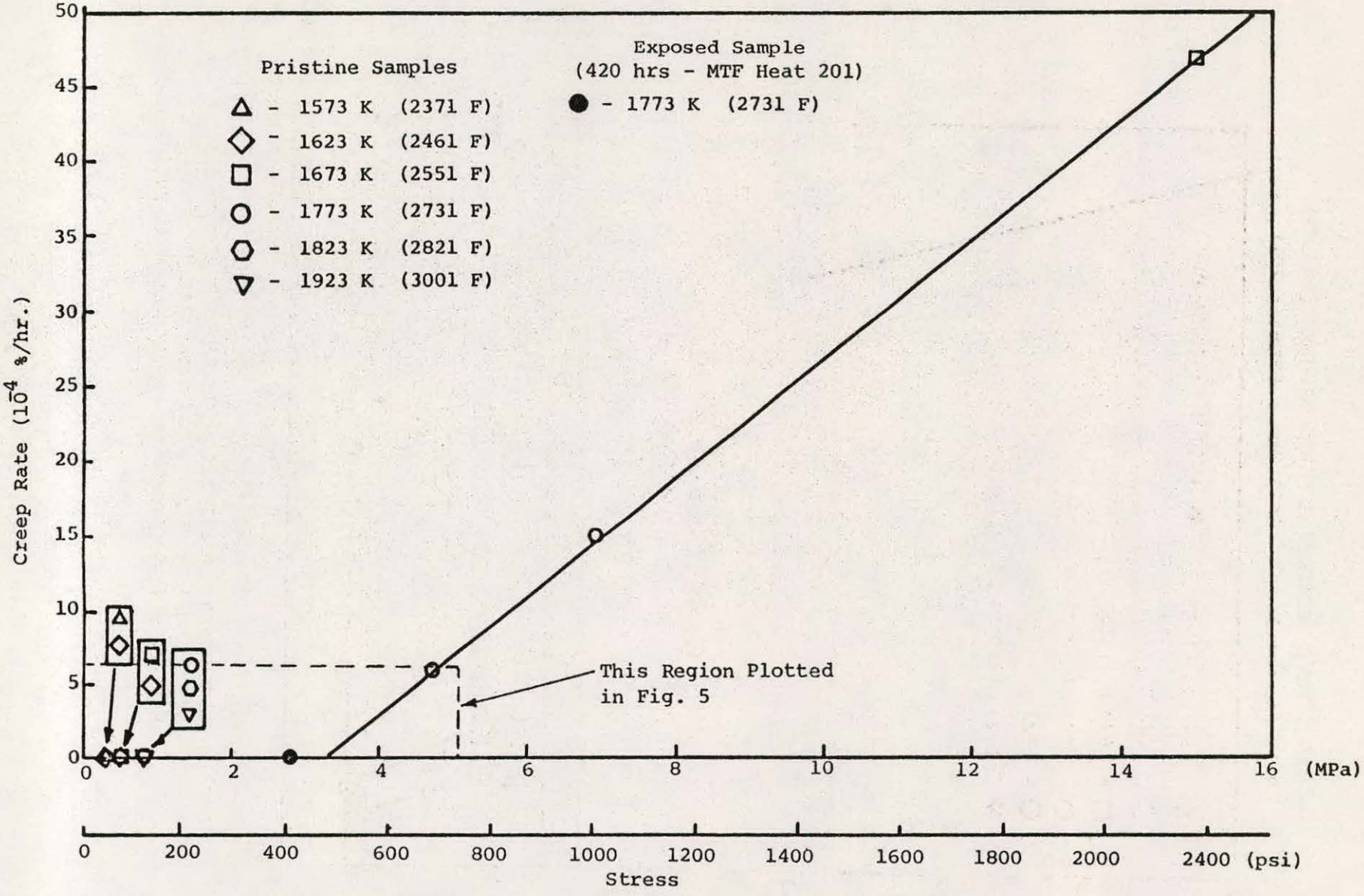

FIGURE 4. STEADY STATE CREEP RATE OF CORHART X-317
(DATA FROM MONTANA TECH MEASUREMENTS)

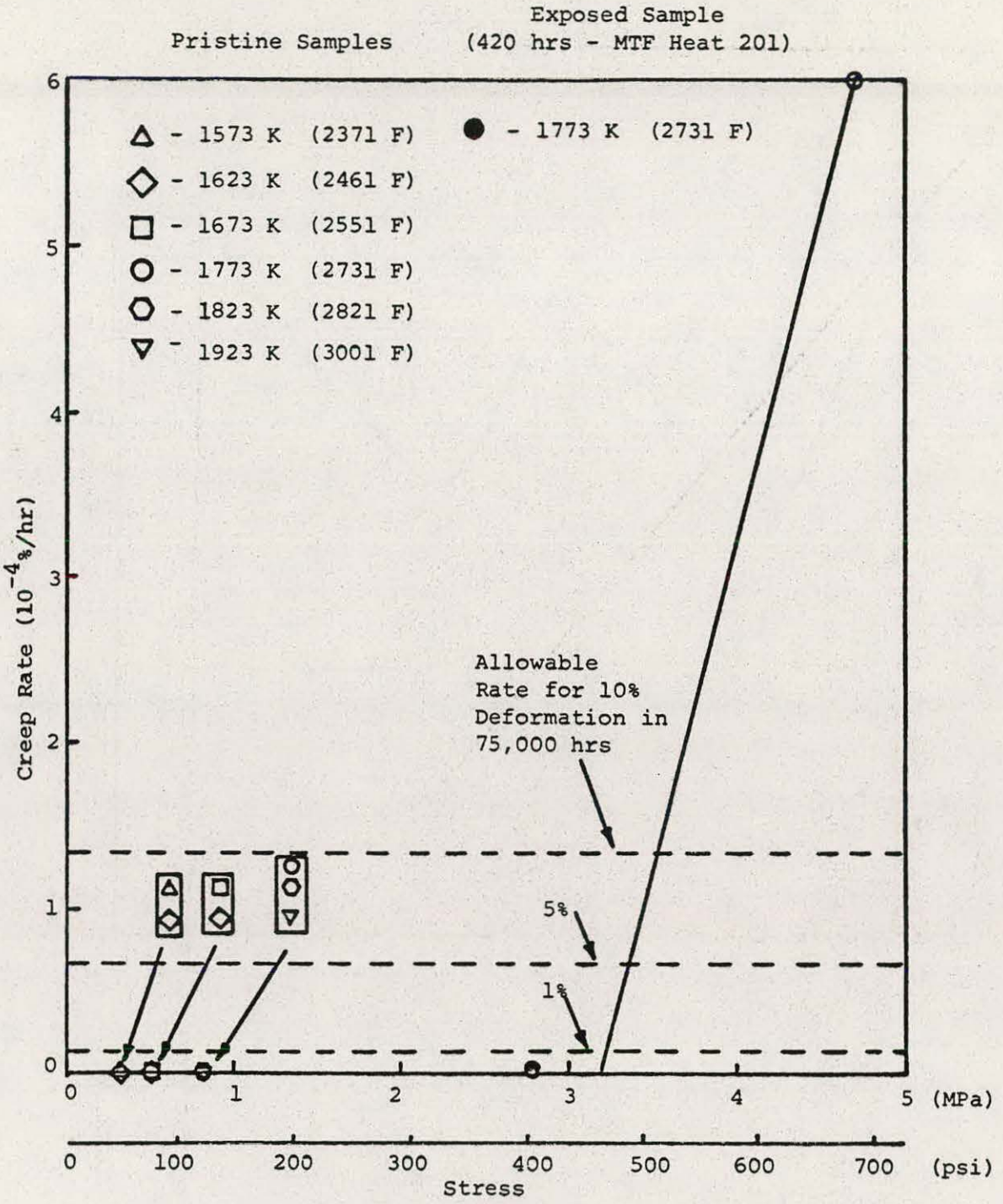

FIGURE 5. STEADY STATE CREEP RATE OF CORHART X-317 COMPARED WITH ALLOWABLE CREEP RATES OVER LIFE OF HTAH MATERIALS (DATA FROM MONTANA TECH MEASUREMENTS)

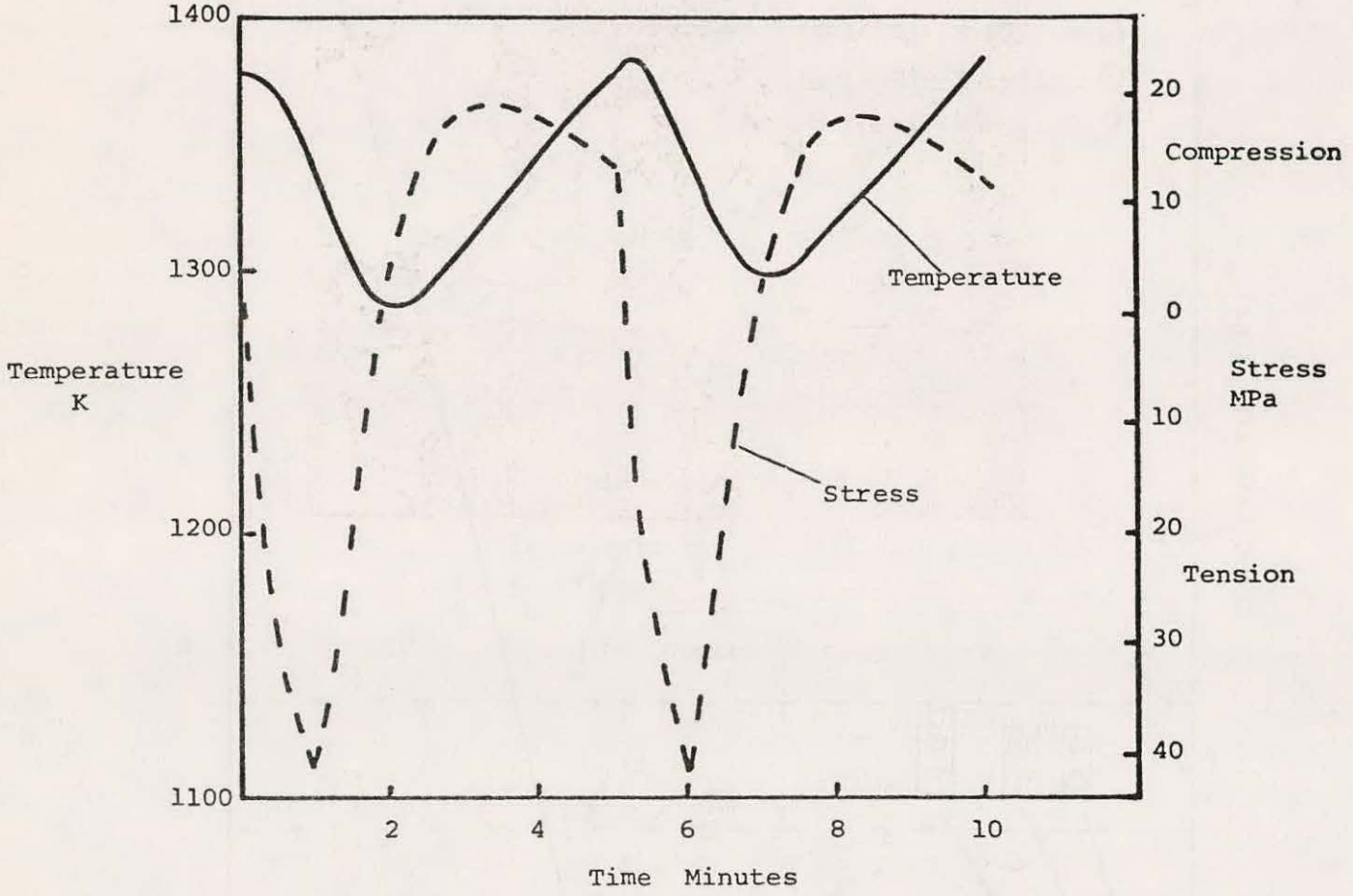

FIGURE 6. CYCLIC TEMPERATURE AND STRESS FOR THERMAL STRESS CYCLING EXPERIMENT

Figure 7.
Unreacted interior of LS812 - 72X

Figure 8.

Hot face of LS812 from Valve Test 3

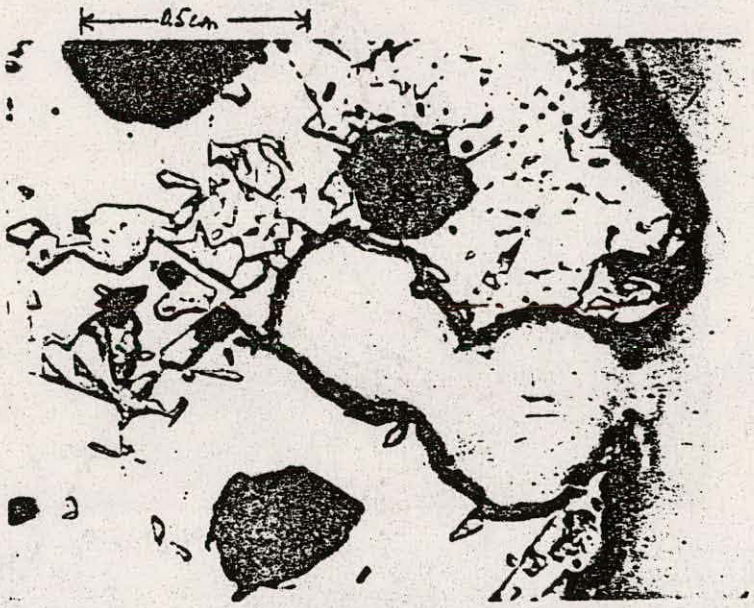

Figure 9

Hot face of LS812 from Valve Test 3
Showing Penetration Solution or Refractory

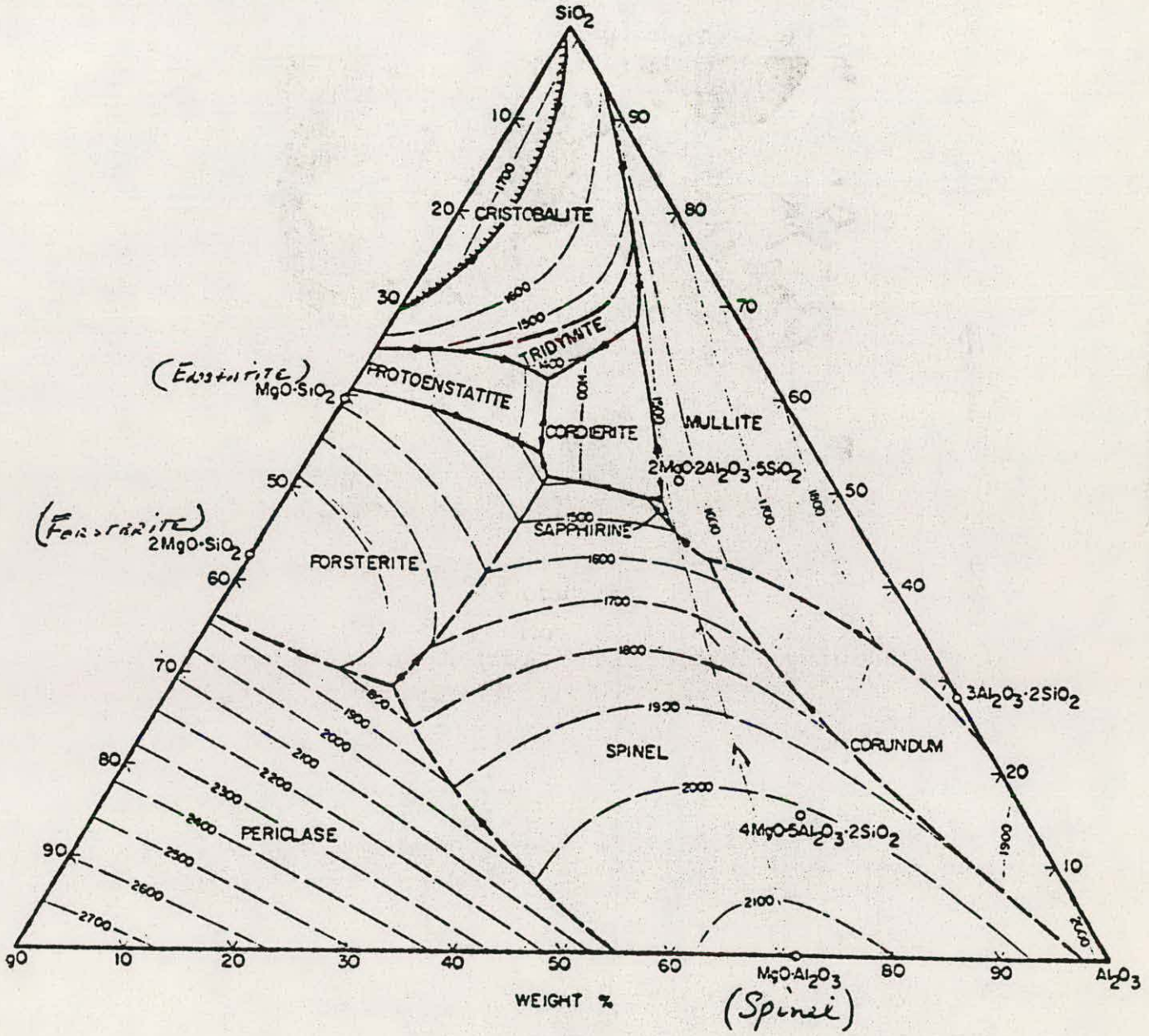

Figure 10. Phase Diagram for the System MgO-Al2O3-SiO2

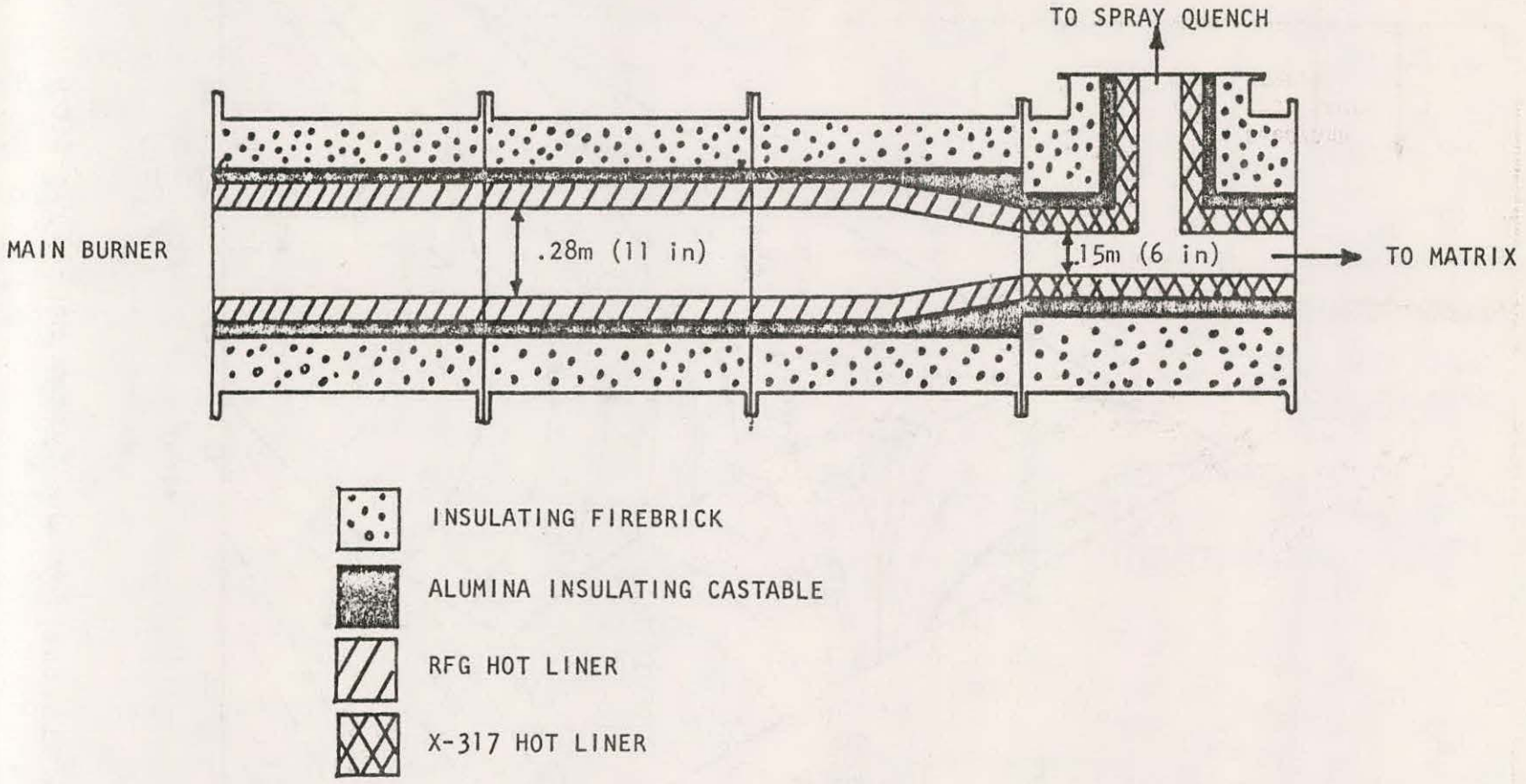

FIGURE 11. MTF HOT GAS SUPPLY DUCT CONFIGURATION

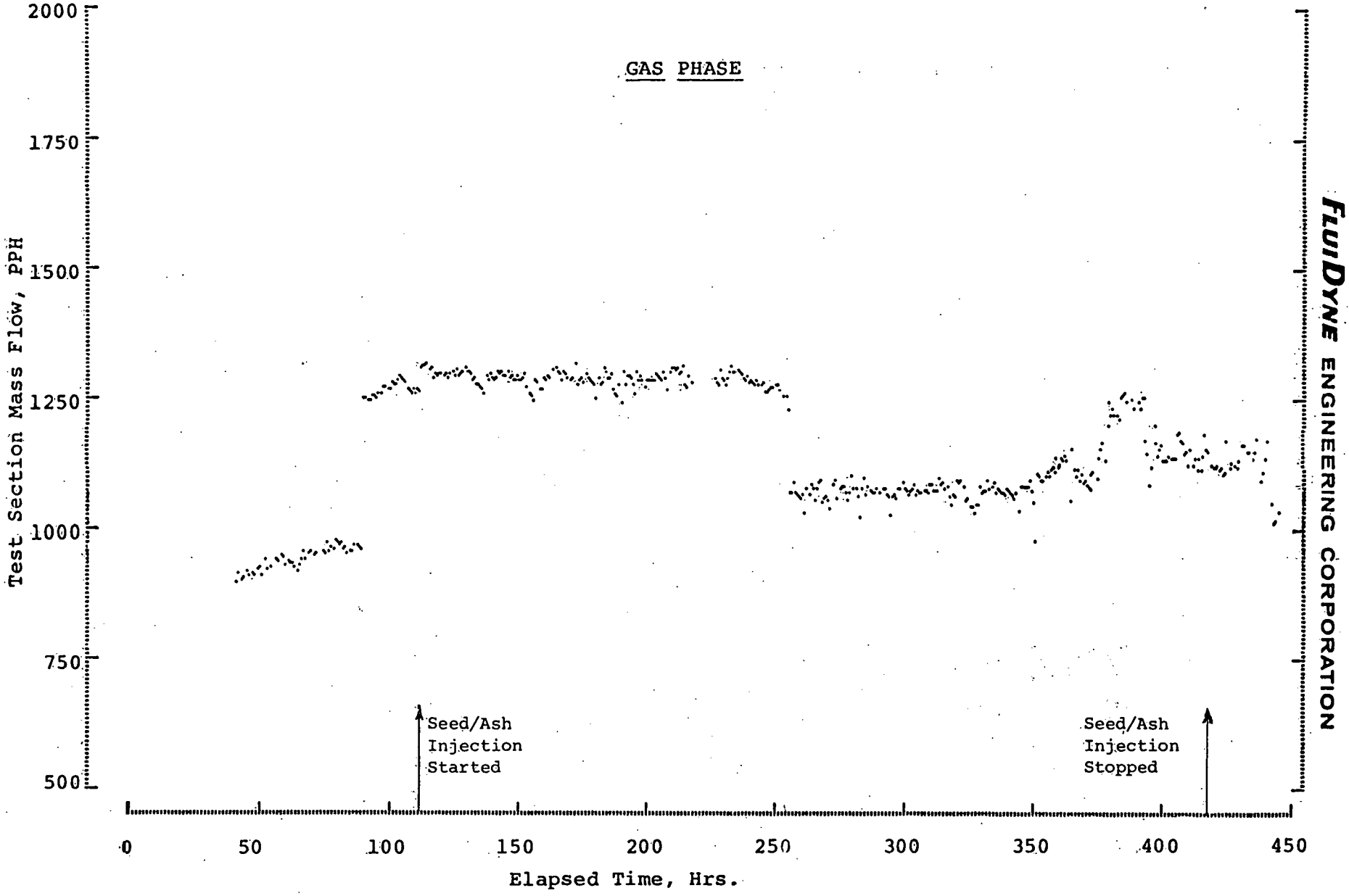

FIGURE 12. MASS FLOW THROUGH MTF CORED BRICK MATRIX ON GAS PHASE - HEAT 203

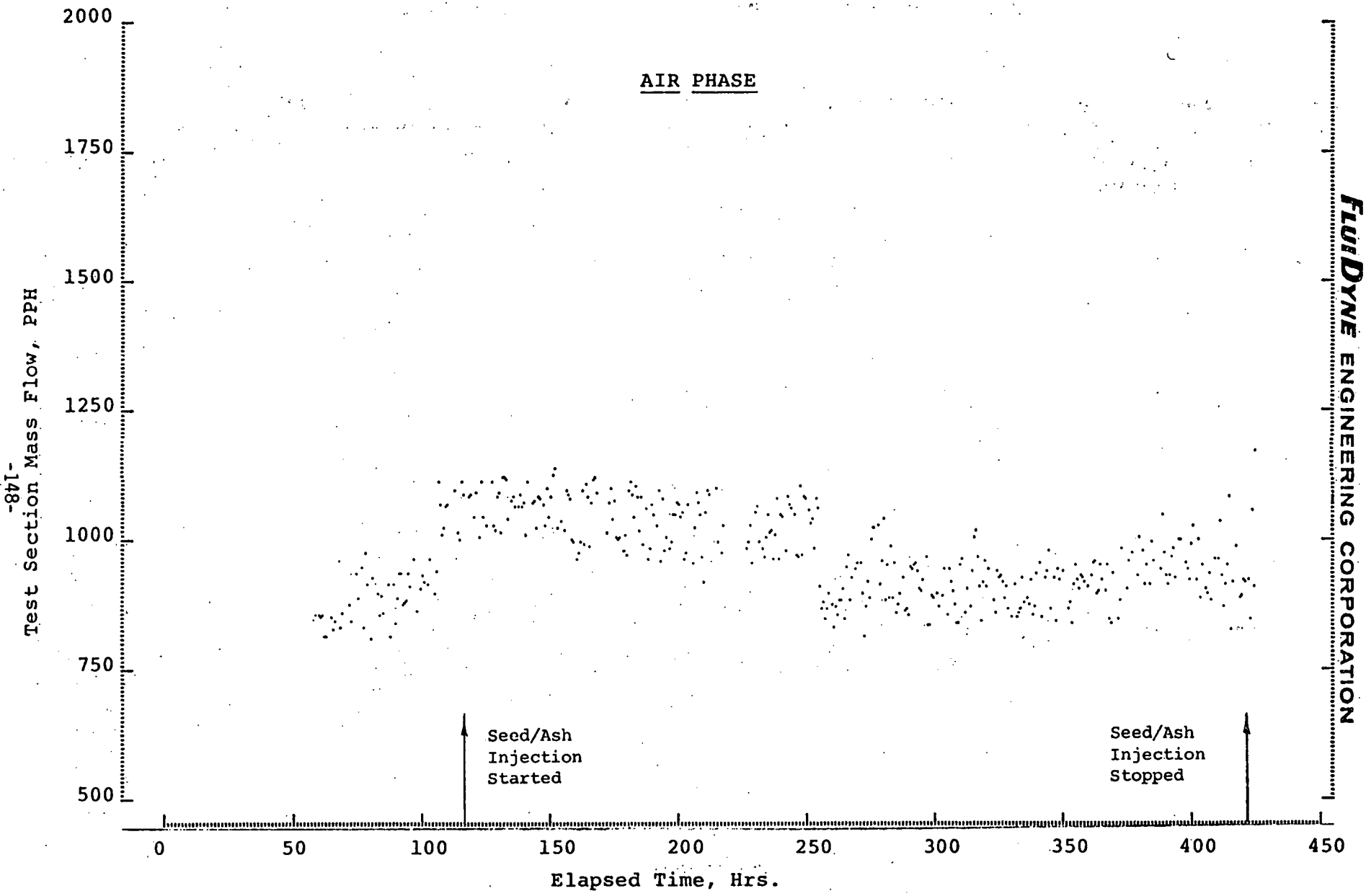

FIGURE 13. MASS FLOW THROUGH MTF CORED BRICK MATRIX ON AIR PHASE - HEAT 203

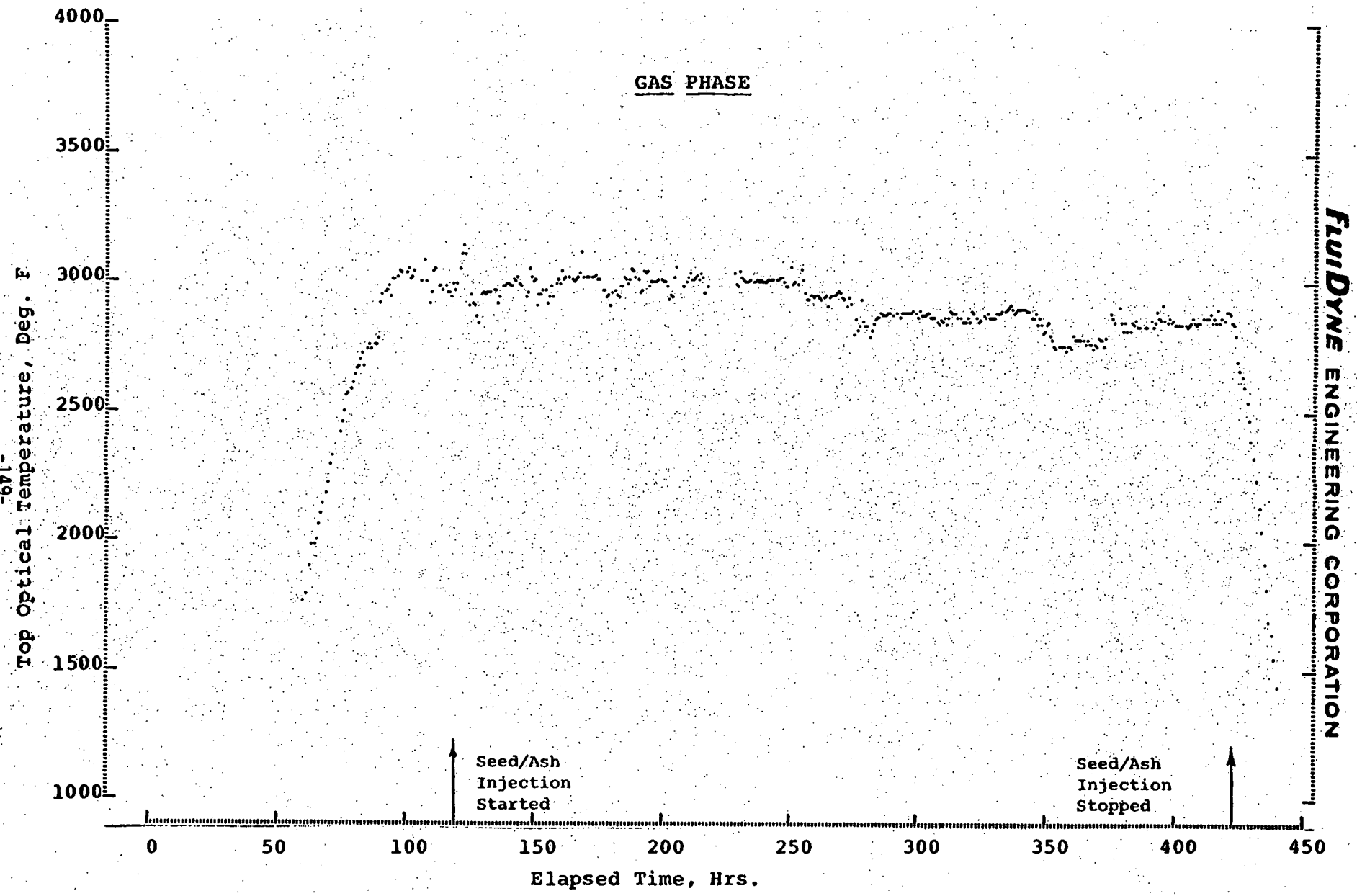

FIGURE 14. TOP OF MATRIX SOLID TEMPERATURE AT END OF GAS PHASE - HEAT 203

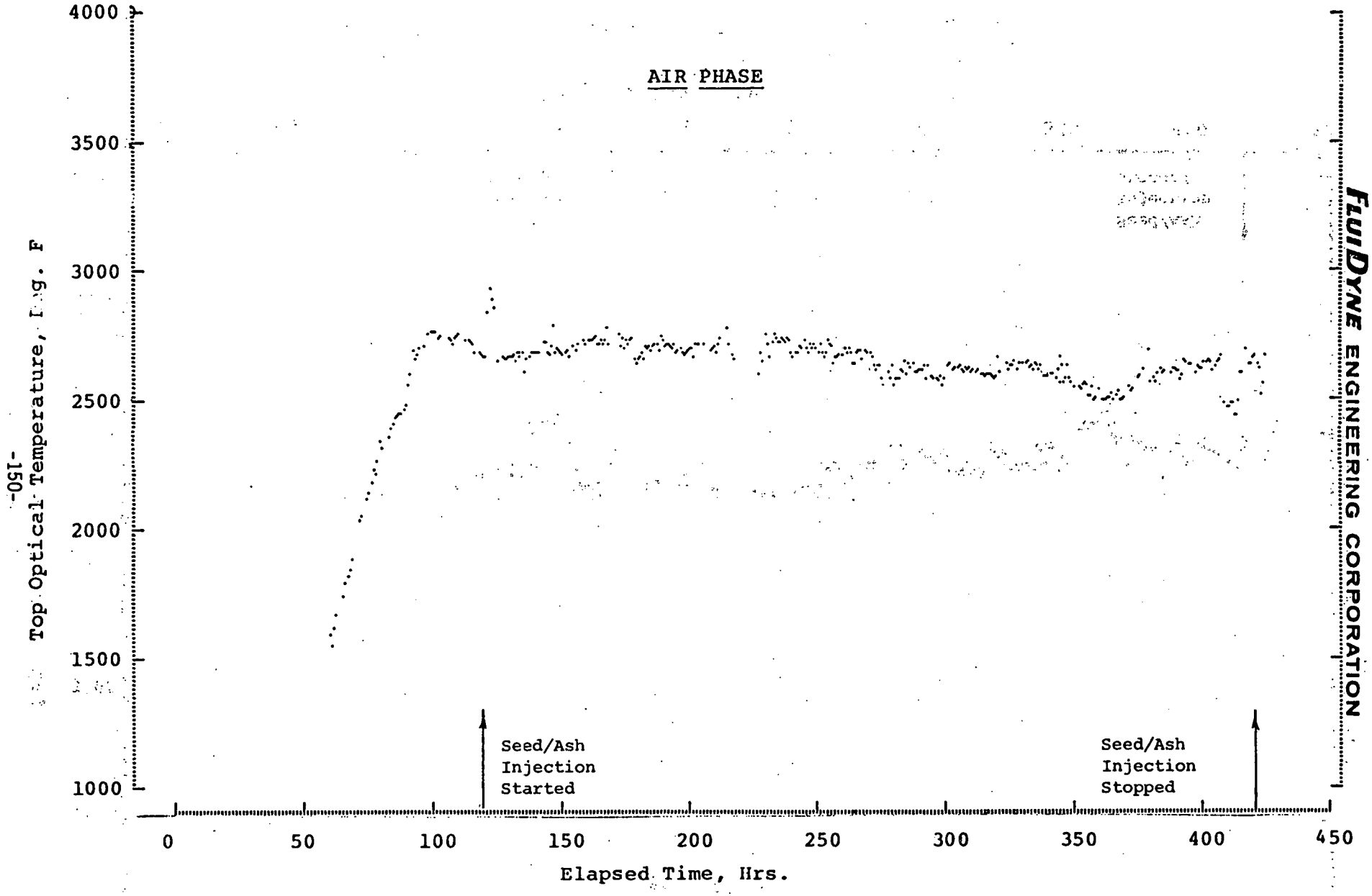

FIGURE 15. TOP OF MATRIX SOLID TEMPERATURE AT END OF AIR PHASE - HEAT 203

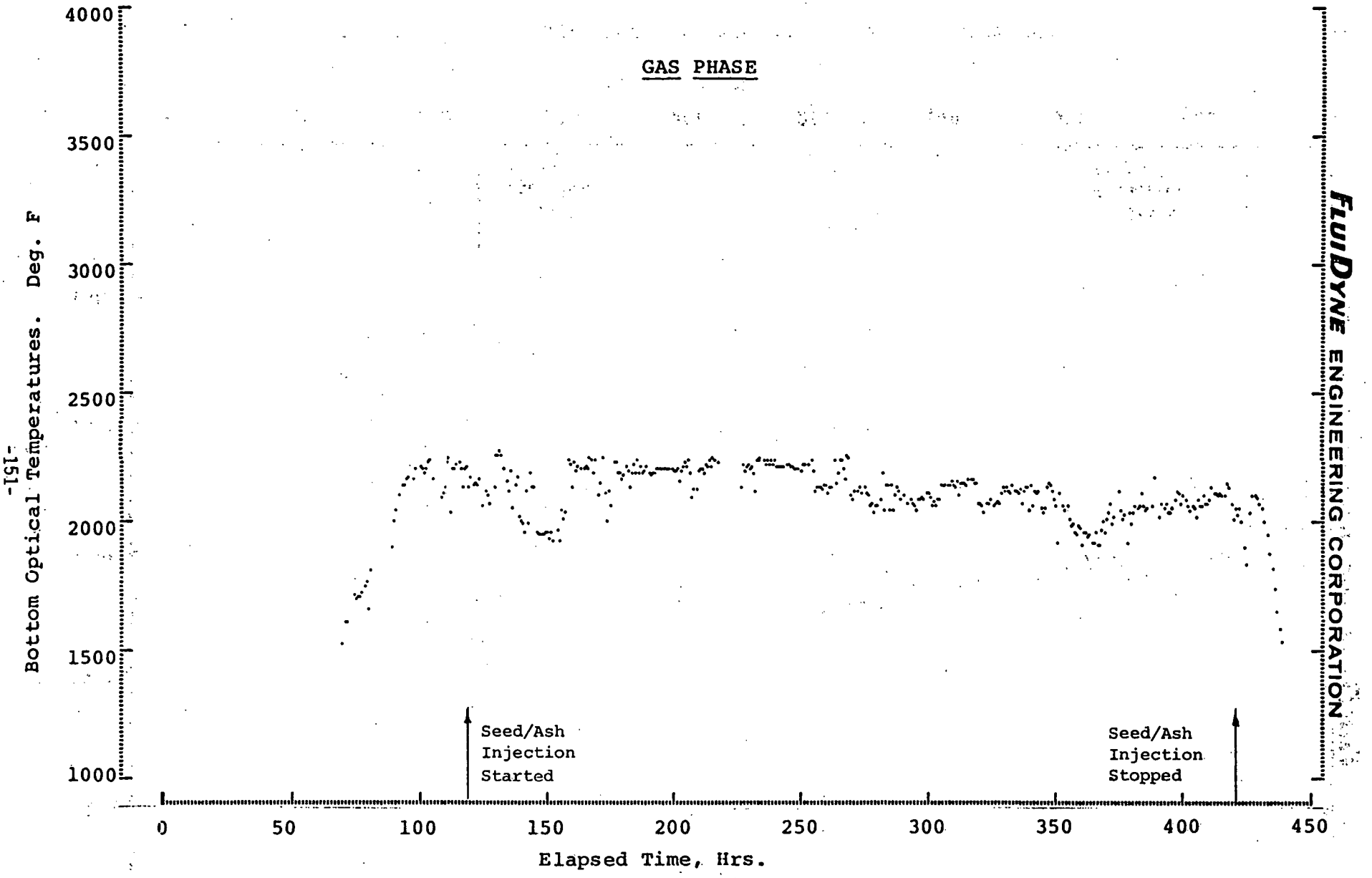

FIGURE 16. BOTTOM OF MATRIX SOLID TEMPERATURE AT END OF GAS PHASE - HEAT 203

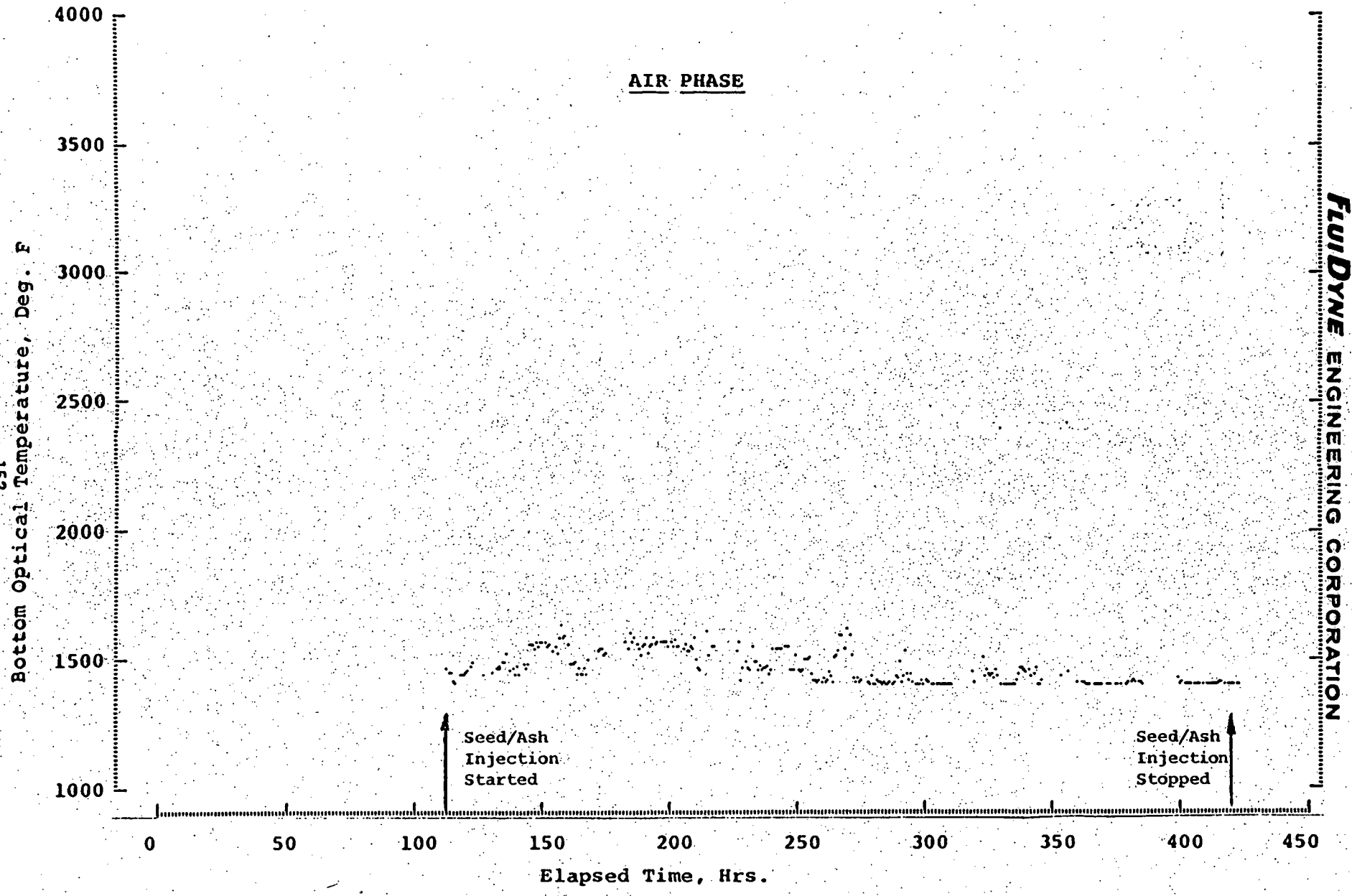

FIGURE 17. BOTTOM OF MATRIX SOLID TEMPERATURE AT END OF AIR PHASE - HEAT 203

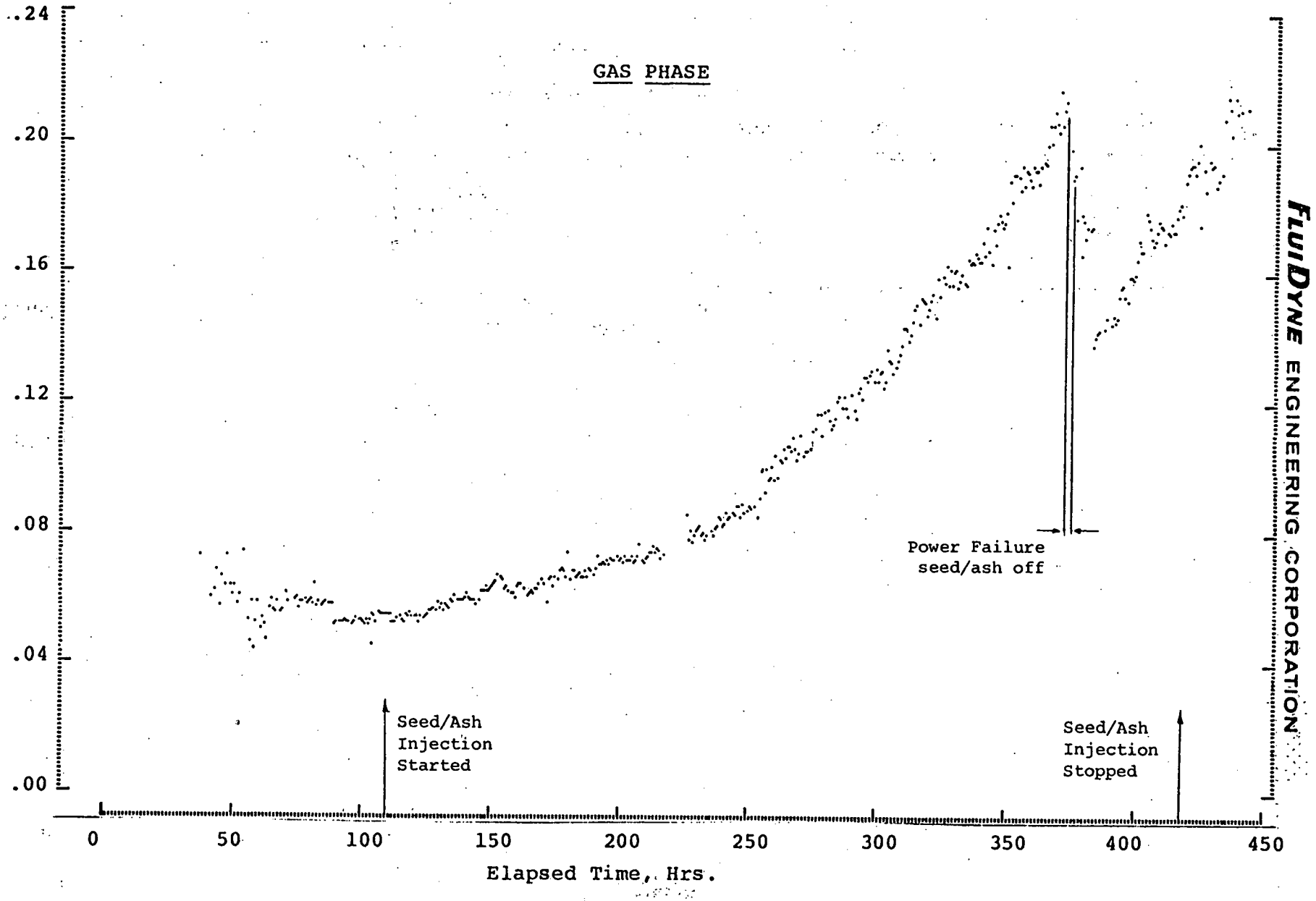

FIGURE 18. MATRIX FRICTION FACTOR AT END OF GAS PHASE - HEAT 203

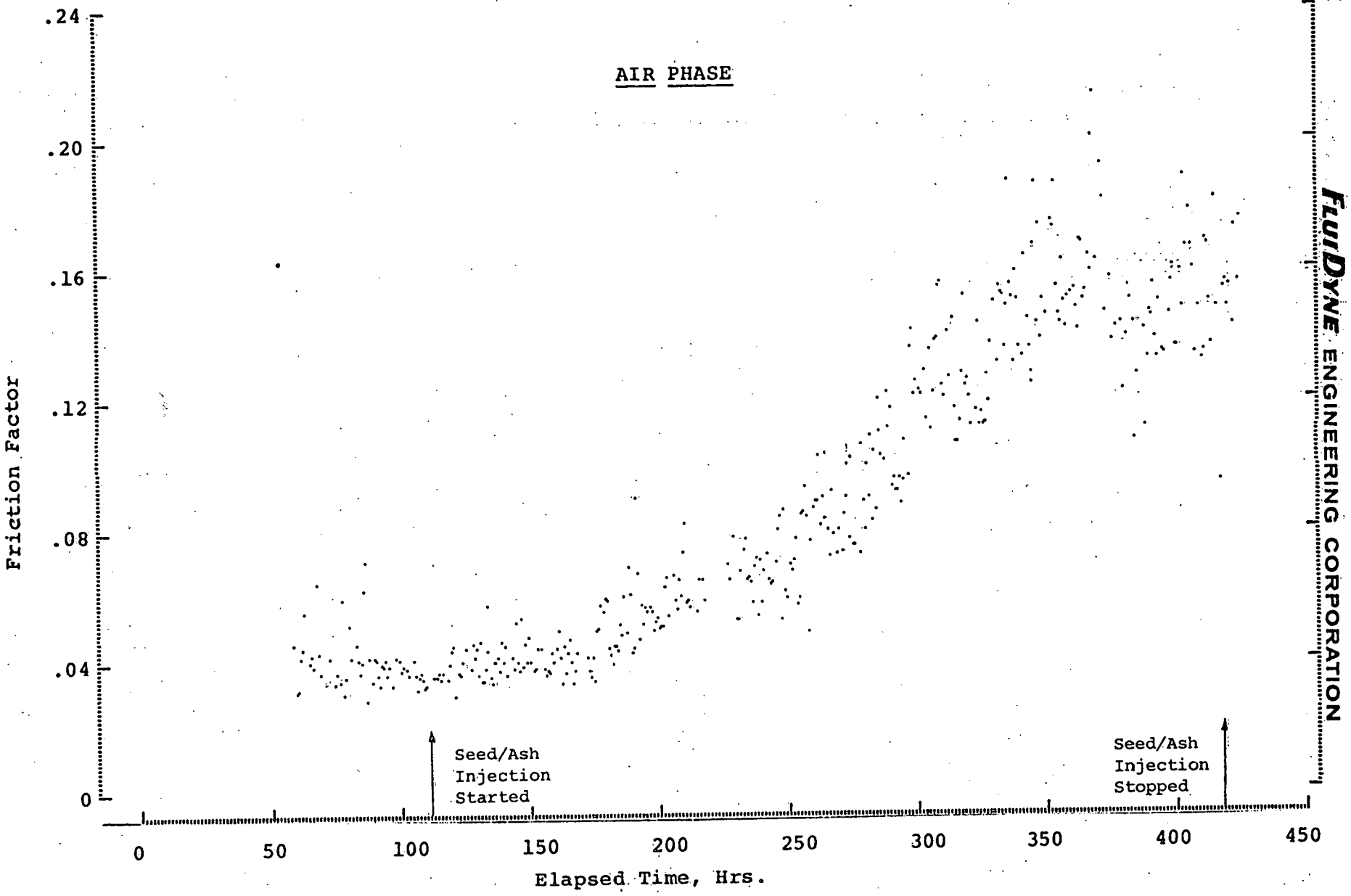

FIGURE 19. MATRIX FRICTION FACTOR AT END OF AIR PHASE - HEAT 203

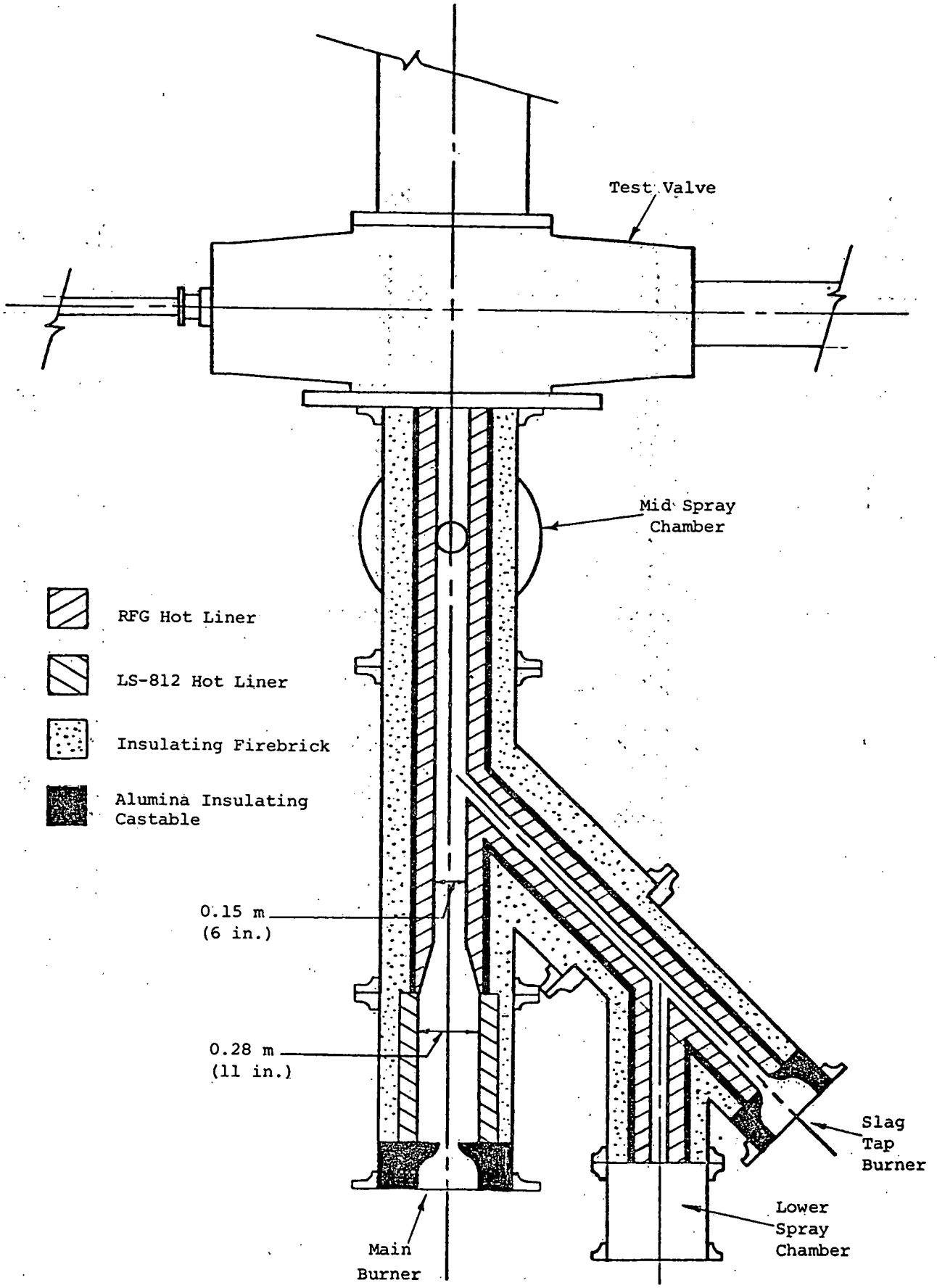

FIGURE 20. CONFIGURATION OF LOWER SECTIONS OF VTF FOR TEST 3A

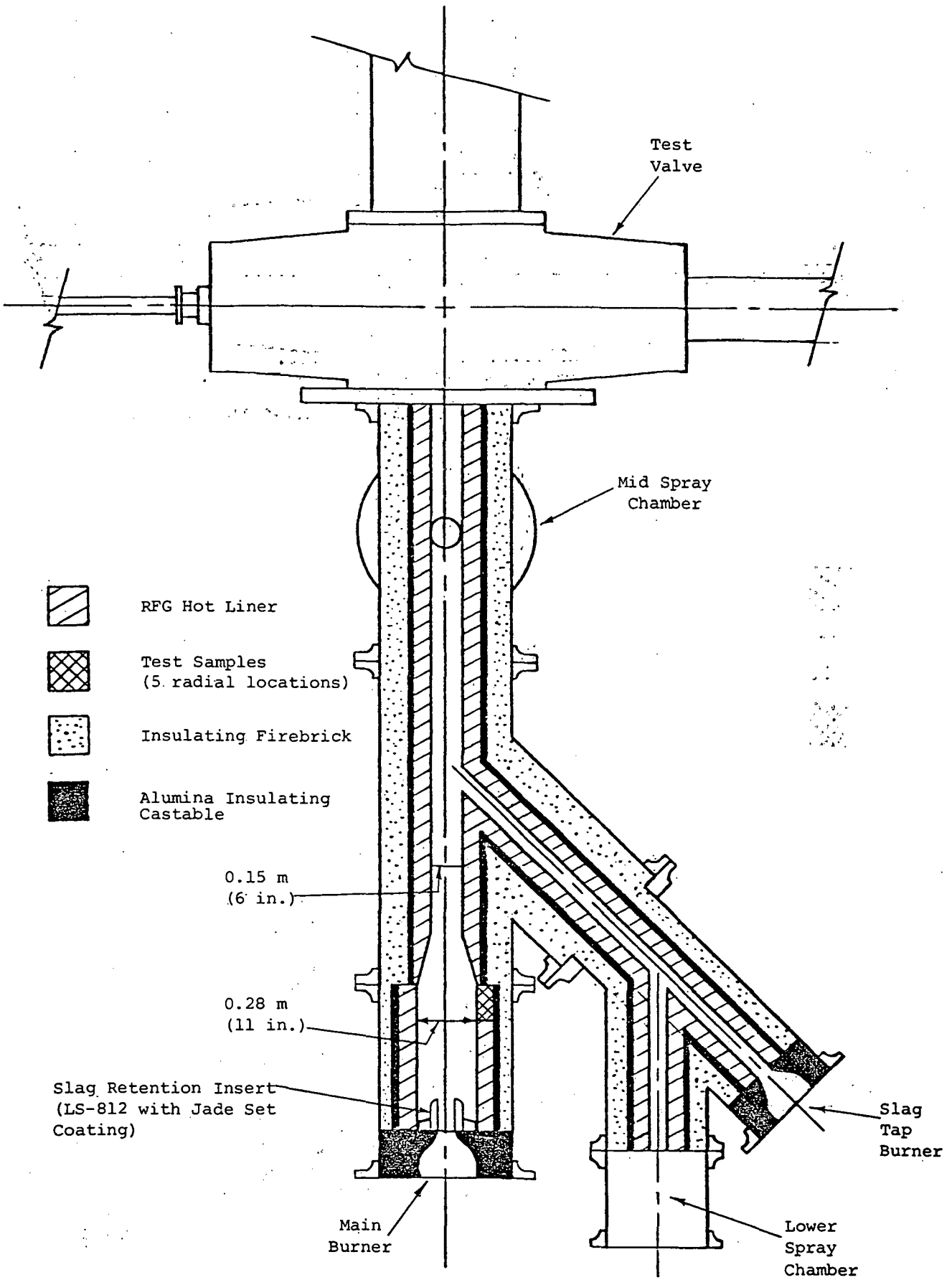

FIGURE 21. CONFIGURATION OF LOWER SECTIONS OF VTF FOR TEST 3B

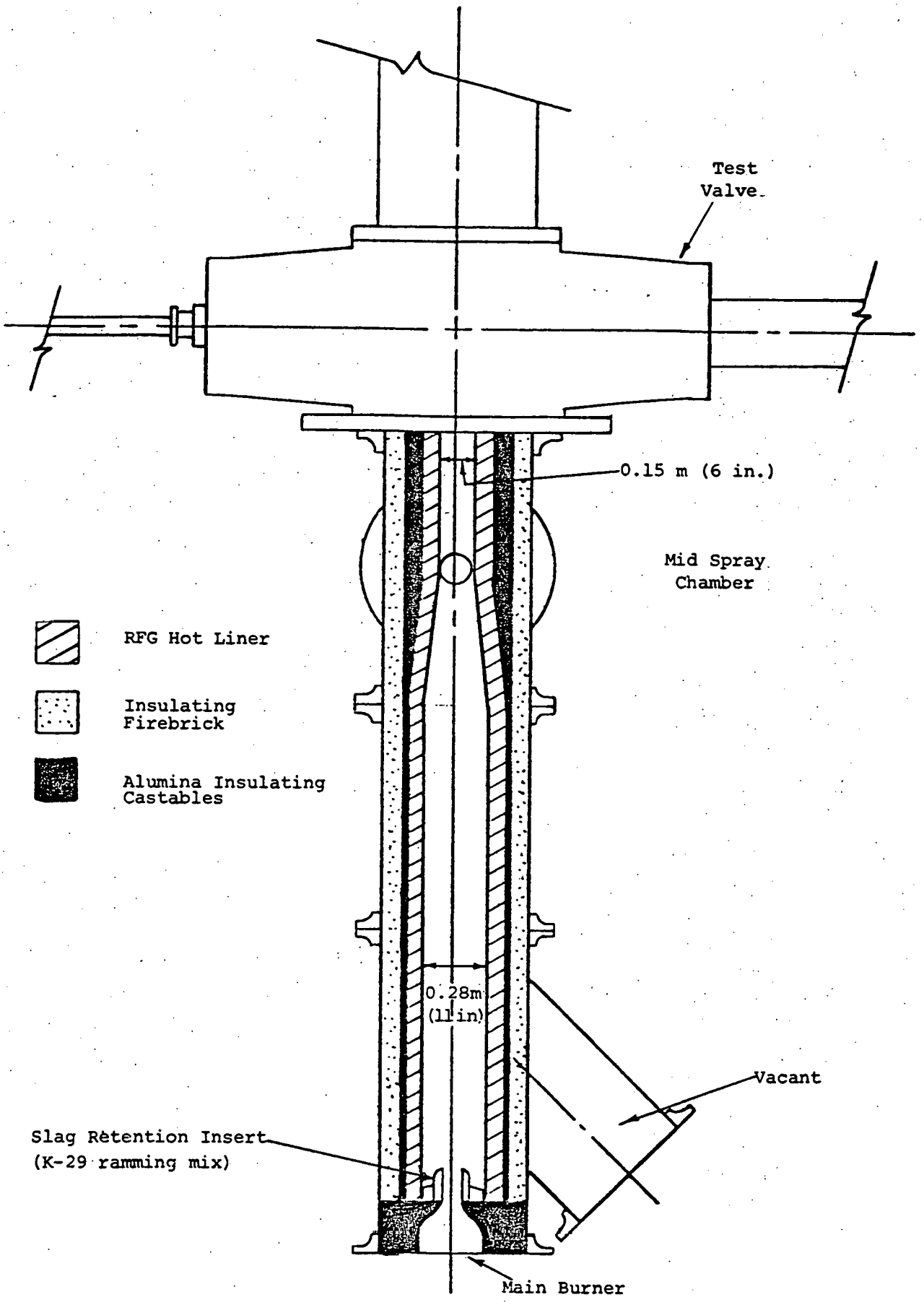

FIGURE 22. CONFIGURATION OF LOWER SECTIONS OF VTF FOR TEST 3C

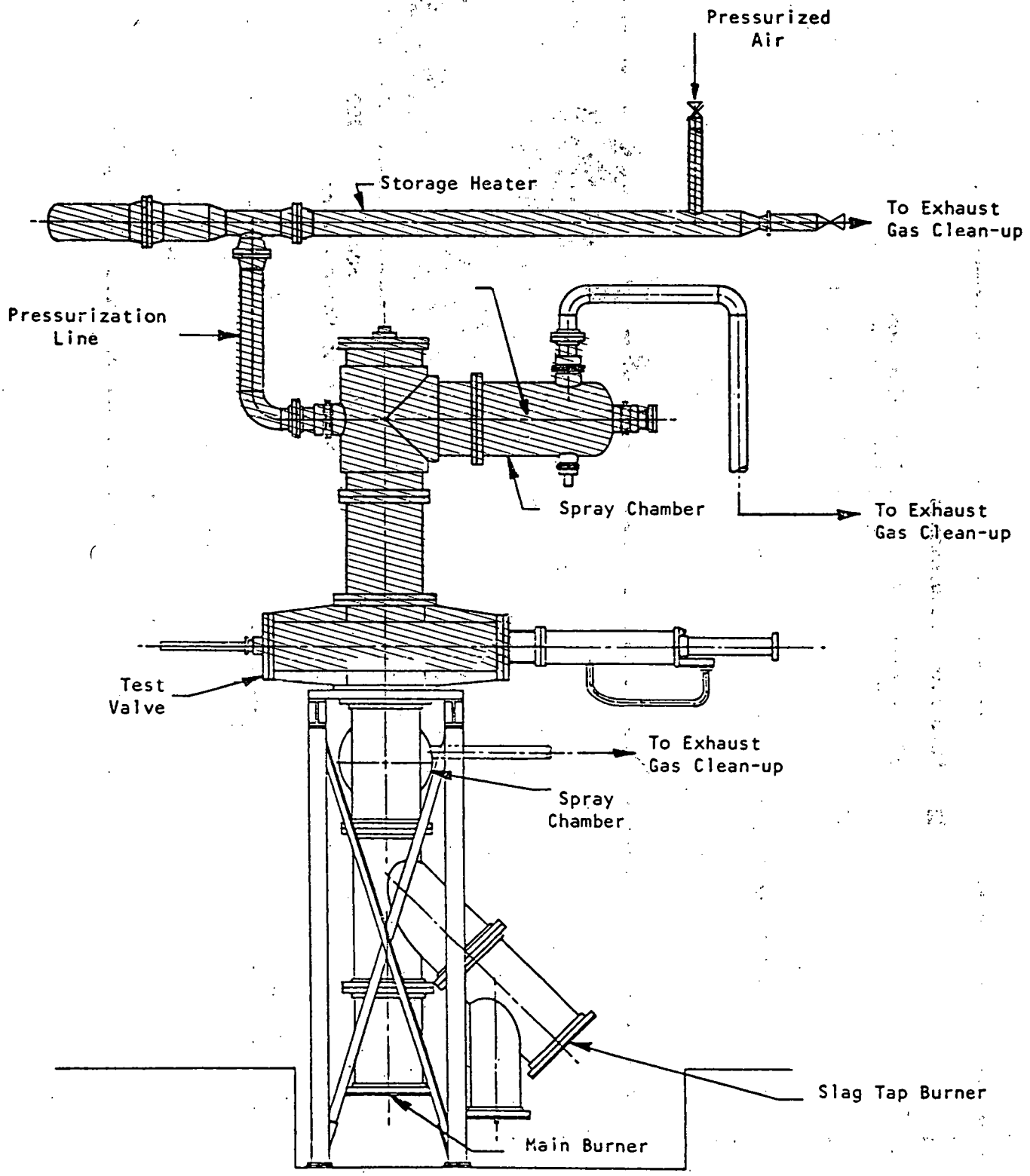

FIGURE 23. VALVE TEST FACILITY DURING AIR PHASE (SHADED AREA IS PRESSURIZED)

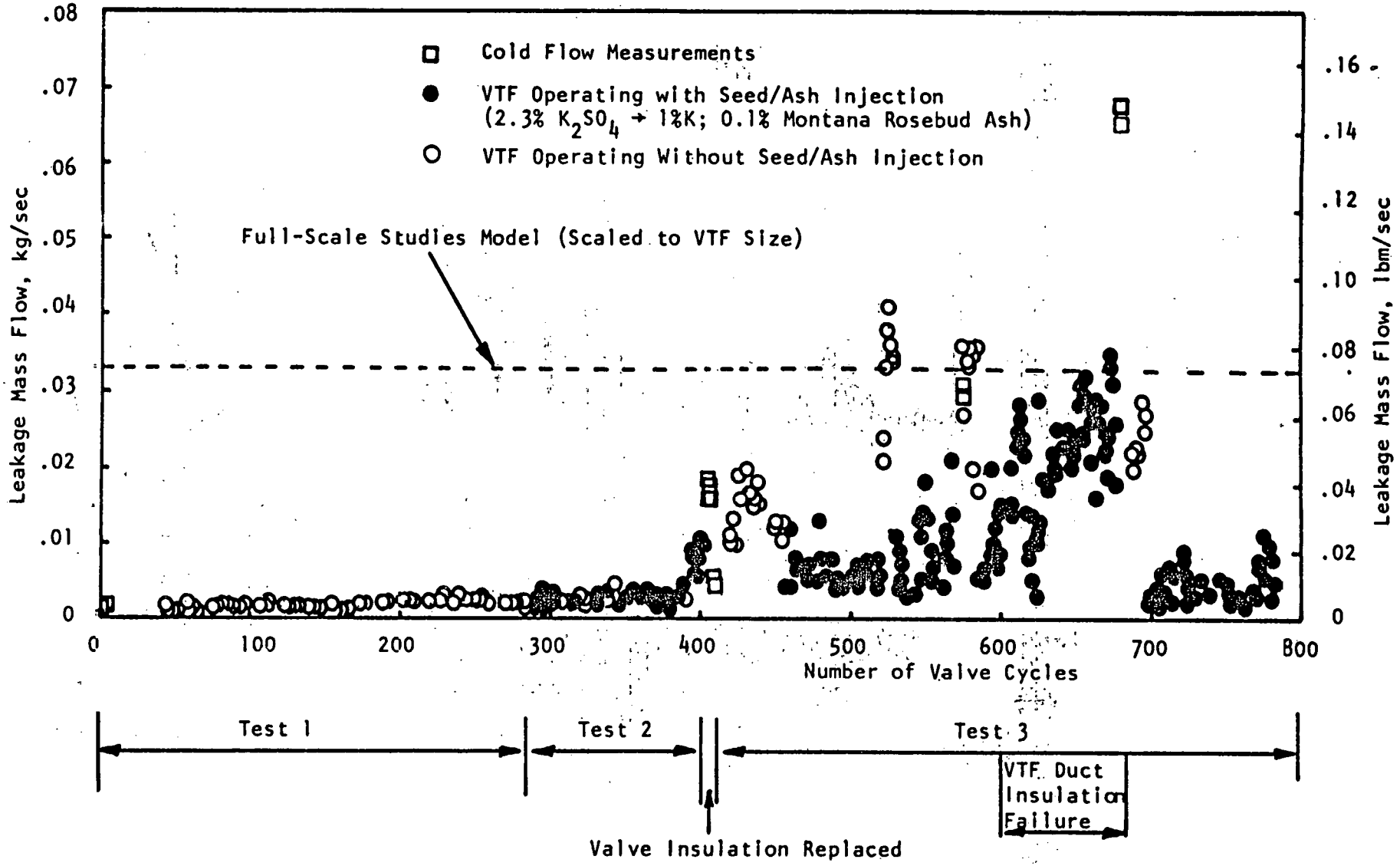

FIG 24. LEAKAGE THROUGH TEST VALVE AT 827 kPa (120 psia)

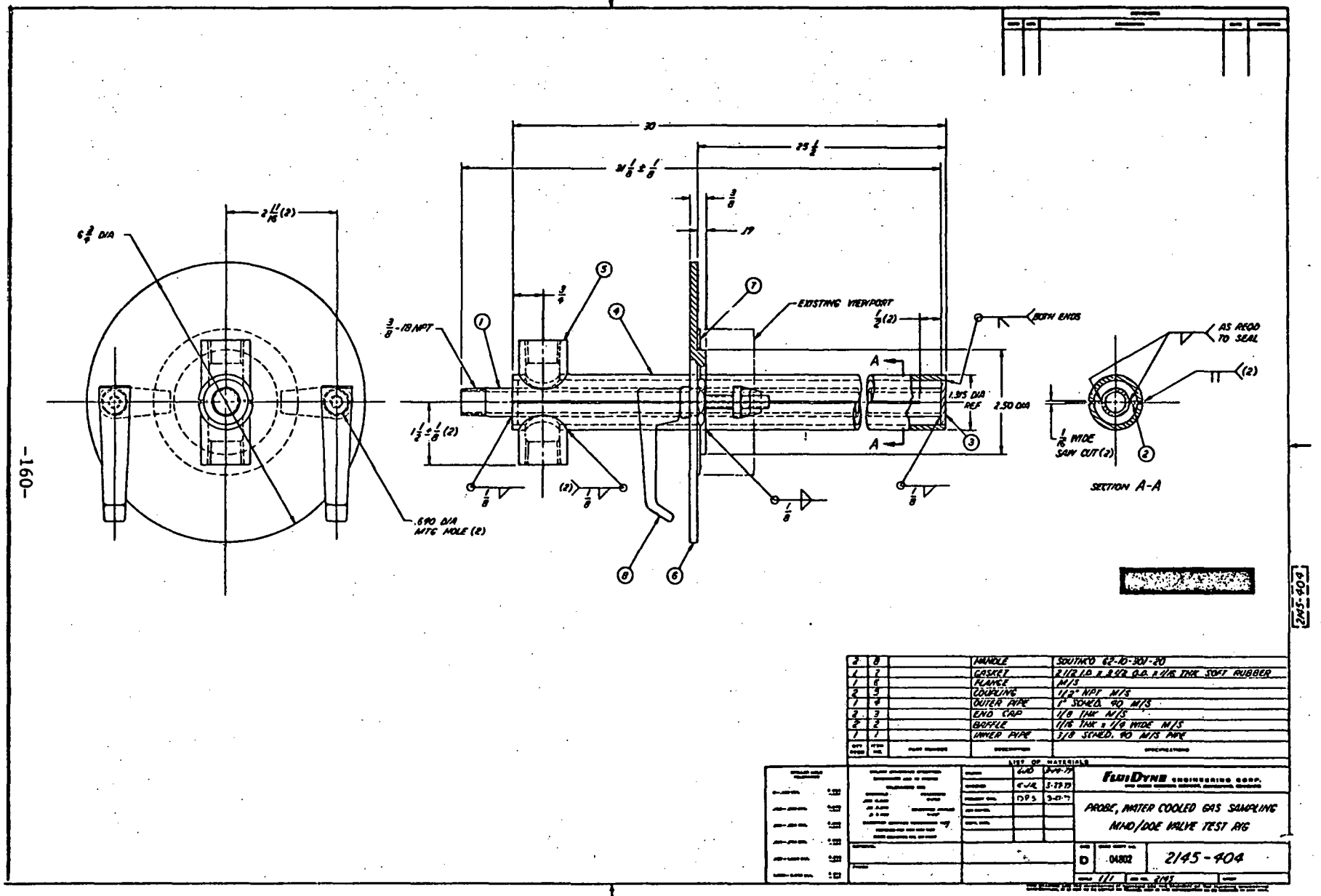

FIGURE 25. WATER-COOLED GAS SAMPLING PROBE

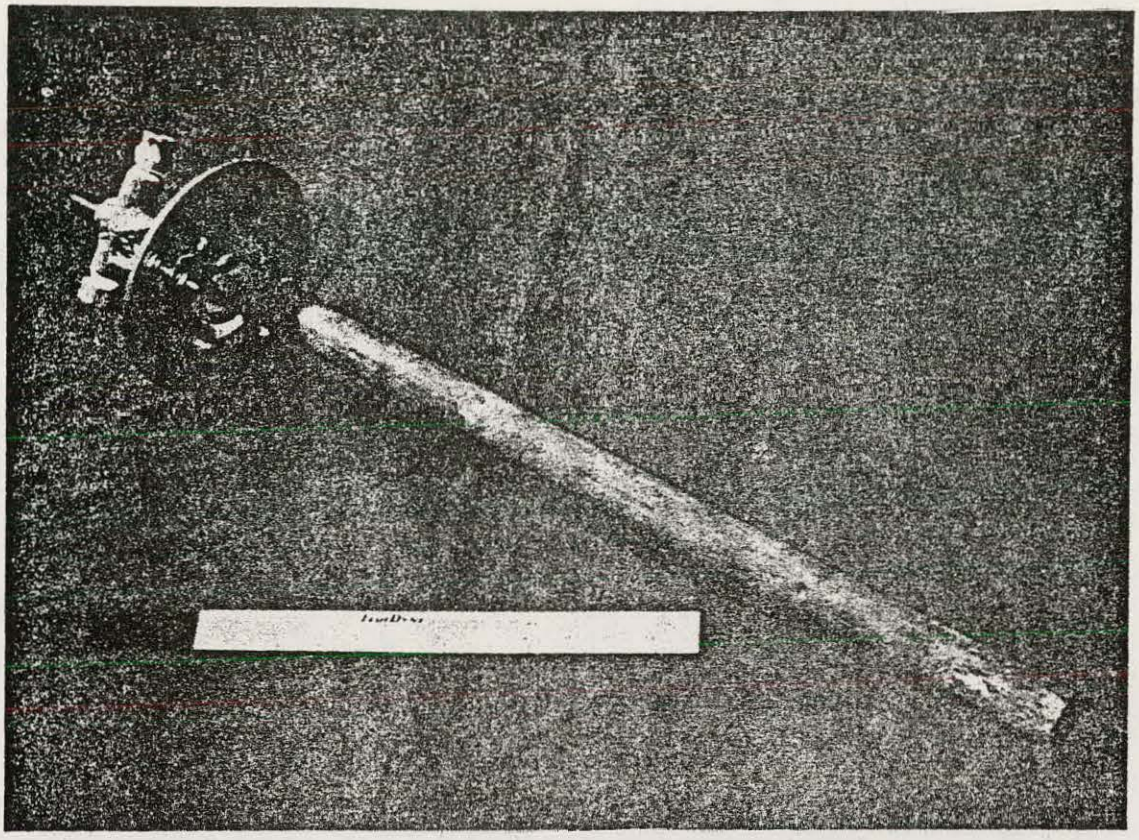

FIGURE 26 WATER - COOLED GAS SAMPLING PROBE

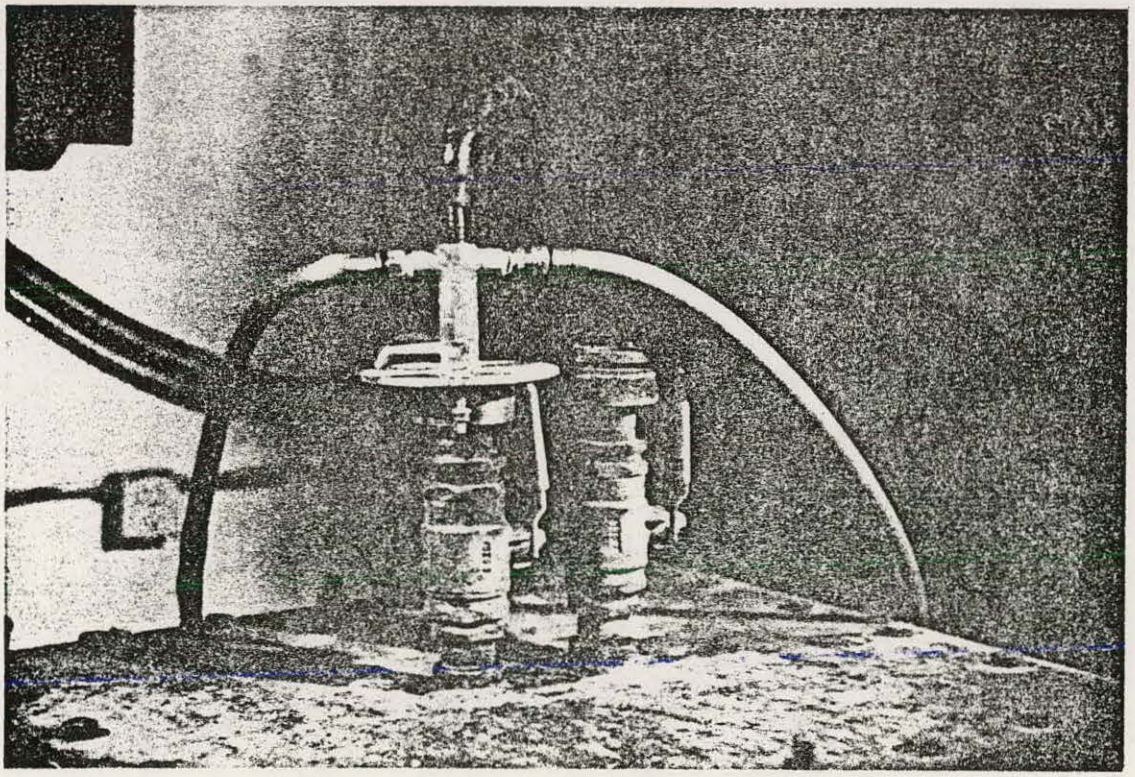

FIGURE 27 WATER - COOLED GAS SAMPLING PROBE INSTALLED AT TOP OF MATRIX IN MATRIX TEST FACILITY

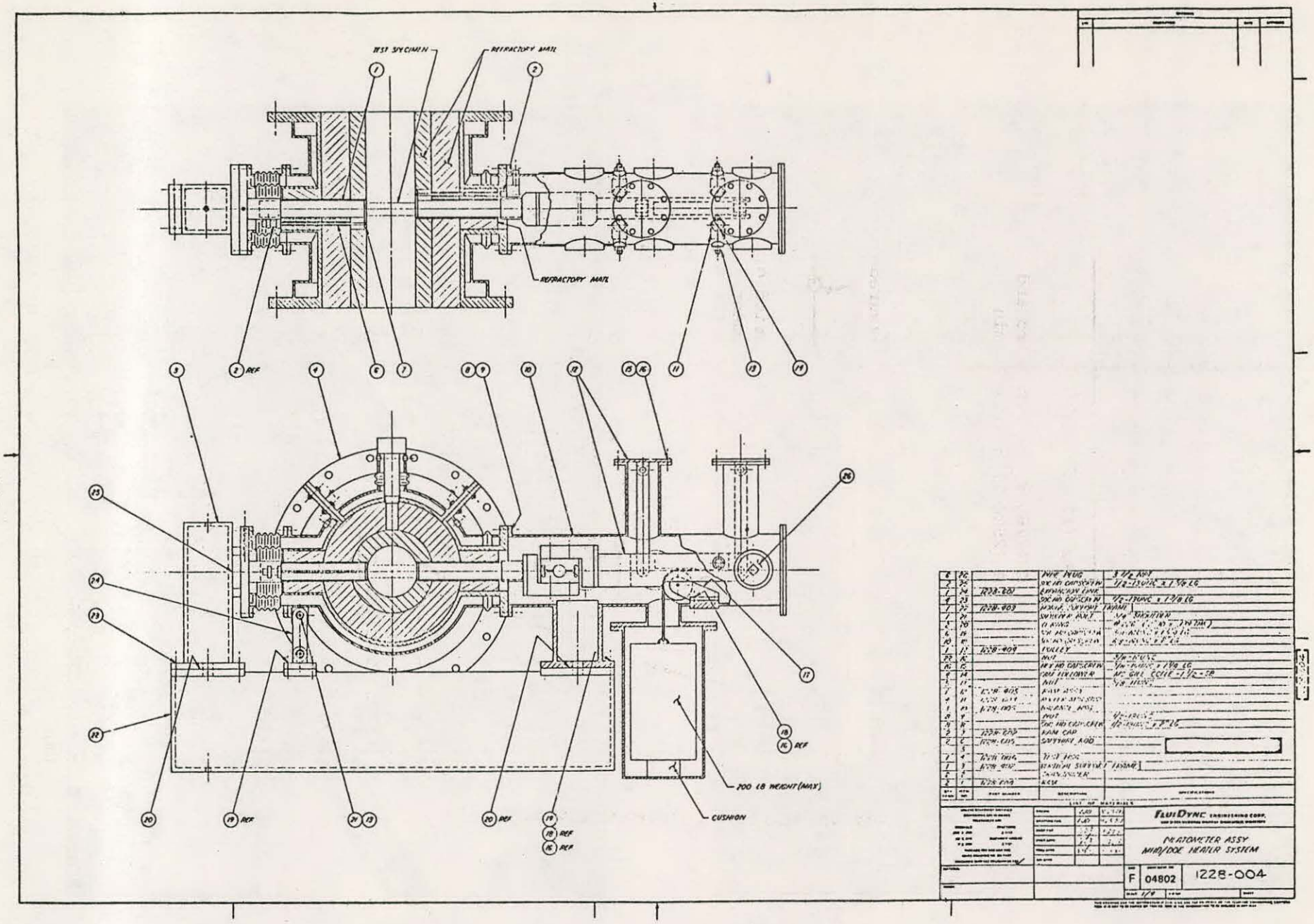

FIGURE 28. DILATOMETER ASSEMBLY DRAWING

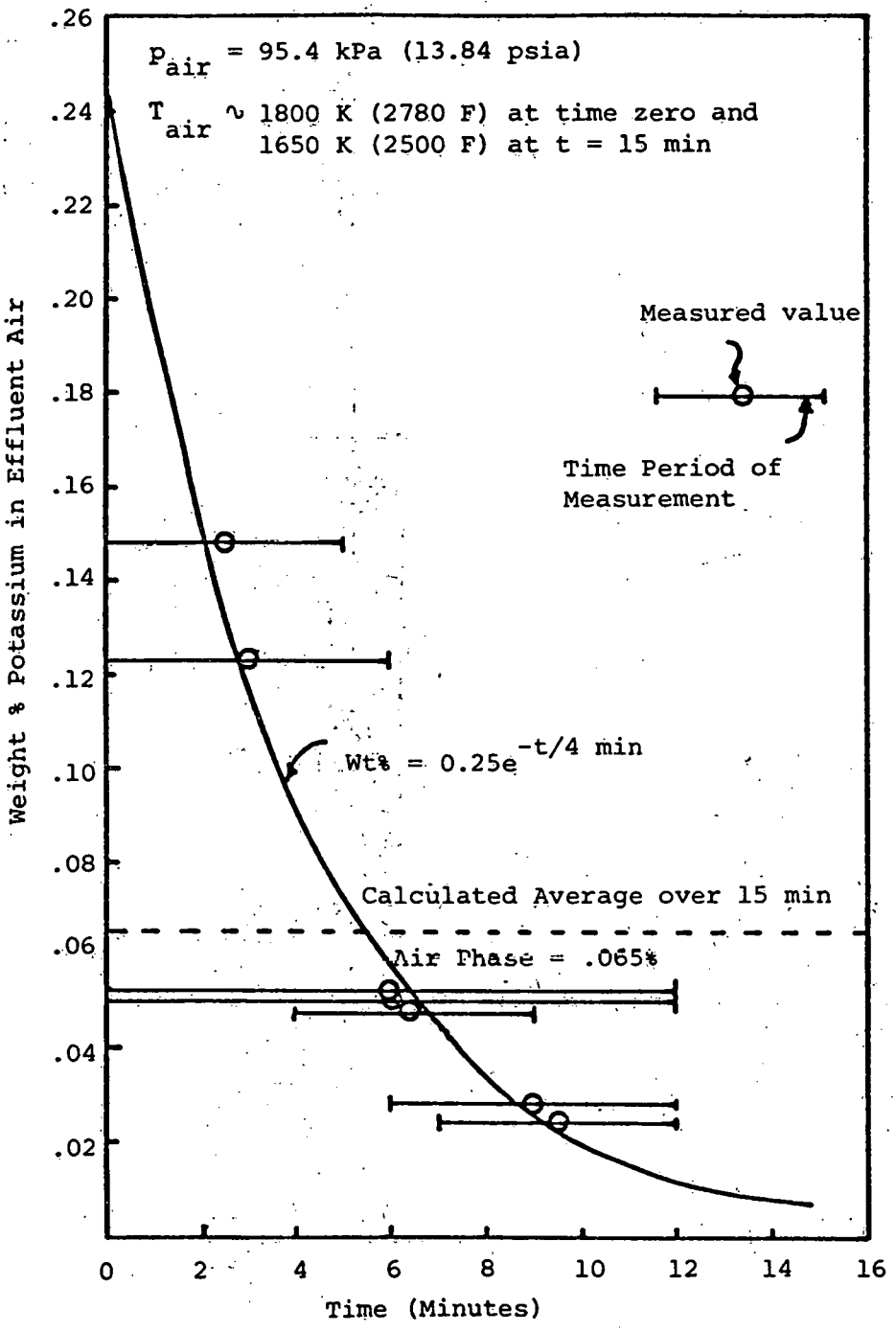

FIGURE 29 MEASUREMENTS OF POTASSIUM IN EFFLUENT AIR STREAM, MTF-HEAT 203

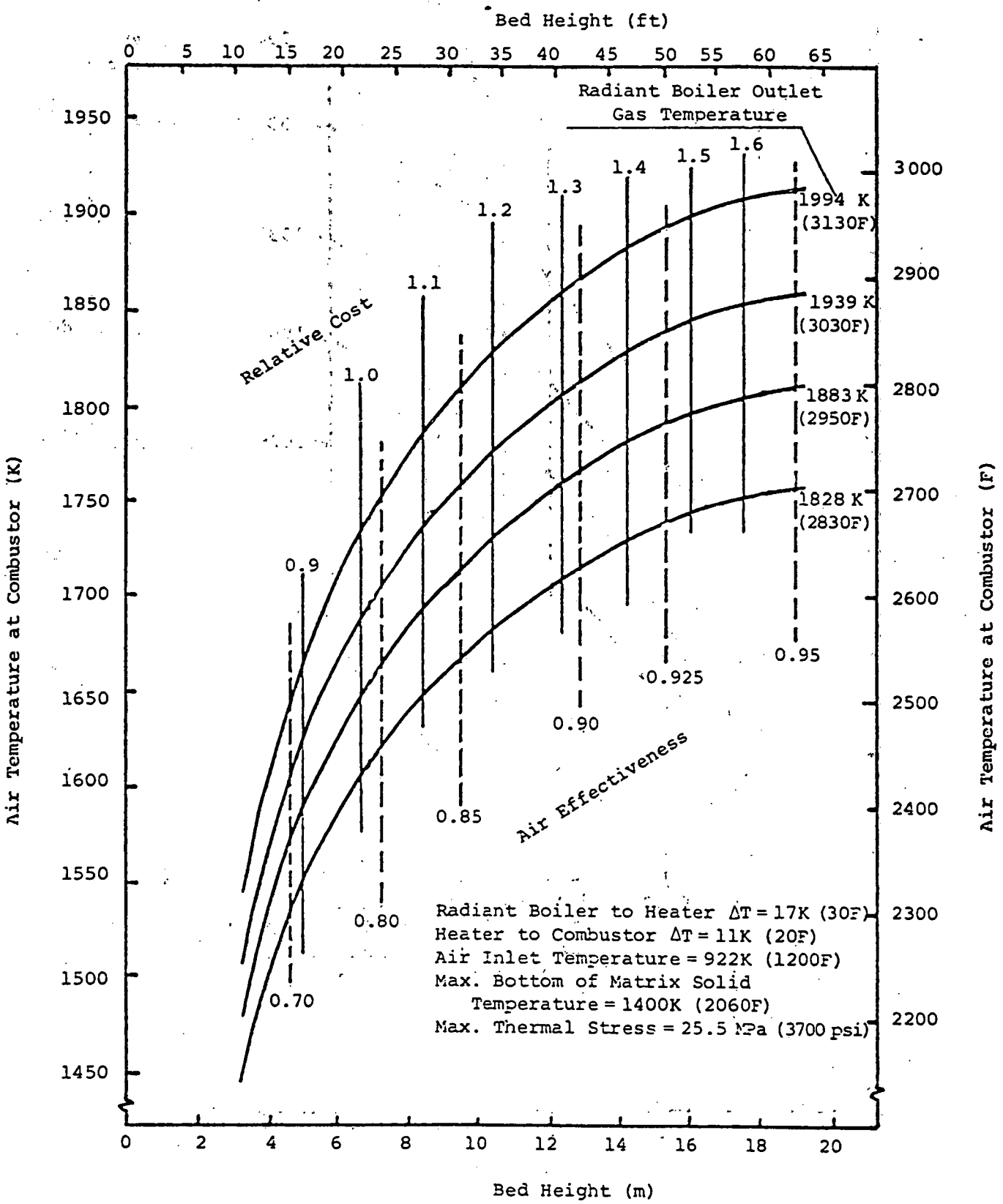

FIGURE 30. DELIVERED AIR TEMPERATURE FOR VARIOUS RADIANT BOILER OUTLET GAS TEMPERATURES;

Hole Diameter = 31.8 mm (1.25 in)
Web Thickness = 10.4 mm (0.409 in)

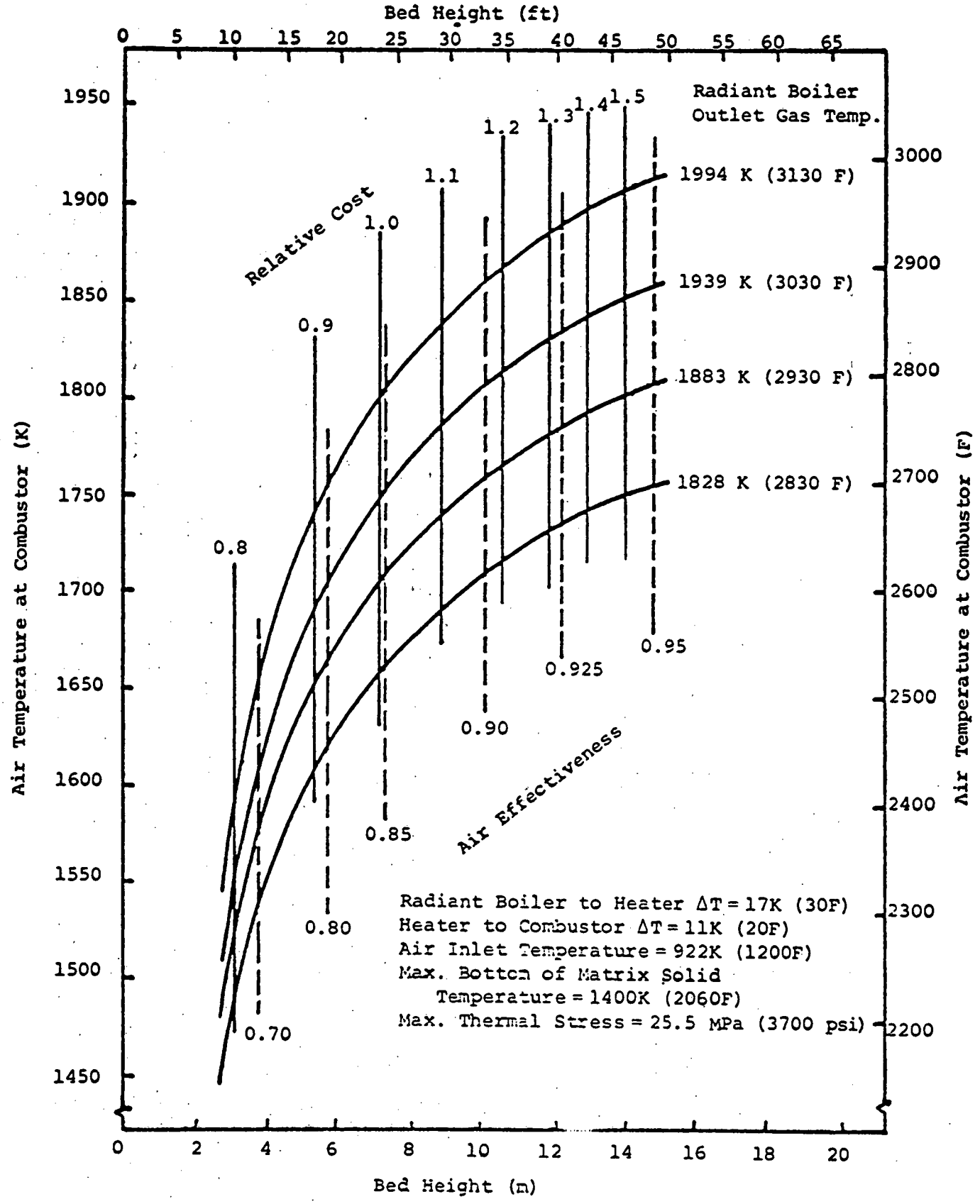

FIGURE 31. DELIVERED AIR TEMPERATURE FOR VARIOUS RADIANT BOILER OUTLET GAS TEMPERATURES;

Hole Diameter = 25.4 mm (1.0 in)
Web Thickness = 13.8 mm (0.545 in)

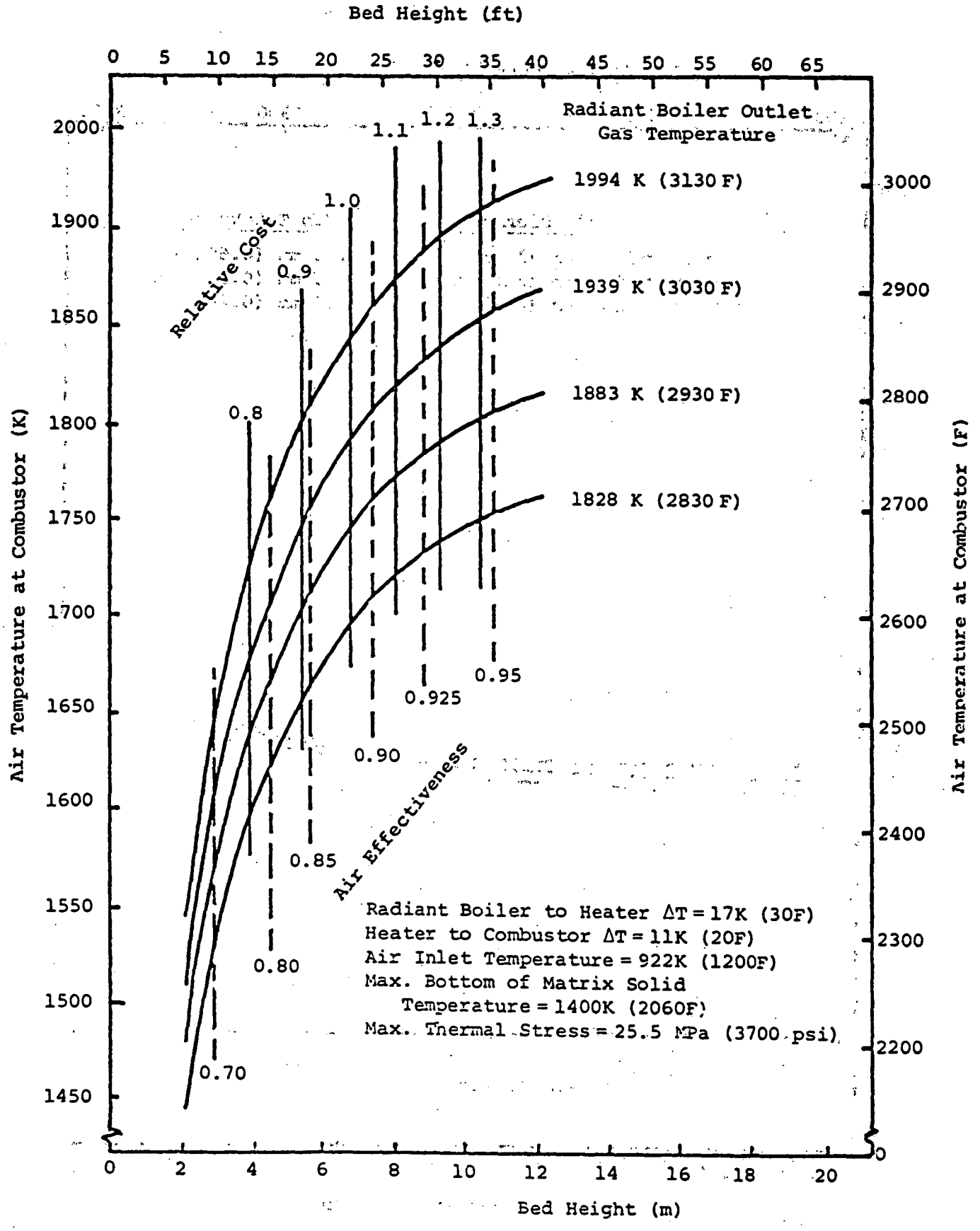

FIGURE 32. DELIVERED AIR TEMPERATURE FOR VARIOUS RADIANT BOILER OUTLET GAS TEMPERATURES;

Hole Diameter = 19.0 mm (0.75 in)
Web Thickness = 10.4 mm (0.409 in)

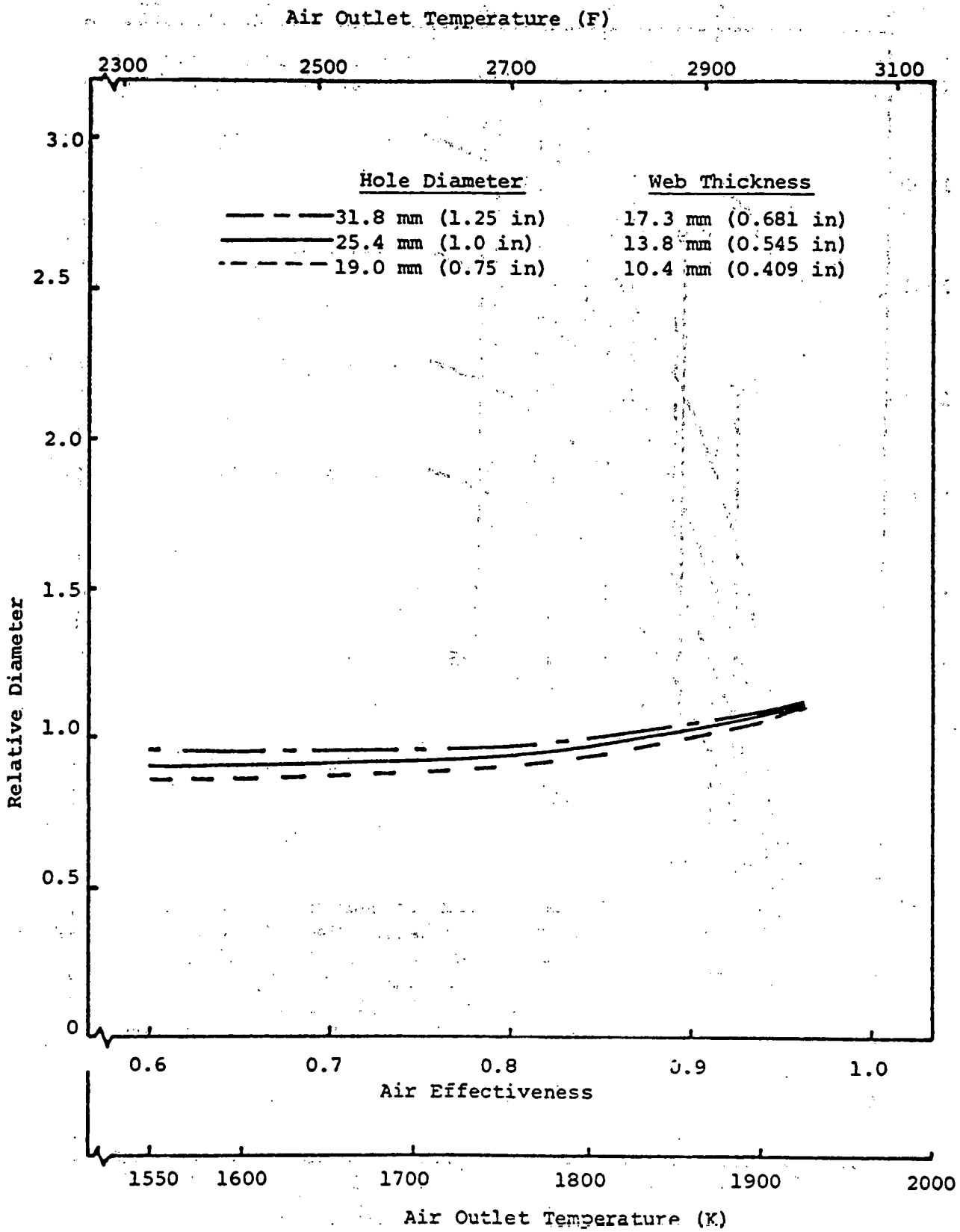

FIGURE 33. BED DIAMETER RELATIVE TO EXAMPLE CASE FOR VARIOUS HOLE DIAMETERS

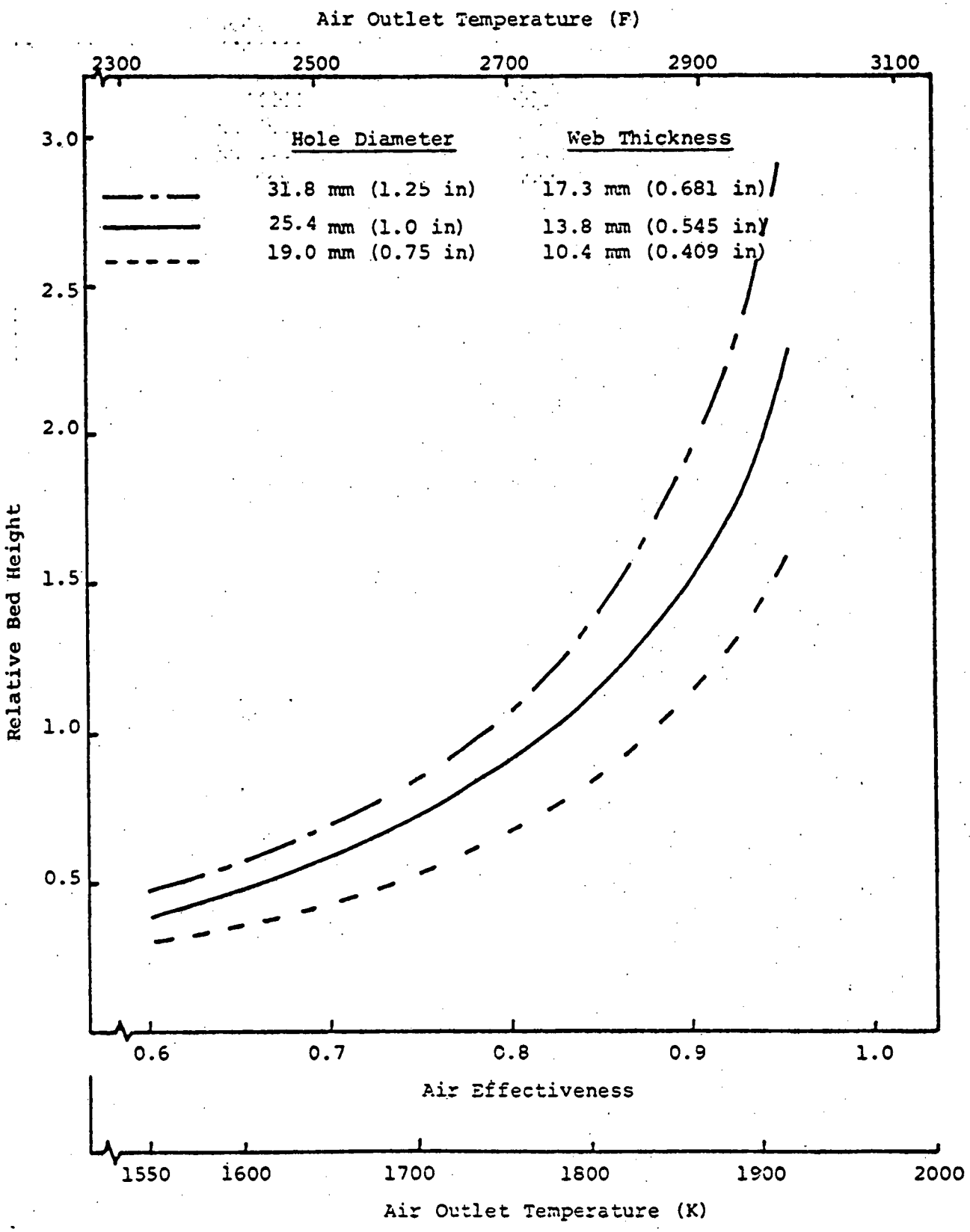

FIGURE 34. BED HEIGHT RELATIVE TO EXAMPLE CASE FOR VARIOUS HOLE DIAMETERS

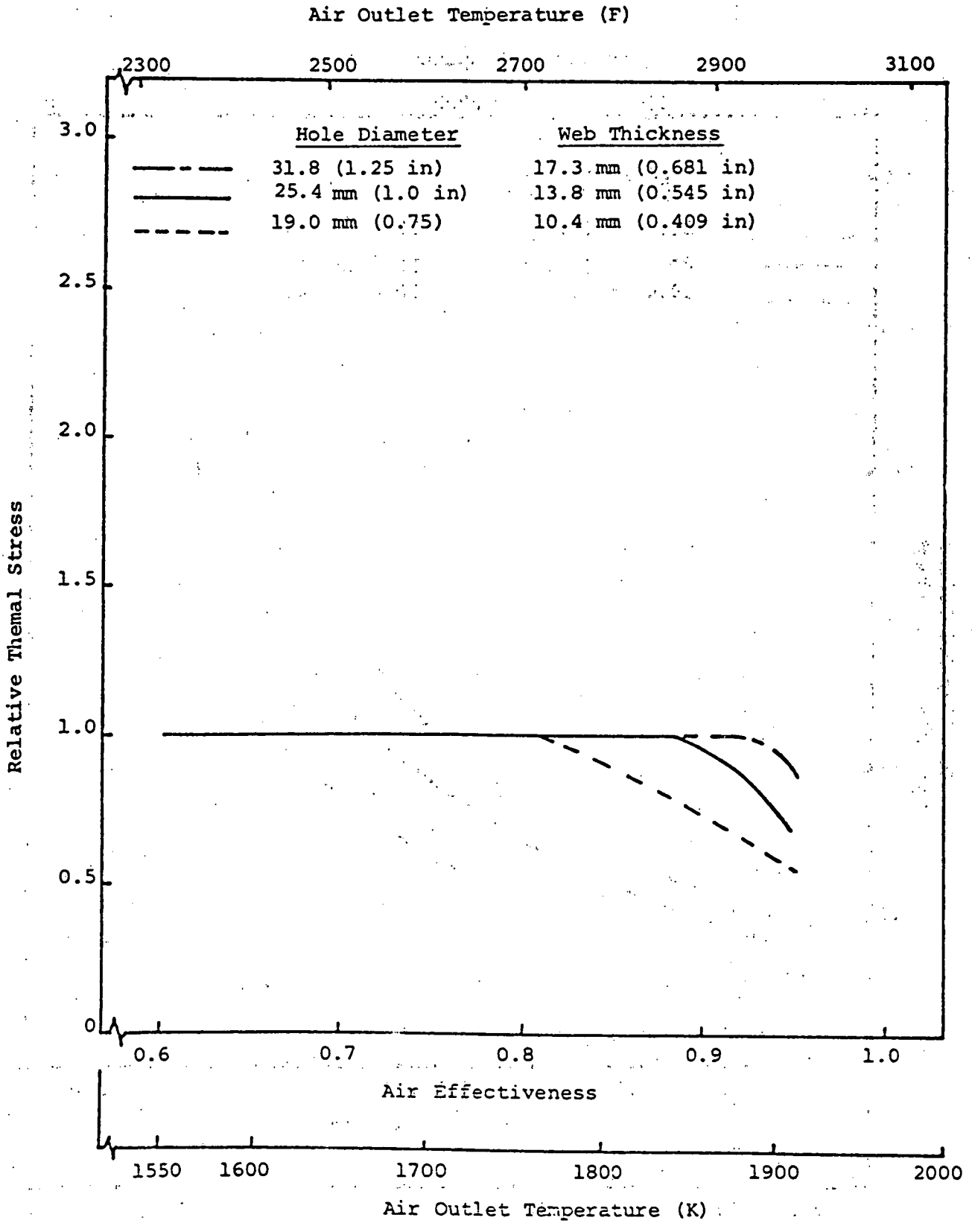

FIGURE 35. THERMAL STRESS RELATIVE TO EXAMPLE CASE FOR VARIOUS HOLE DIAMETERS

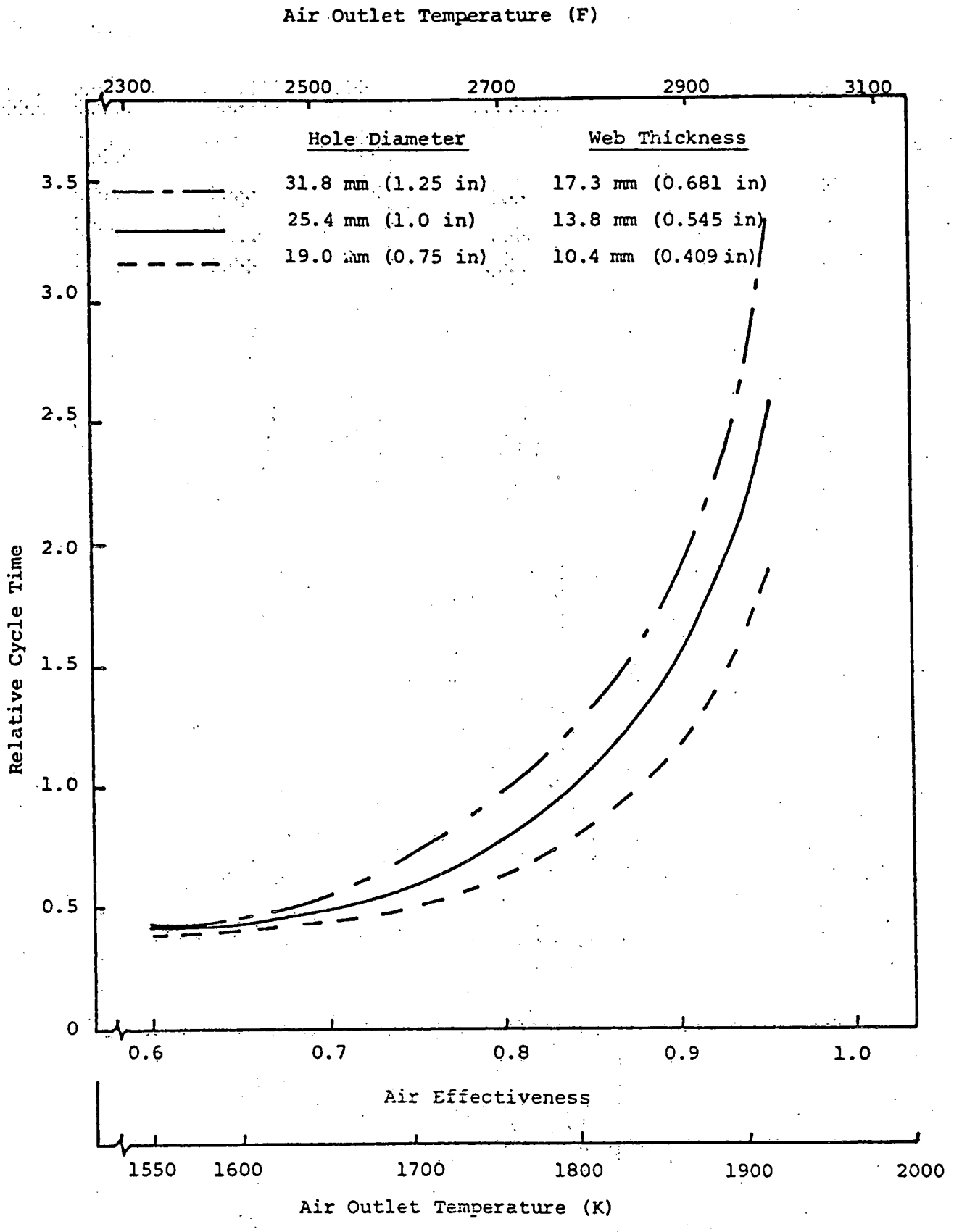

FIGURE 36. CYCLE TIME RELATIVE TO EXAMPLE CASE FOR VARIOUS HOLE DIAMETERS

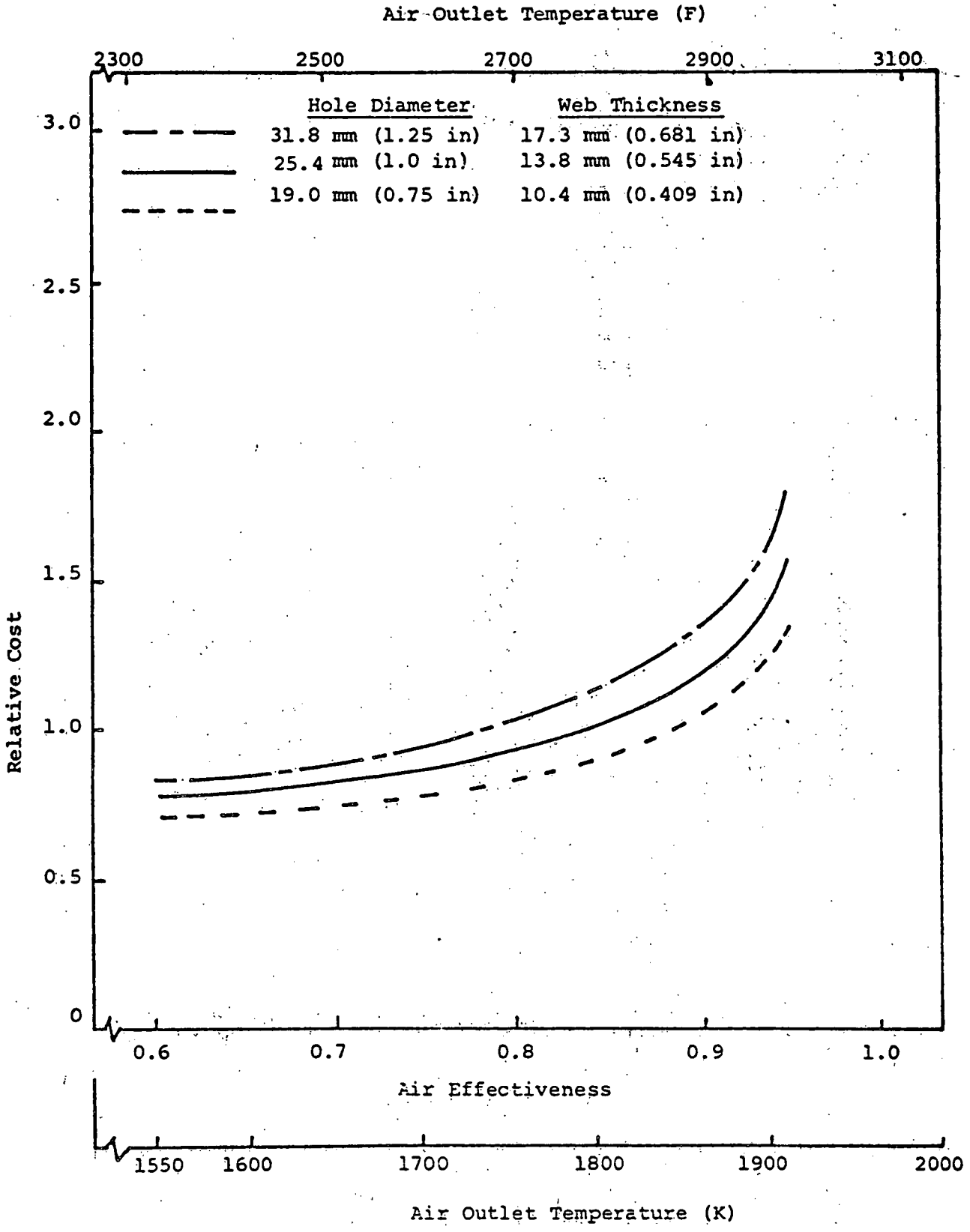

FIGURE 37. COST RELATIVE TO EXAMPLE CASE FOR VARIOUS HOLE DIAMETERS

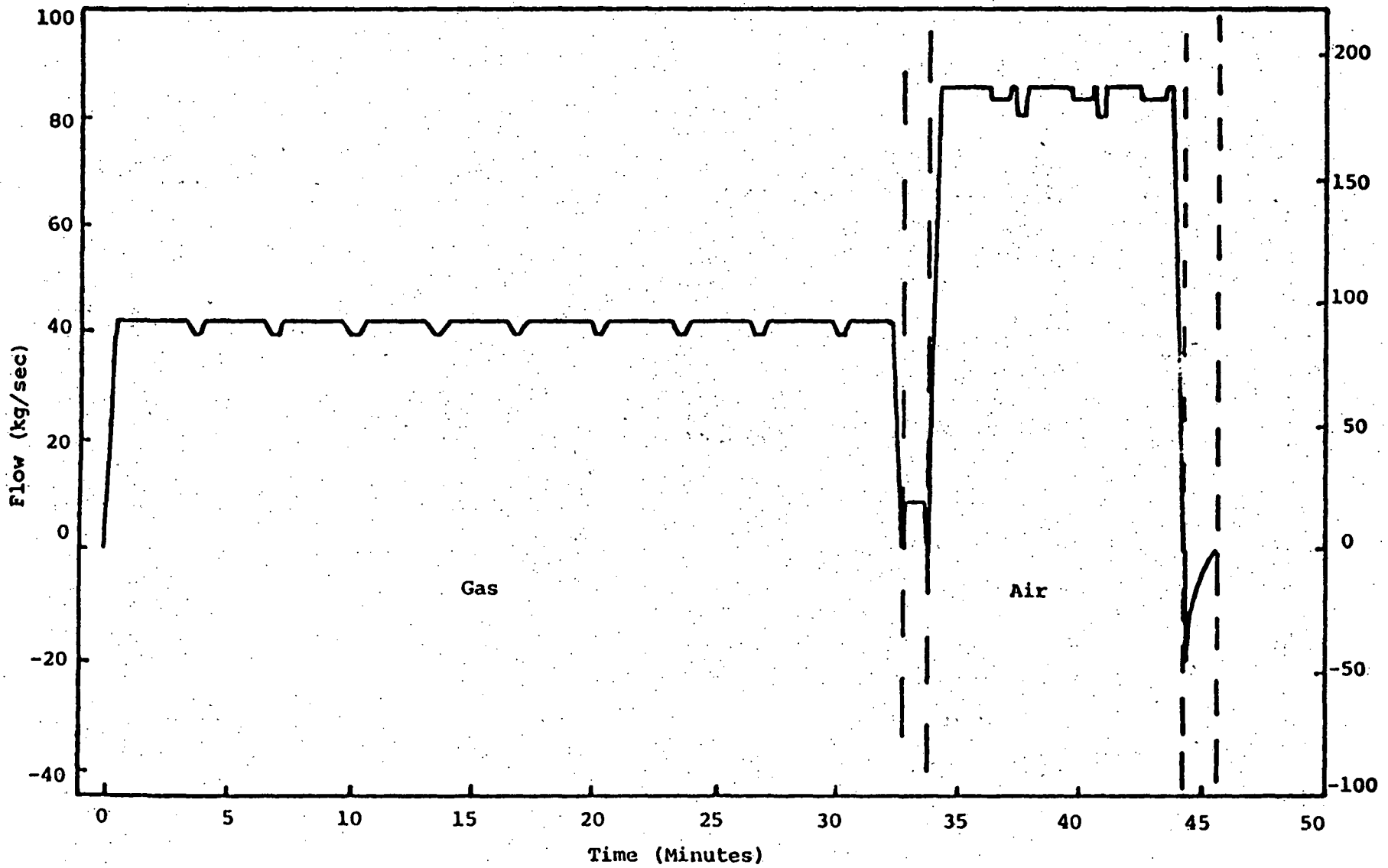

FIGURE 38. GAS AND AIR FLOW RATES FOR AN INDIVIDUAL HEATER WITH IDEAL FLOW DISTRIBUTION (INCLUDING PRESSURIZATION/DEPRESSURIZATION MASS EXCHANGE) EXAMPLE HTAH

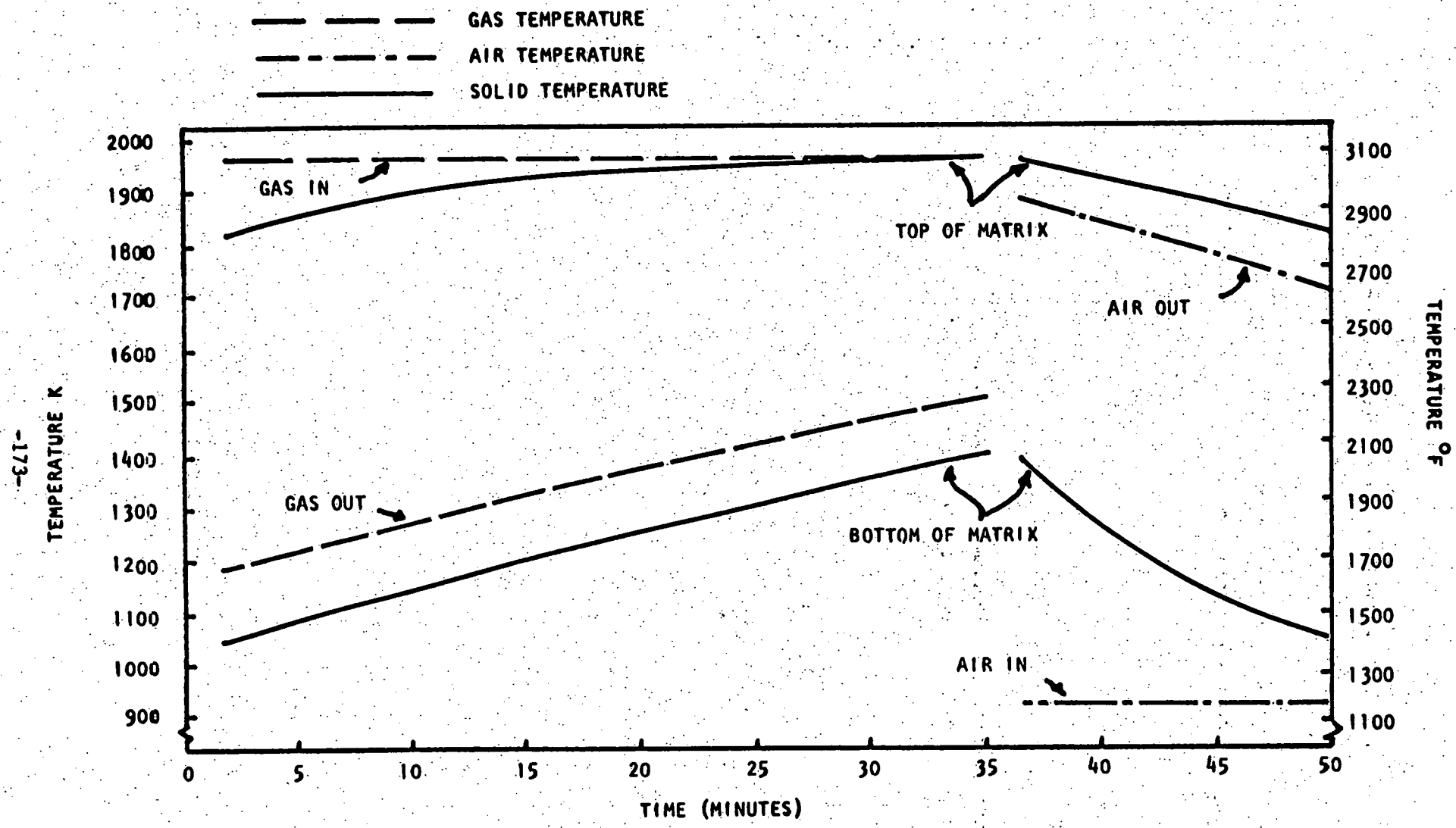

FIGURE 39. INDIVIDUAL HEATER PERFORMANCE FOR EXAMPLE HTAH BASED ON IDEAL HEATER CYCLE (STRHEX CODE)

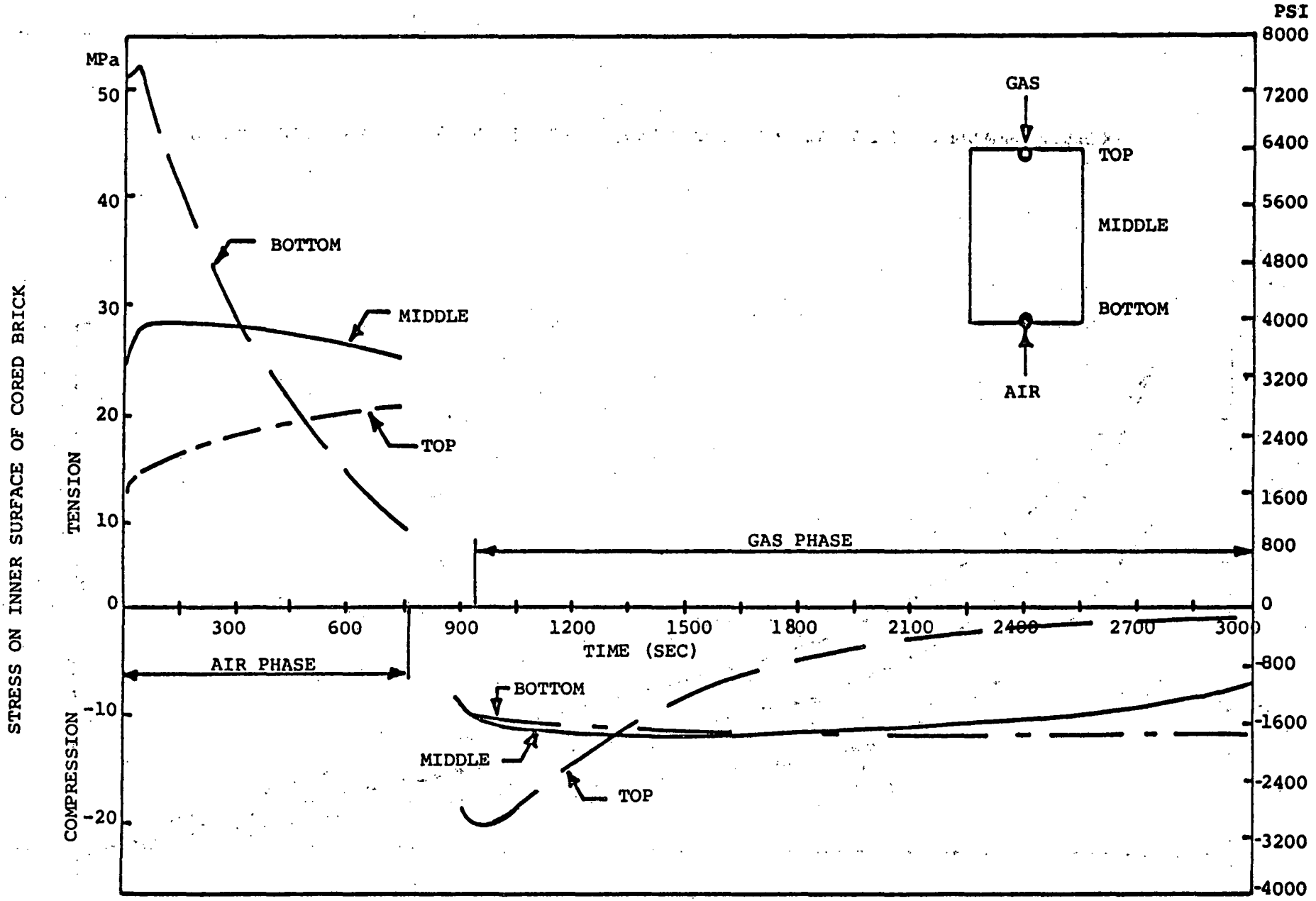

FIGURE 40. THERMAL STRESS AT VARIOUS AXIAL POSITIONS IN MATRIX FOR EXAMPLE HTAH

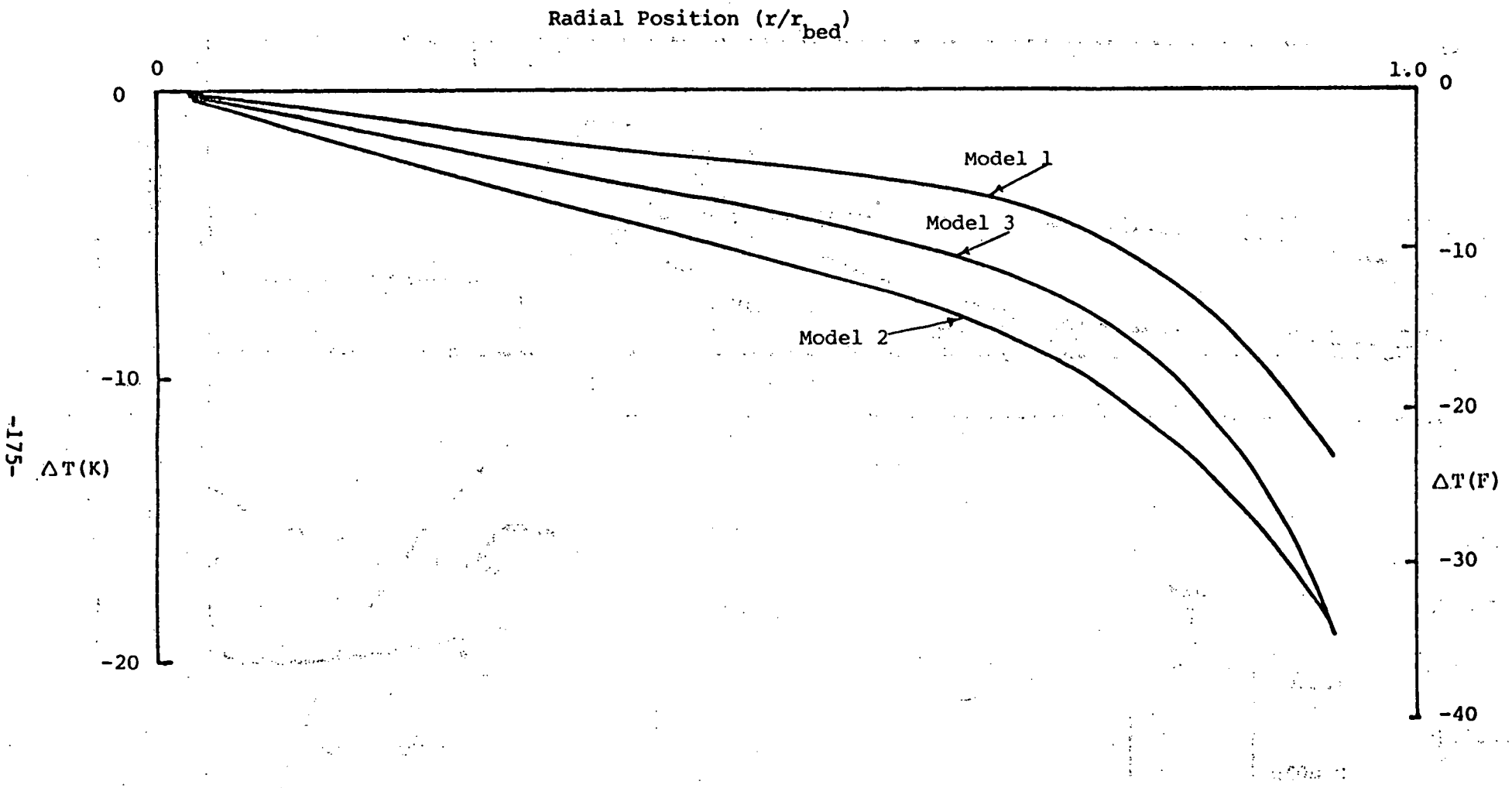

FIGURE 41. END OF GAS PHASE TEMPERATURE DIFFERENCE FOR RADIAL ELEMENTS, STRHEX

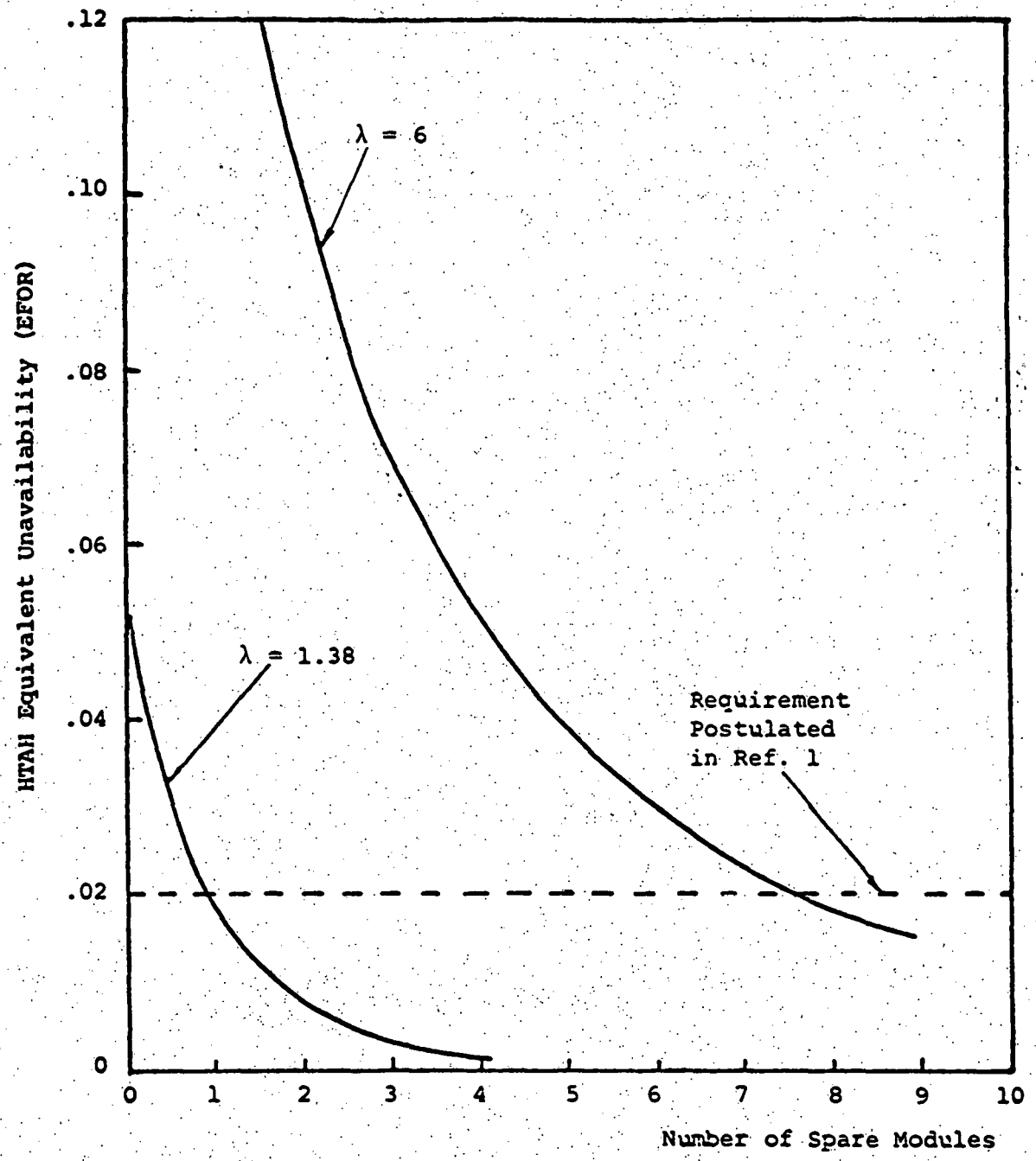

FIGURE 42. NUMBER OF SPARE HEATER MODULES REQUIRED FOR A GIVEN HTAH UNAVAILABILITY FOLLOWING METHOD OF REFERENCES 1-3

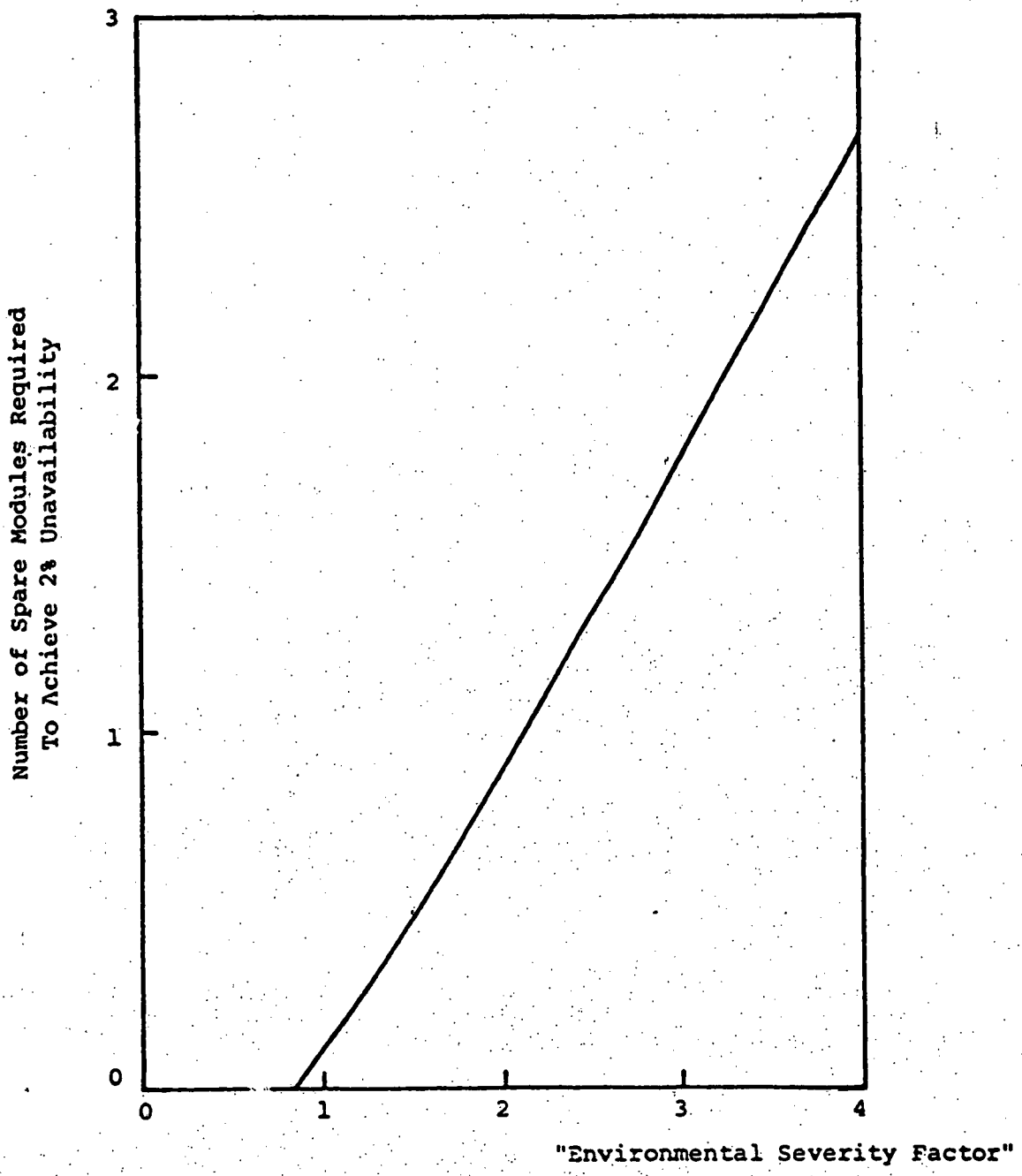

FIGURE 43. NUMBER OF SPARE HEATERS REQUIRED TO ACHIEVE 2% UNAVAILABILITY FOR $\lambda = 1.38$ VS. ASSUMED SEVERITY FACTOR

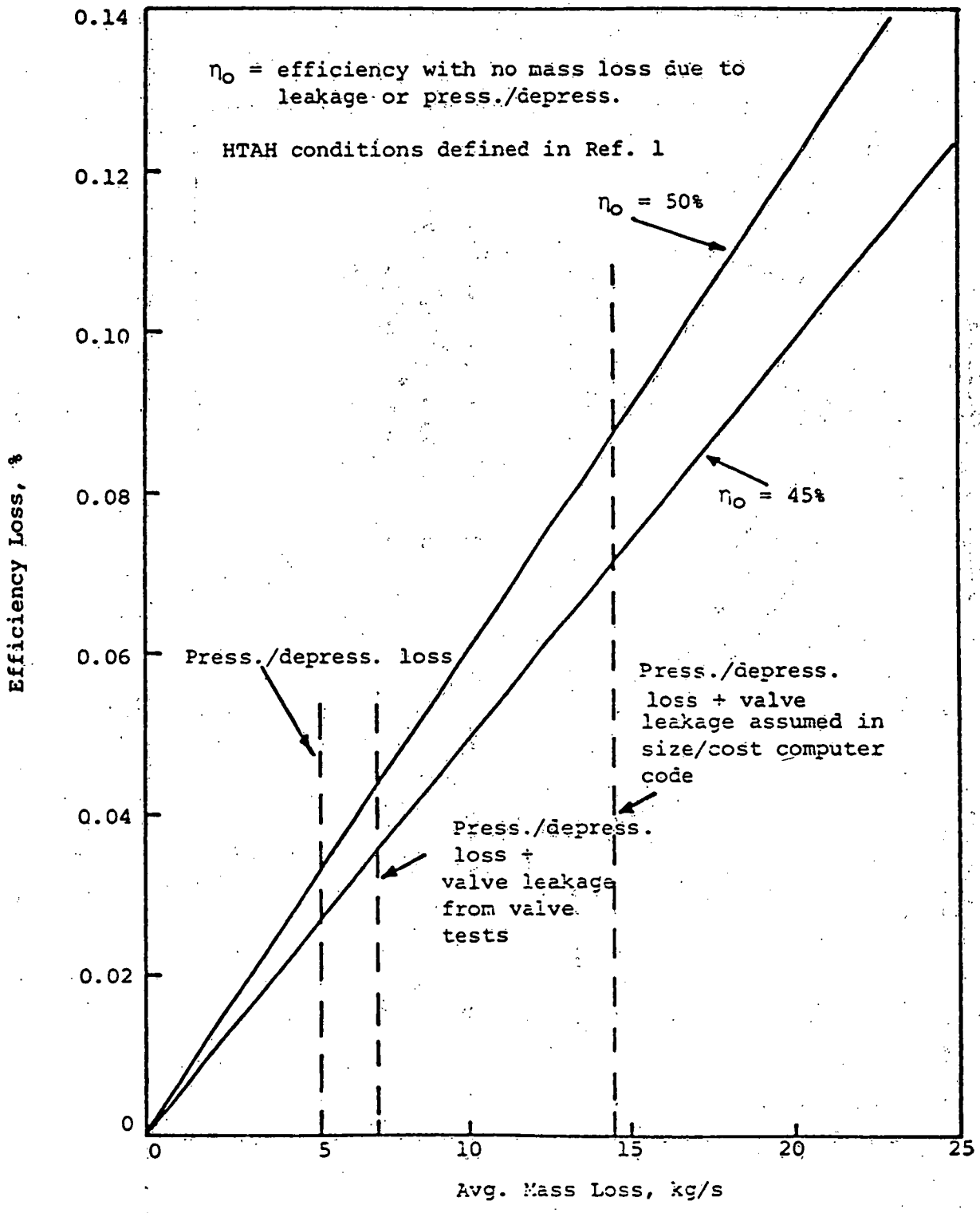

FIGURE 44. LOSS IN OVERALL PLANT EFFICIENCY DUE TO HTAH VALVE LEAKAGE AND PRESSURIZATION/DEPRESSURIZATION MASS LOSS FOR 1000 MW_e PLANT

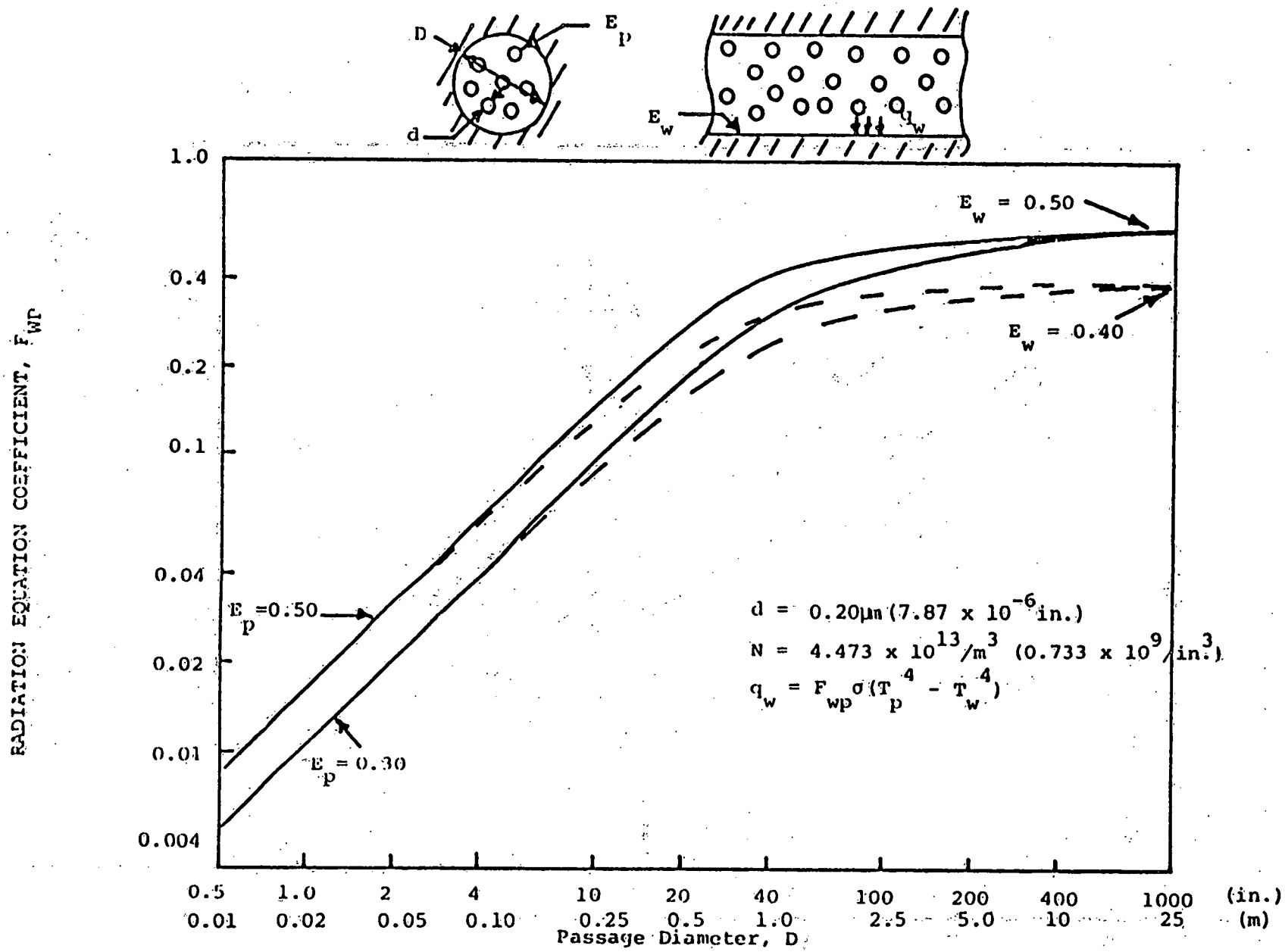

FIGURE 45. INTERCHANGE FACTOR OF CYLINDRICAL WALL WITH RESPECT TO PARTICLES FOR MHD CHANNEL EXHAUST GAS

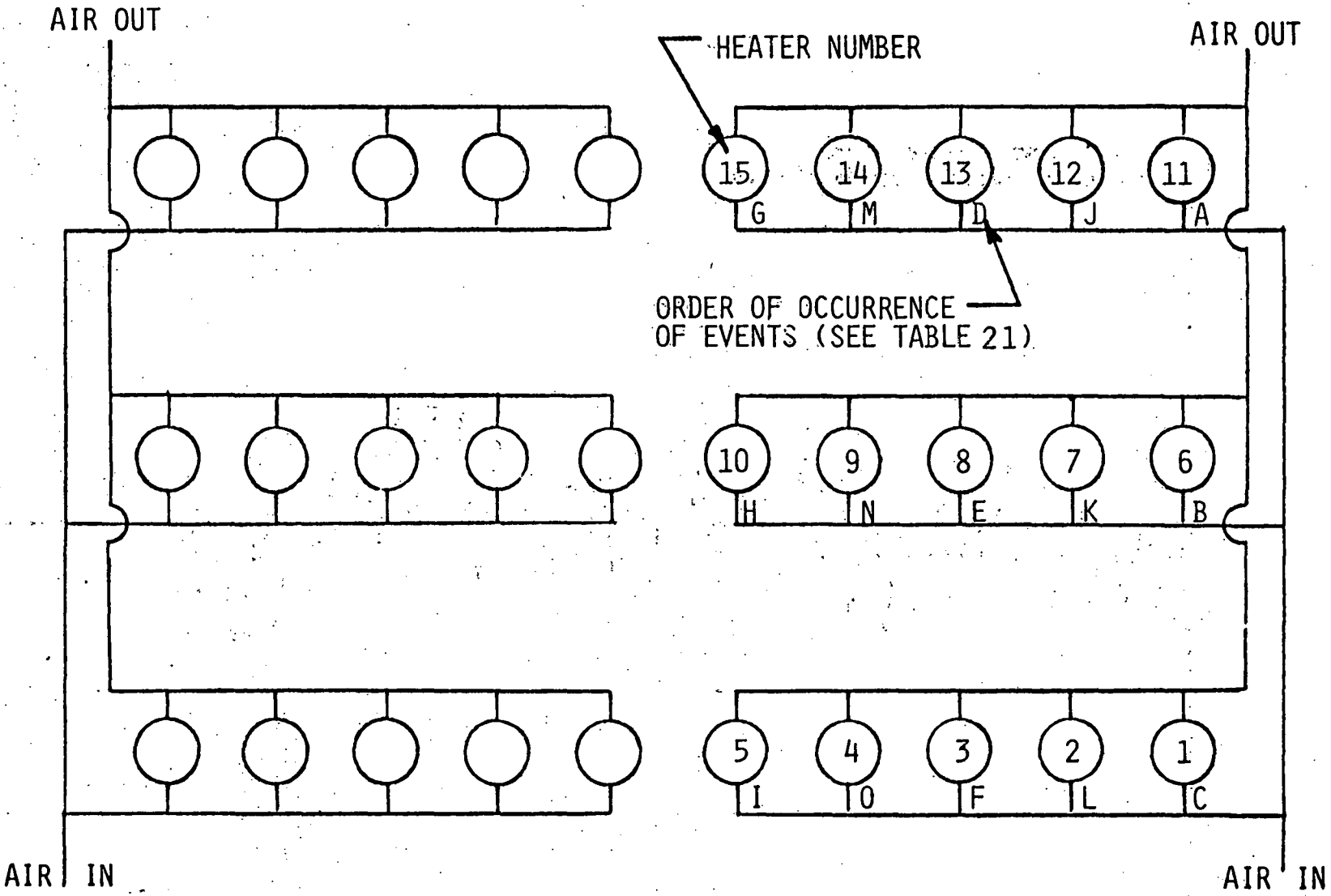

FIGURE 46. IDENTIFICATION OF HEATERS AND SEQUENCE FOR EXAMPLE HTAH PERFORMANCE CALCULATIONS

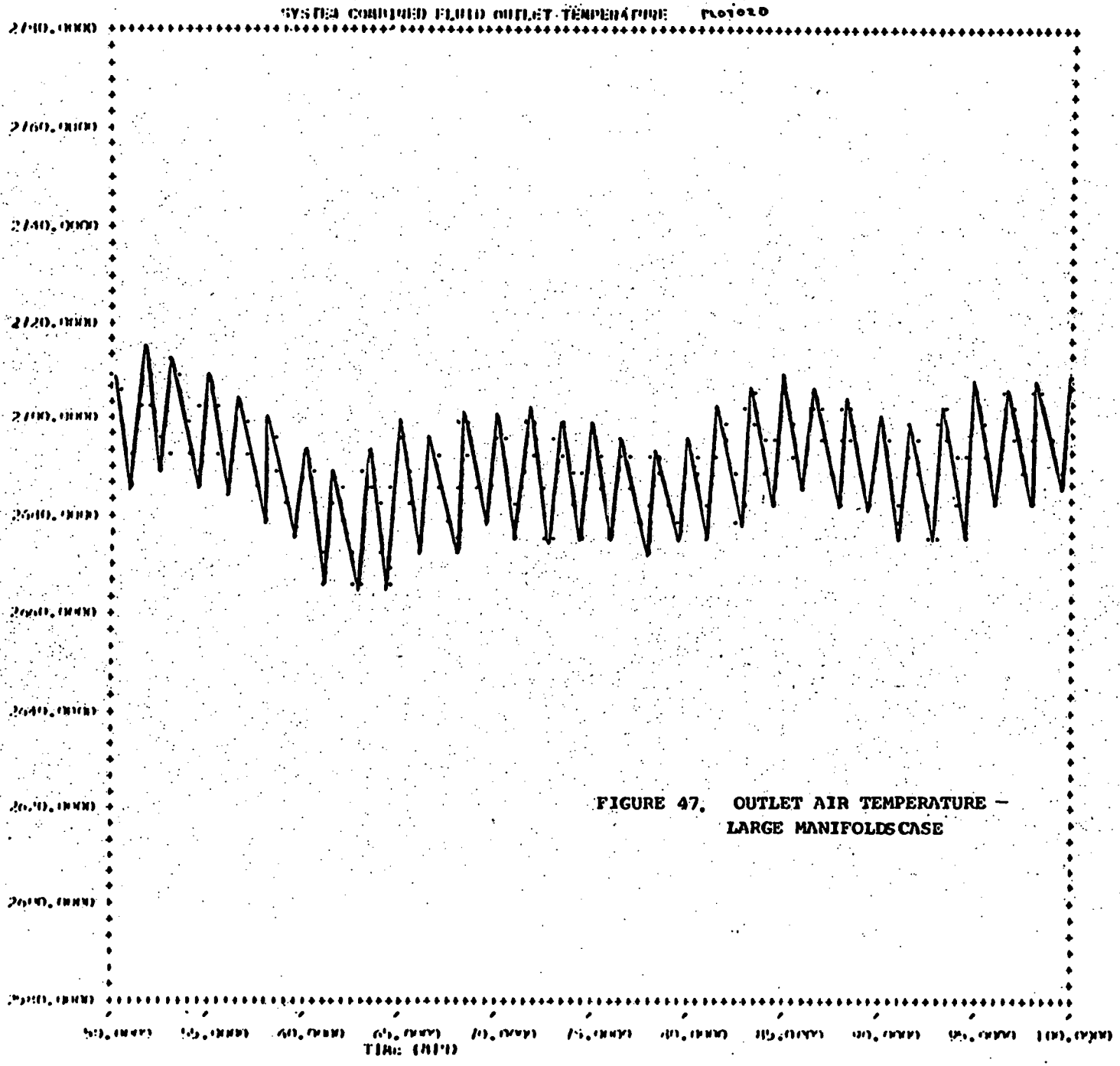

FIGURE 47. OUTLET AIR TEMPERATURE – LARGE MANIFOLDS CASE

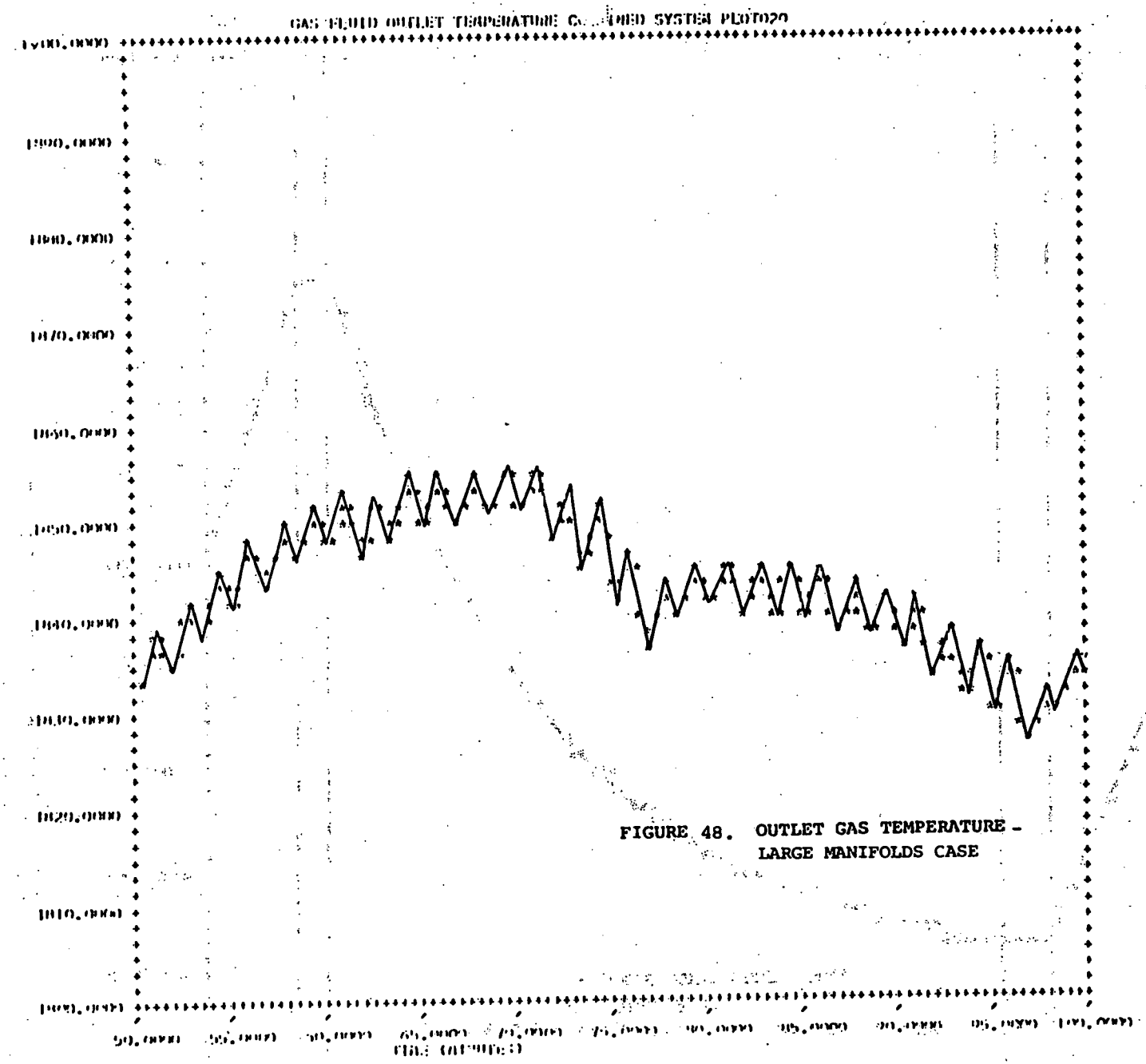

FIGURE 48. OUTLET GAS TEMPERATURE - LARGE MANIFOLDS CASE

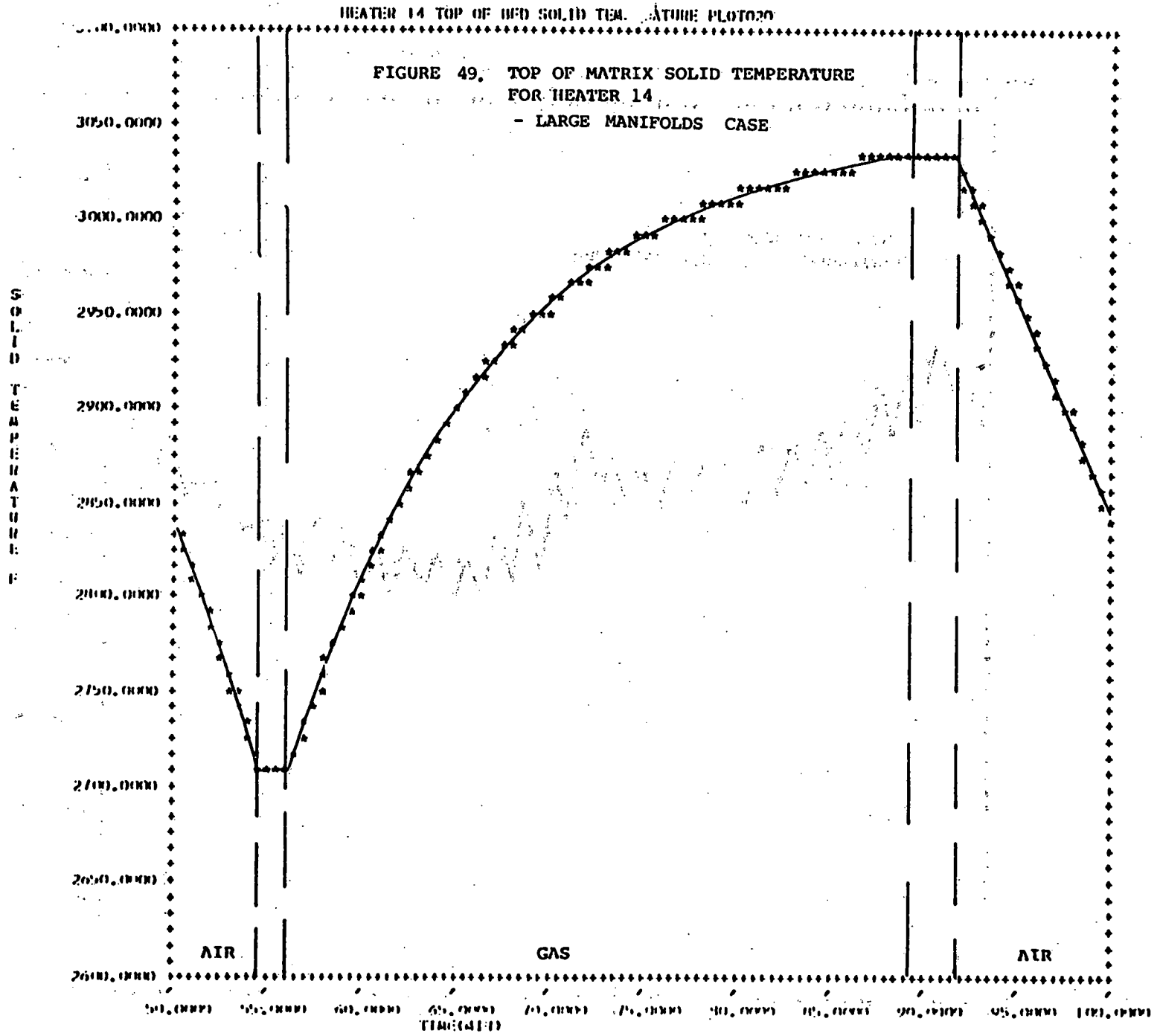

FIGURE 49. TOP OF MATRIX SOLID TEMPERATURE FOR HEATER 14 - LARGE MANIFOLDS CASE

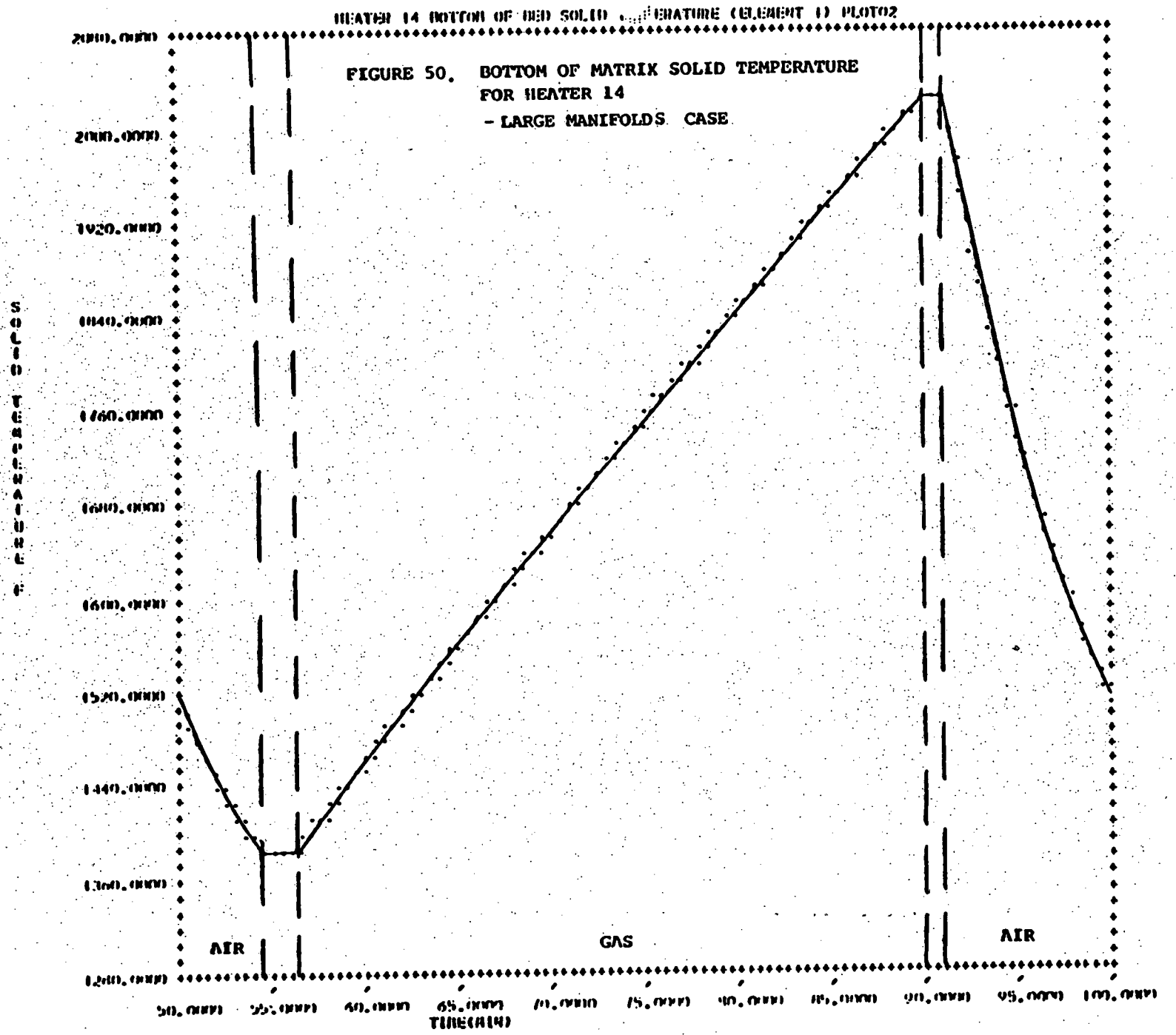

FIGURE 50. BOTTOM OF MATRIX SOLID TEMPERATURE FOR HEATER 14 - LARGE MANIFOLDS CASE

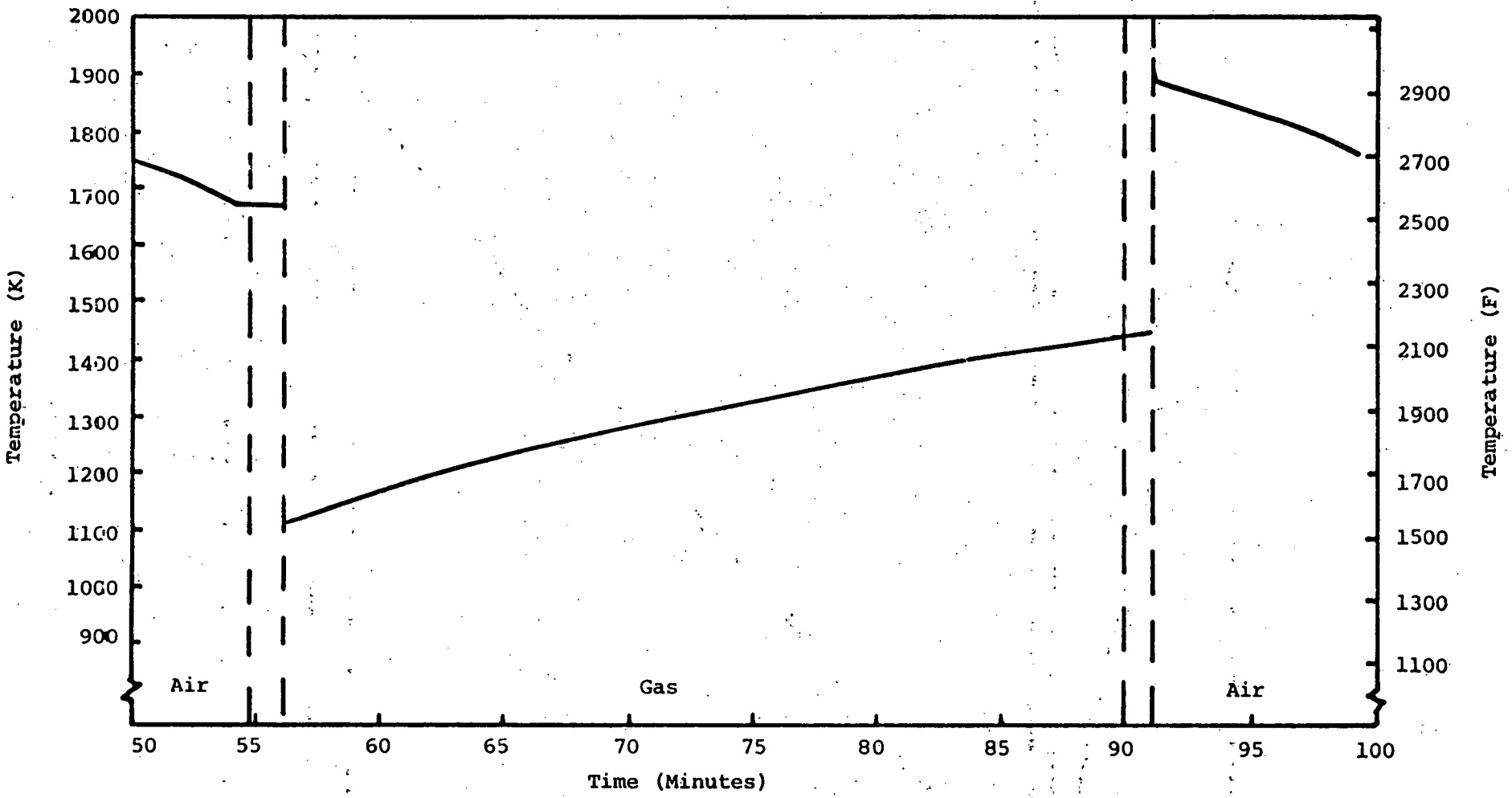

FIGURE 51. OUTLET AIR AND GAS TEMPERATURES FOR HEATER 14, LARGE MANIFOLDS CASE

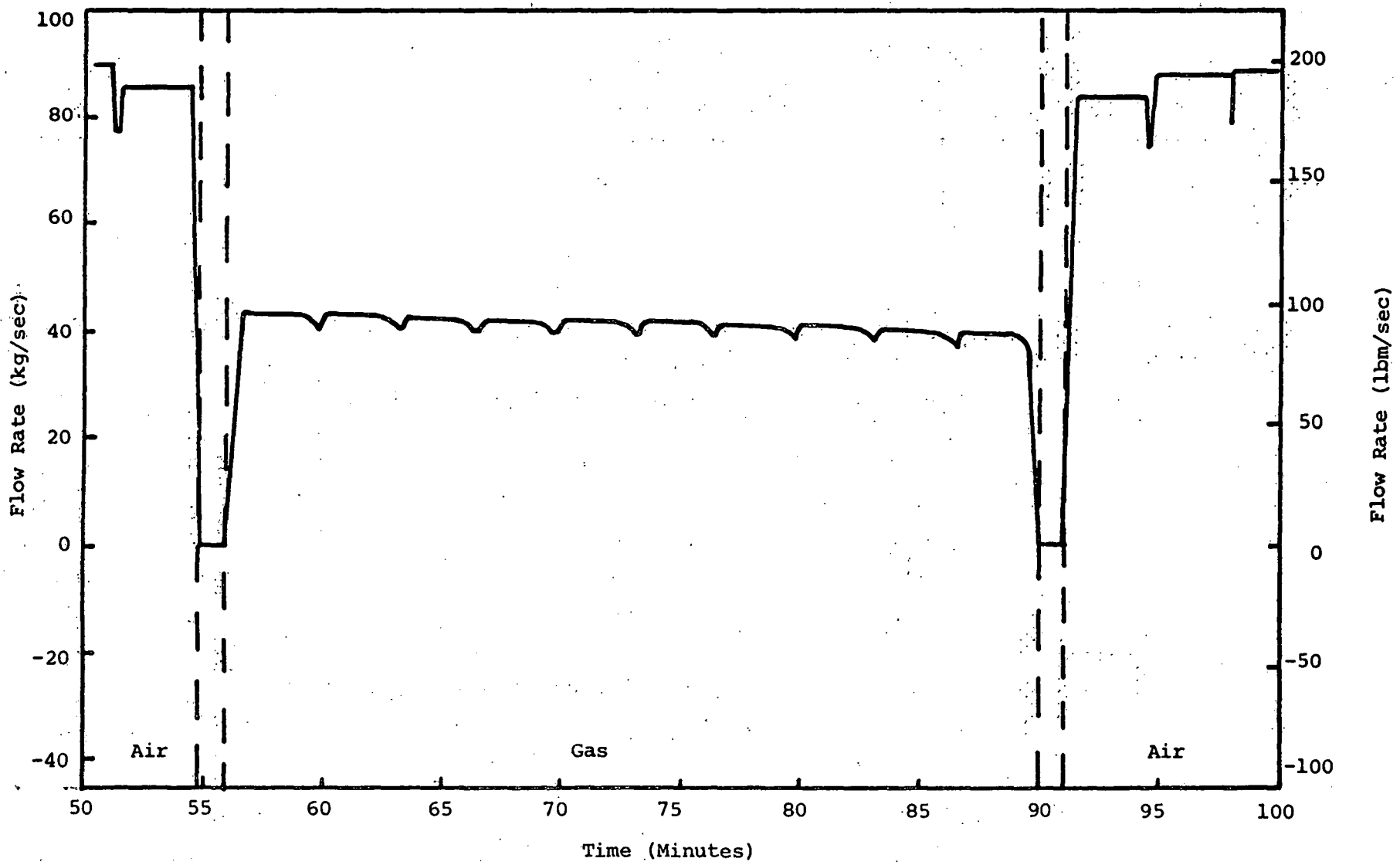

FIGURE 52. AIR AND GAS FLOW RATES THROUGH HEATER 14 - LARGE MANIFOLDS CASE

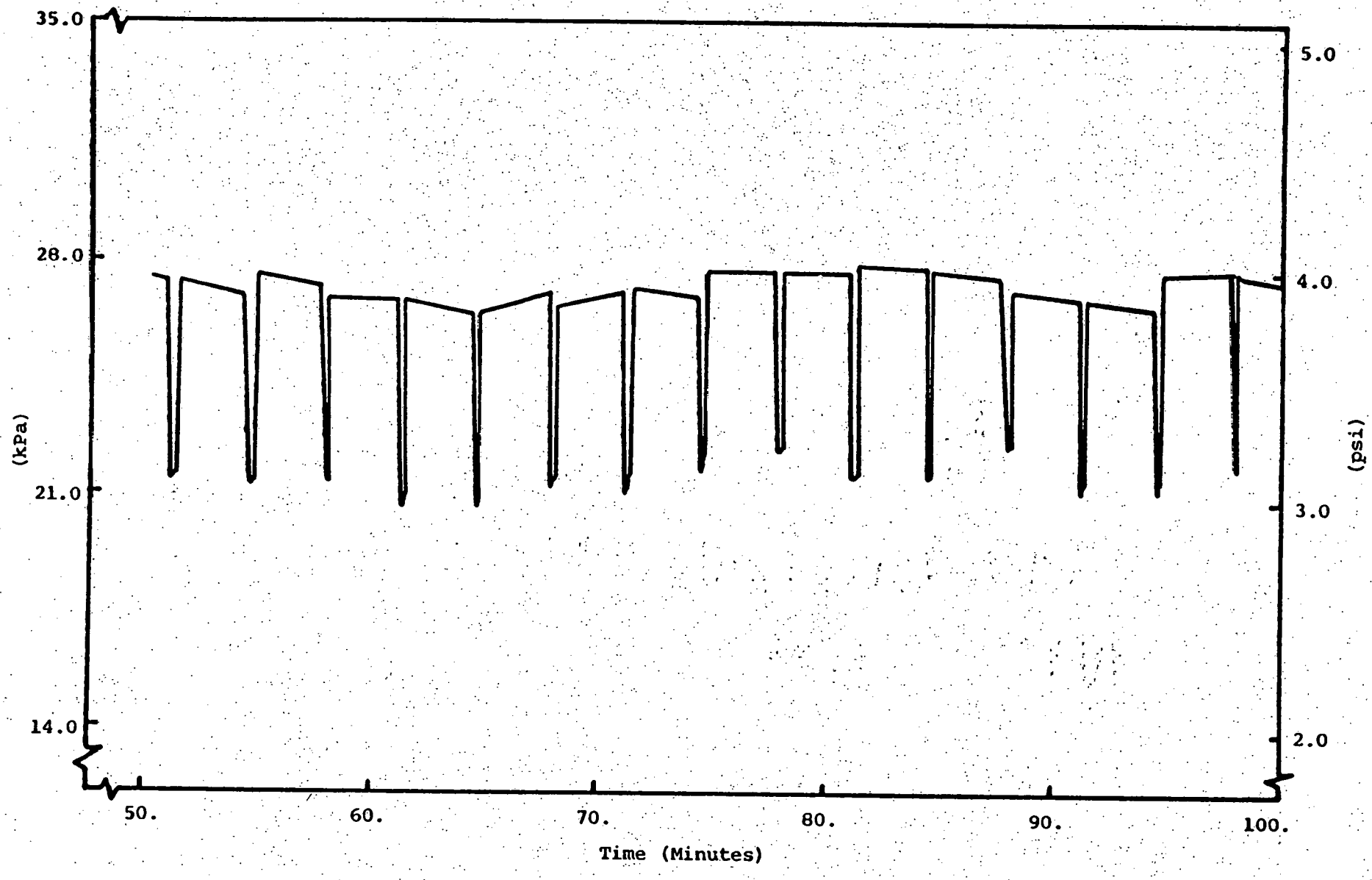

FIGURE 53. AIR SIDE PRESSURE LOSS THROUGH HTAH - LARGE MANIFOLDS CASE

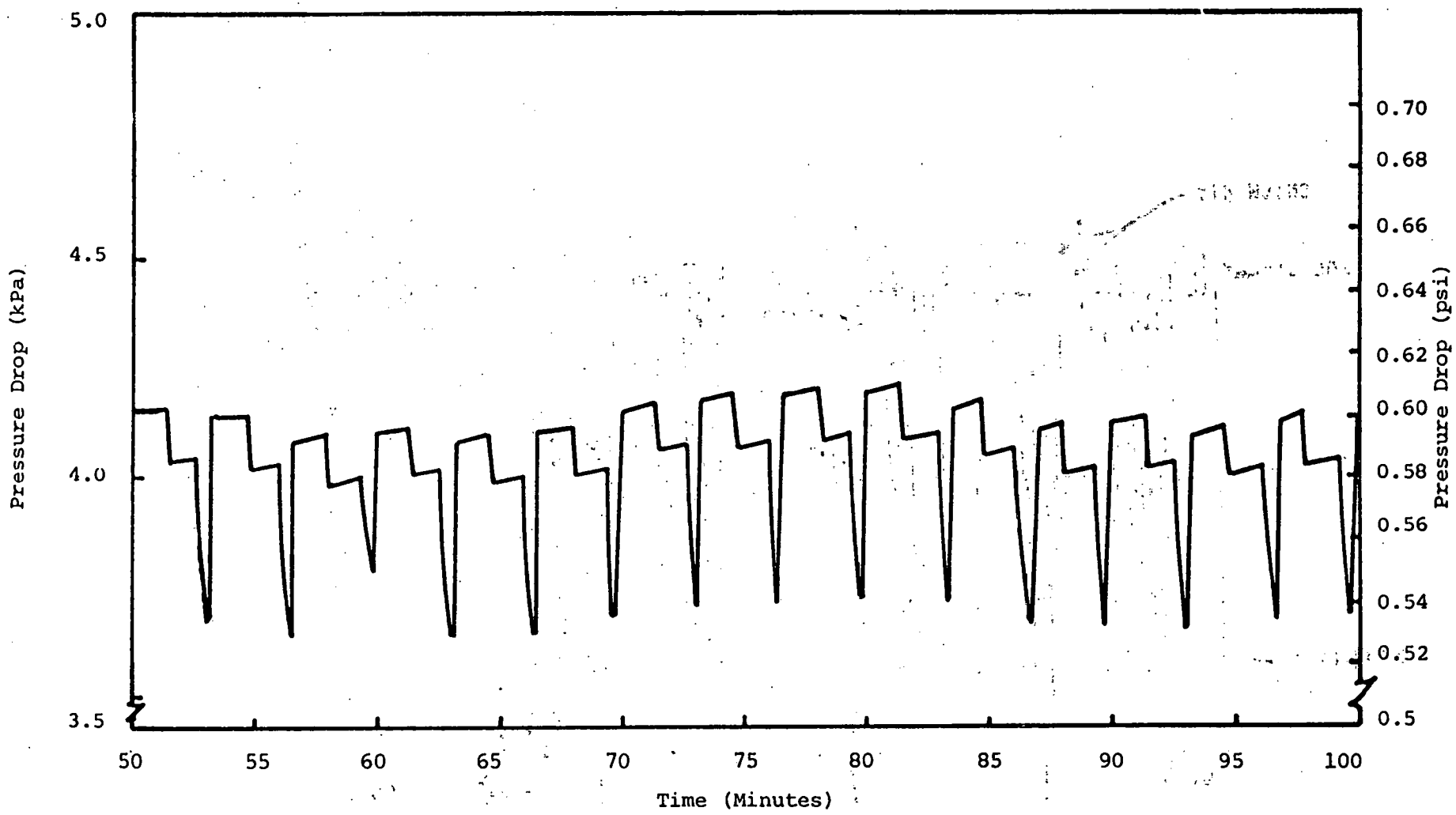

FIGURE 54. GAS SIDE PRESSURE LOSS THROUGH HTAH - LARGE MANIFOLDS CASE

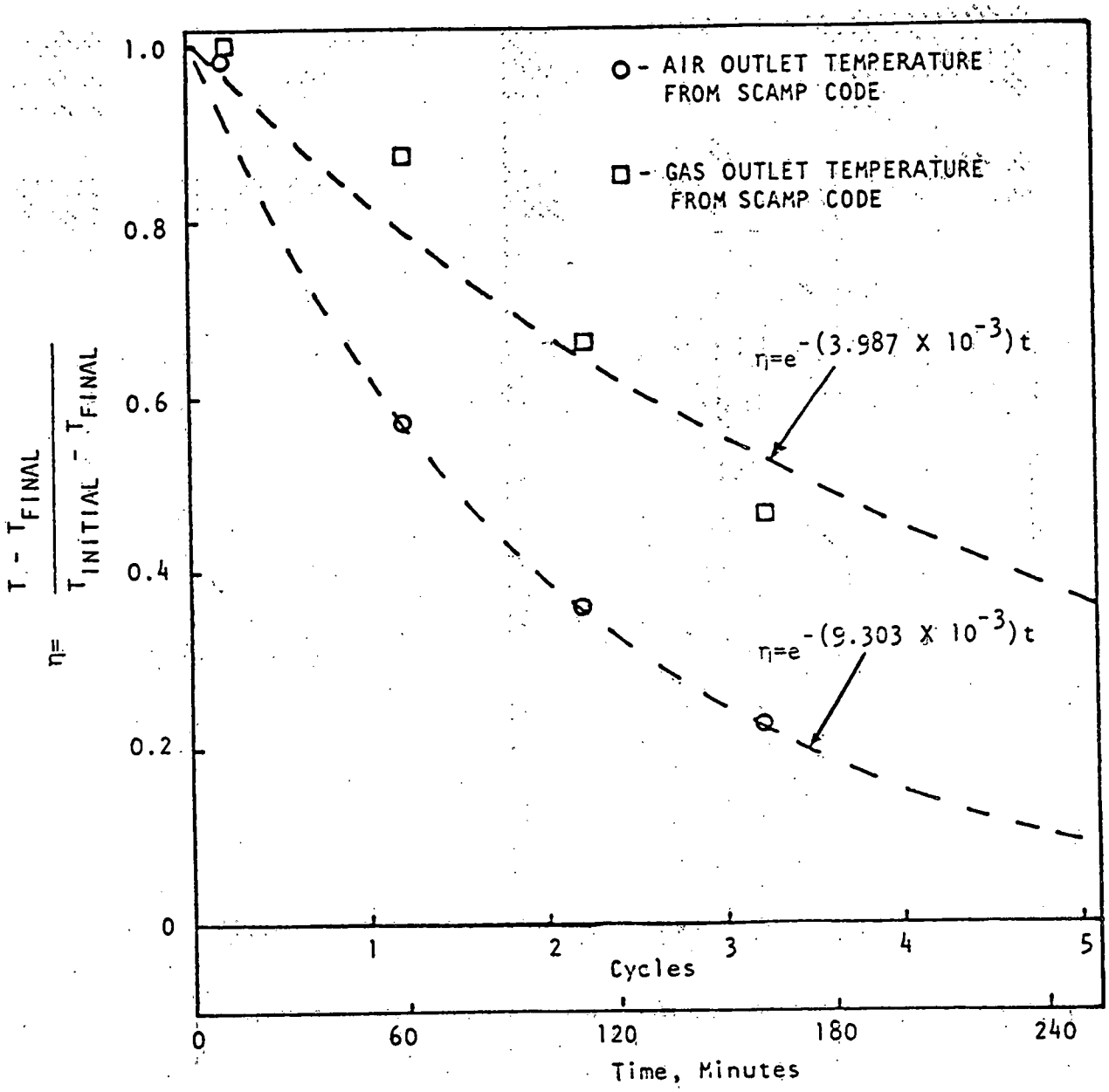

FIGURE 55. TRANSFER FUNCTIONS FOR HTAH AIR AND GAS OUTLET TEMPERATURES

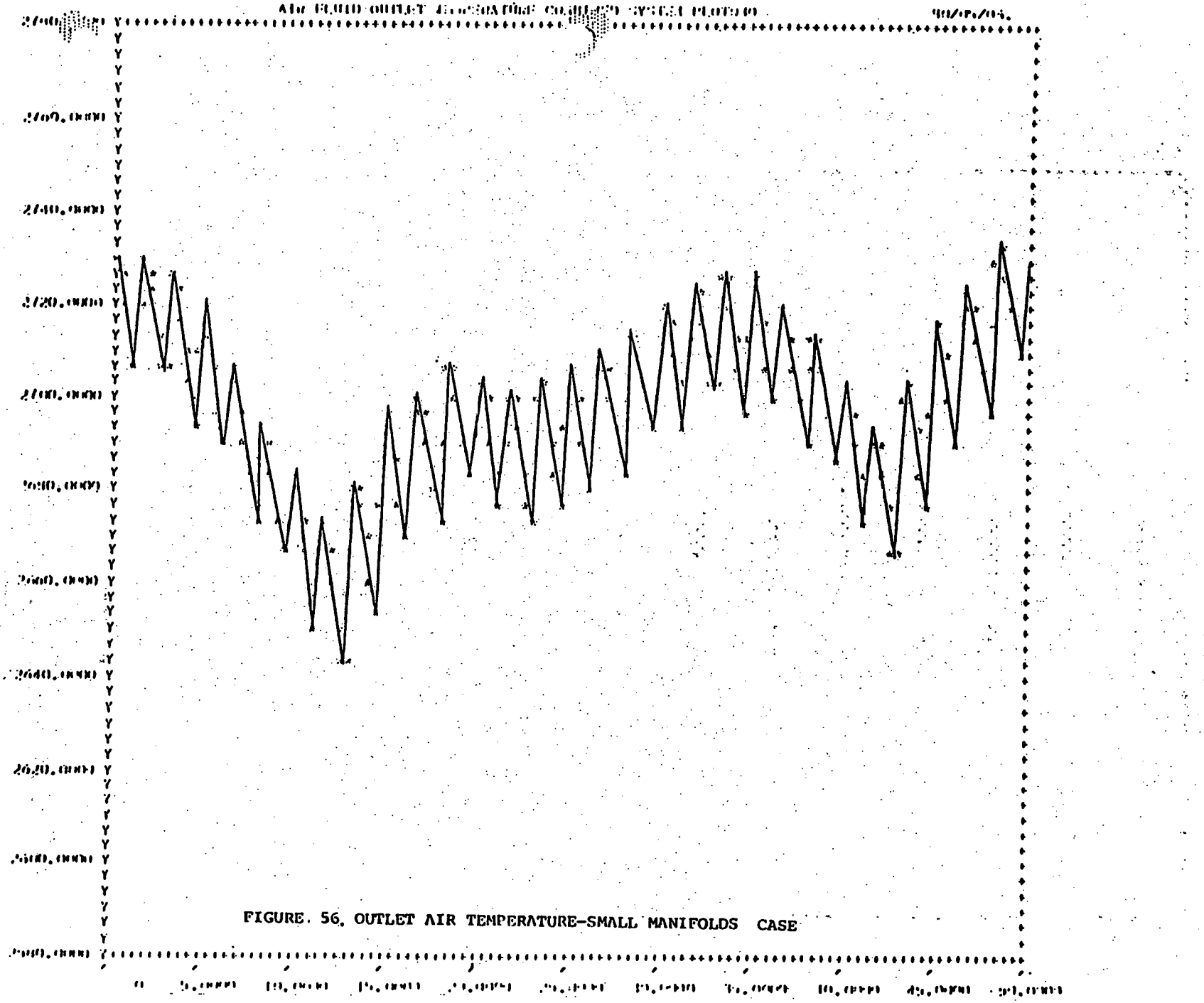

FIGURE. 56. OUTLET AIR TEMPERATURE–SMALL MANIFOLDS CASE

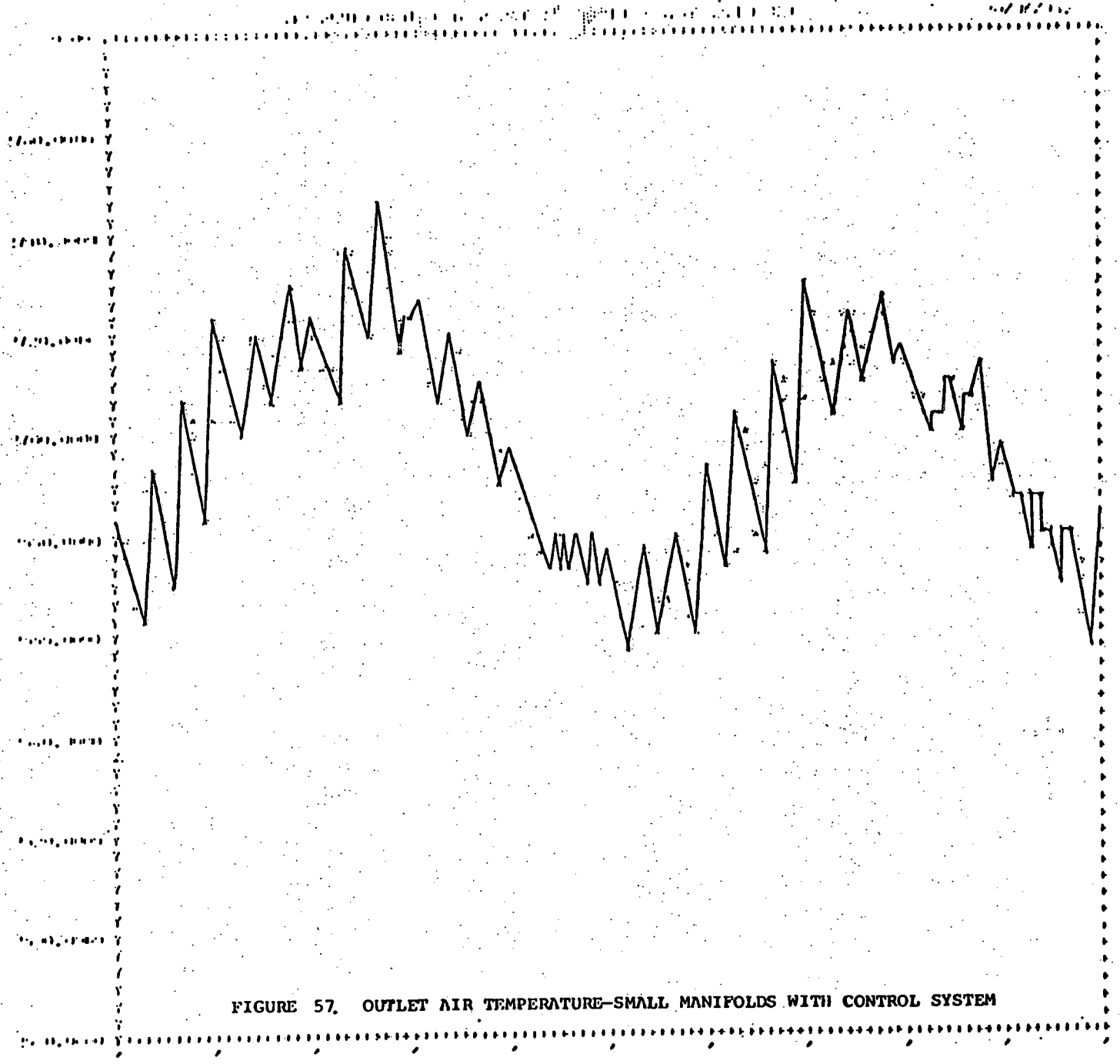

FIGURE 57. OUTLET AIR TEMPERATURE–SMALL MANIFOLDS WITH CONTROL SYSTEM

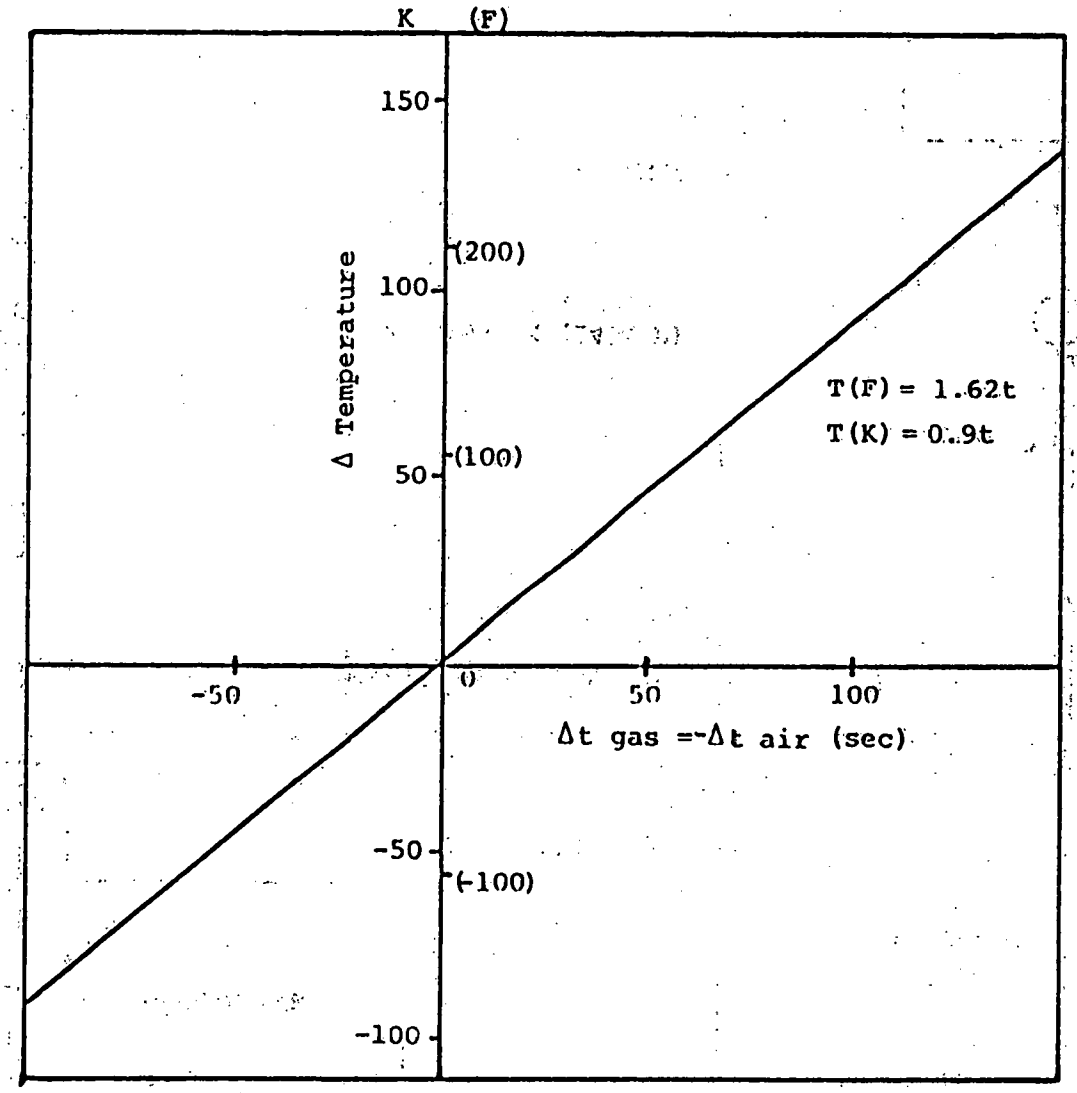

FIGURE 58. CHANGE IN MAXIMUM BOTTOM OF BED SOLID TEMPERATURE WITH CHANGE IN GAS-AIR CYCLE TIME FROM STRIEX

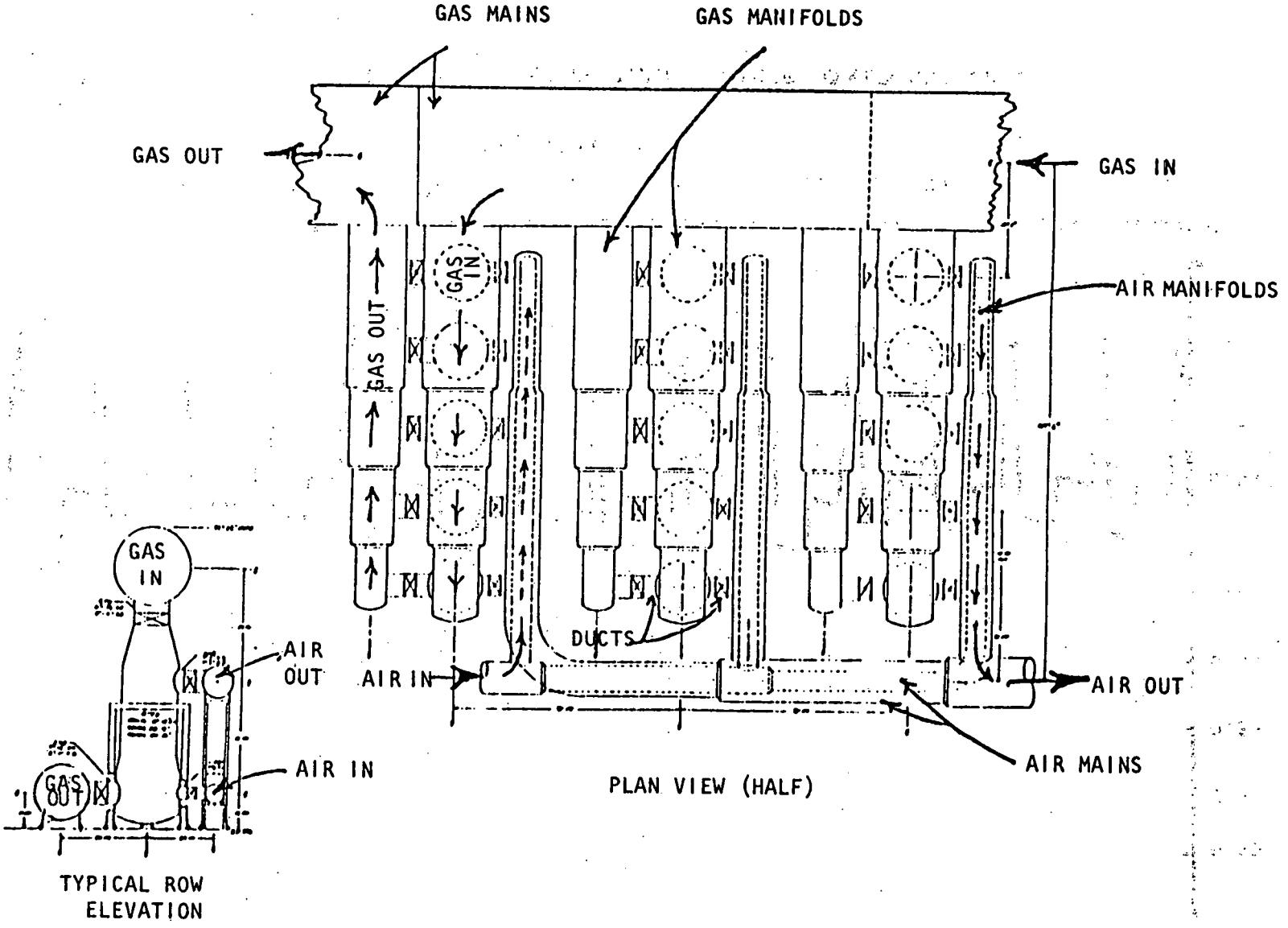

FIGURE 59. LAYOUT OF EXAMPLE HTAH FOR 1000 MW_e PLANT

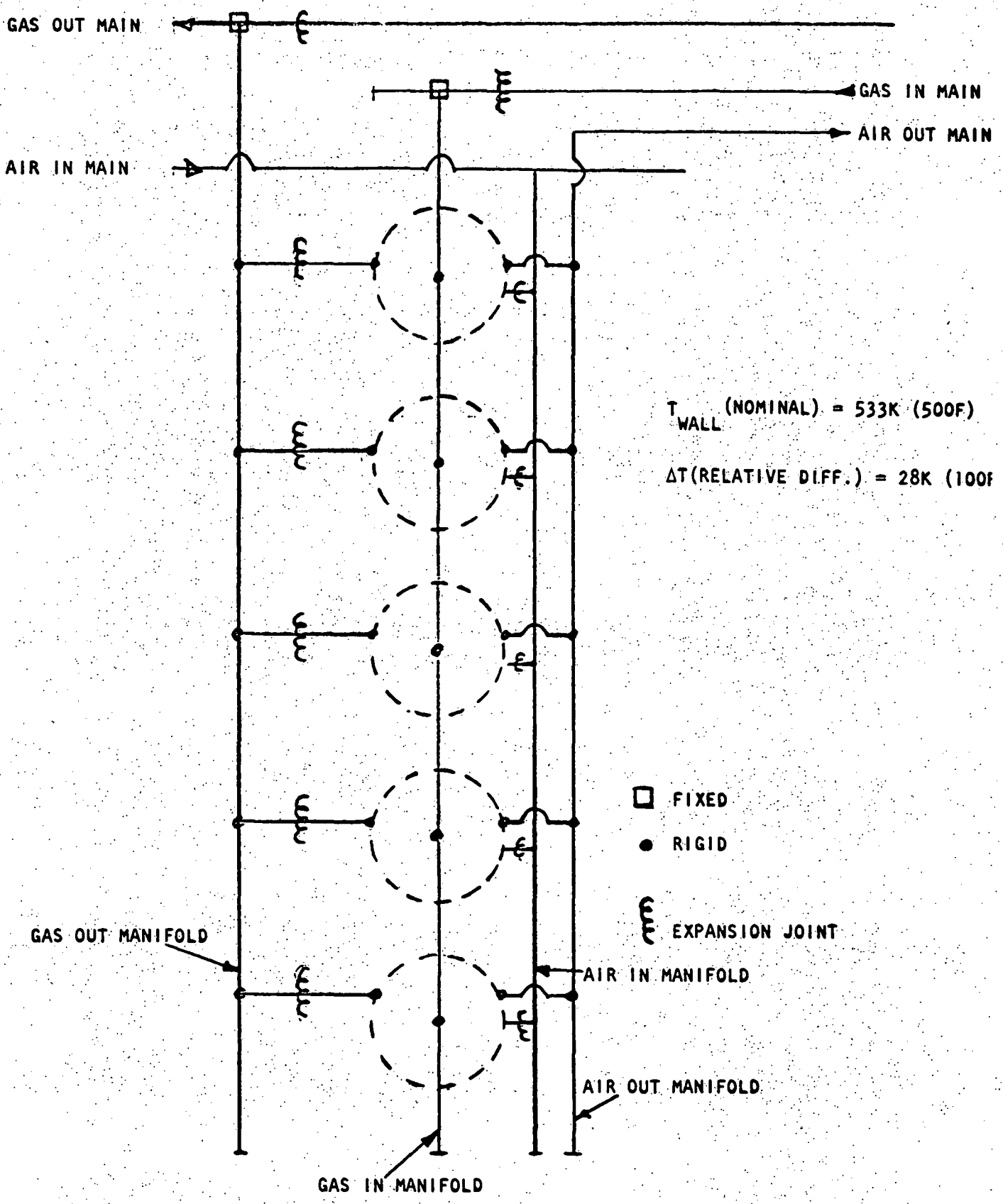

FIGURE 60. TYPICAL HEATER ROW SHOWING THERMAL EXPANSION CONCEPT

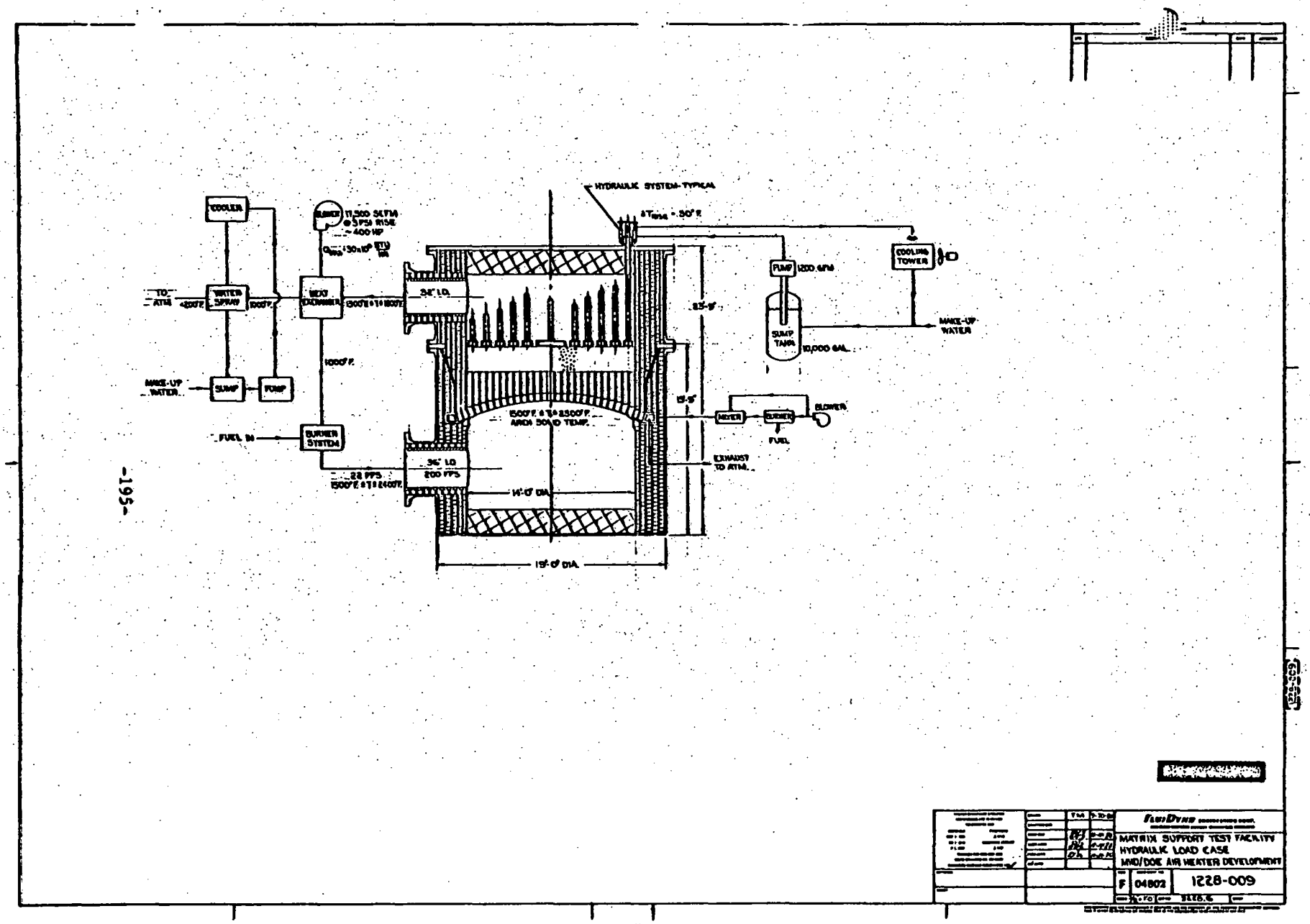

FIGURE 61. MATRIX SUPPORT TEST FACILITY CONCEPT WITH HYDRAULIC LOAD

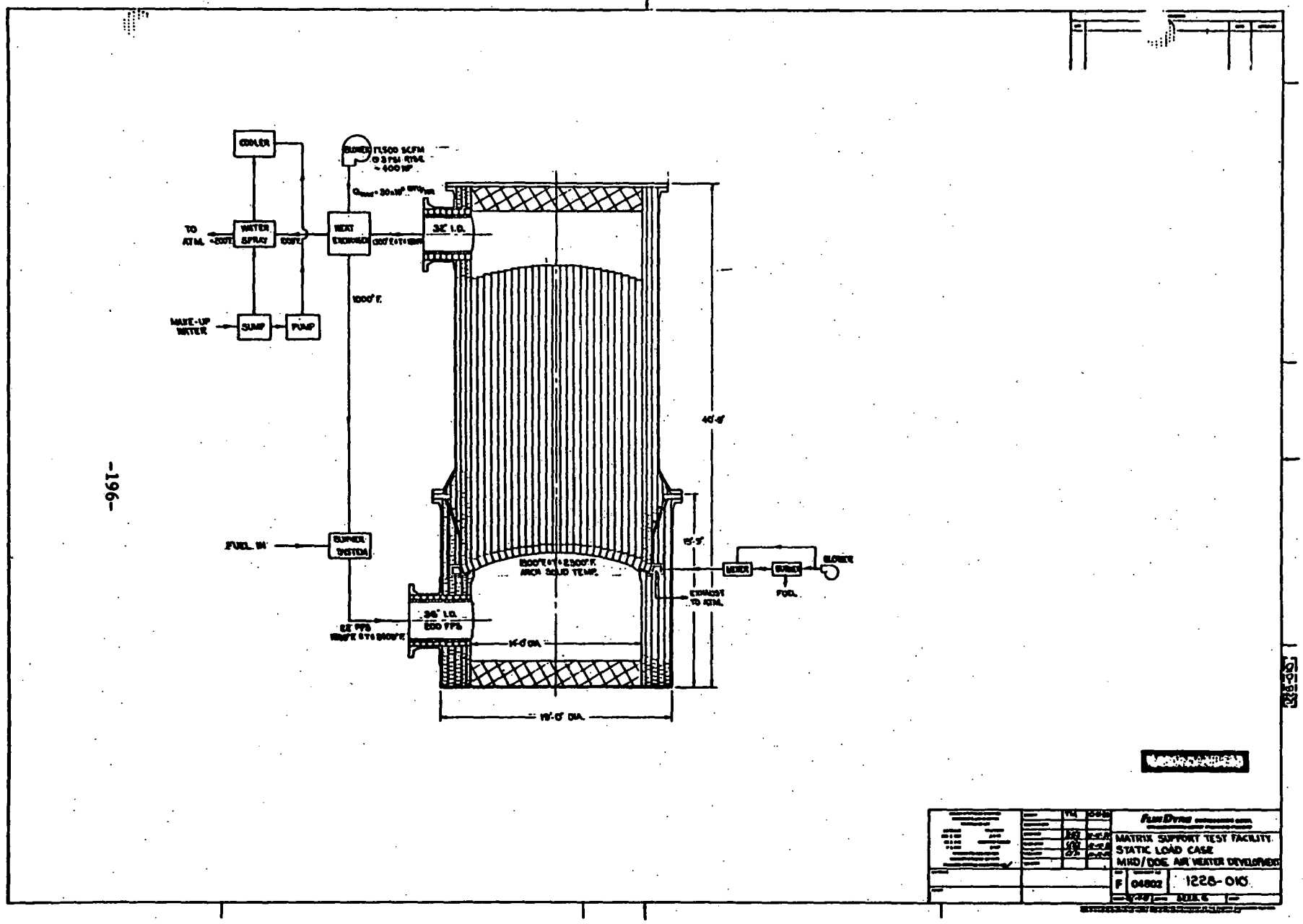

FIGURE 62. MATRIX SUPPORT TEST FACILITY CONCEPT WITH STATIC LOAD

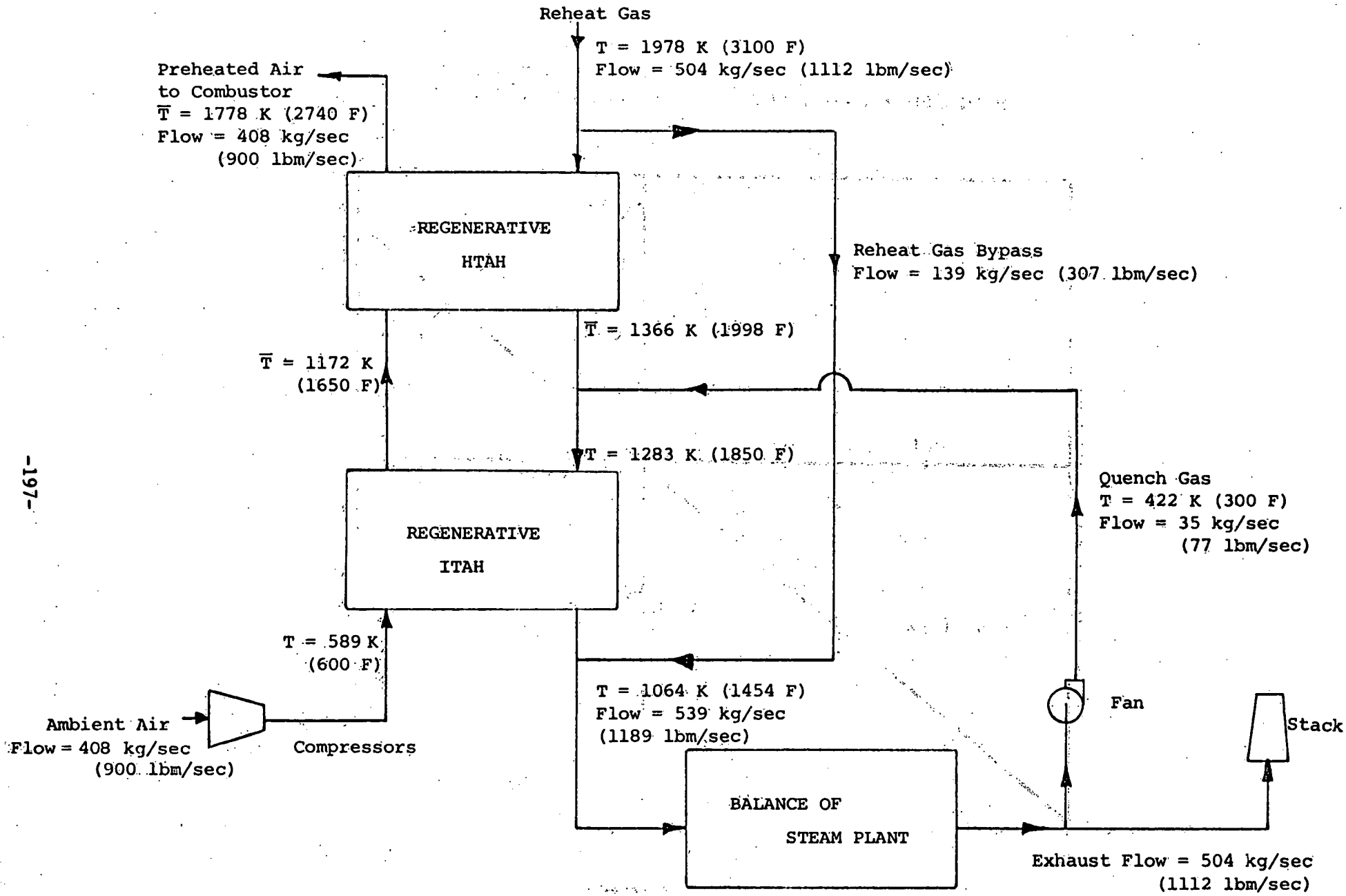

FIGURE 63. SCHEMATIC FLOW DIAGRAM FOR INTEGRATED ITAH/HTAH SYSTEM

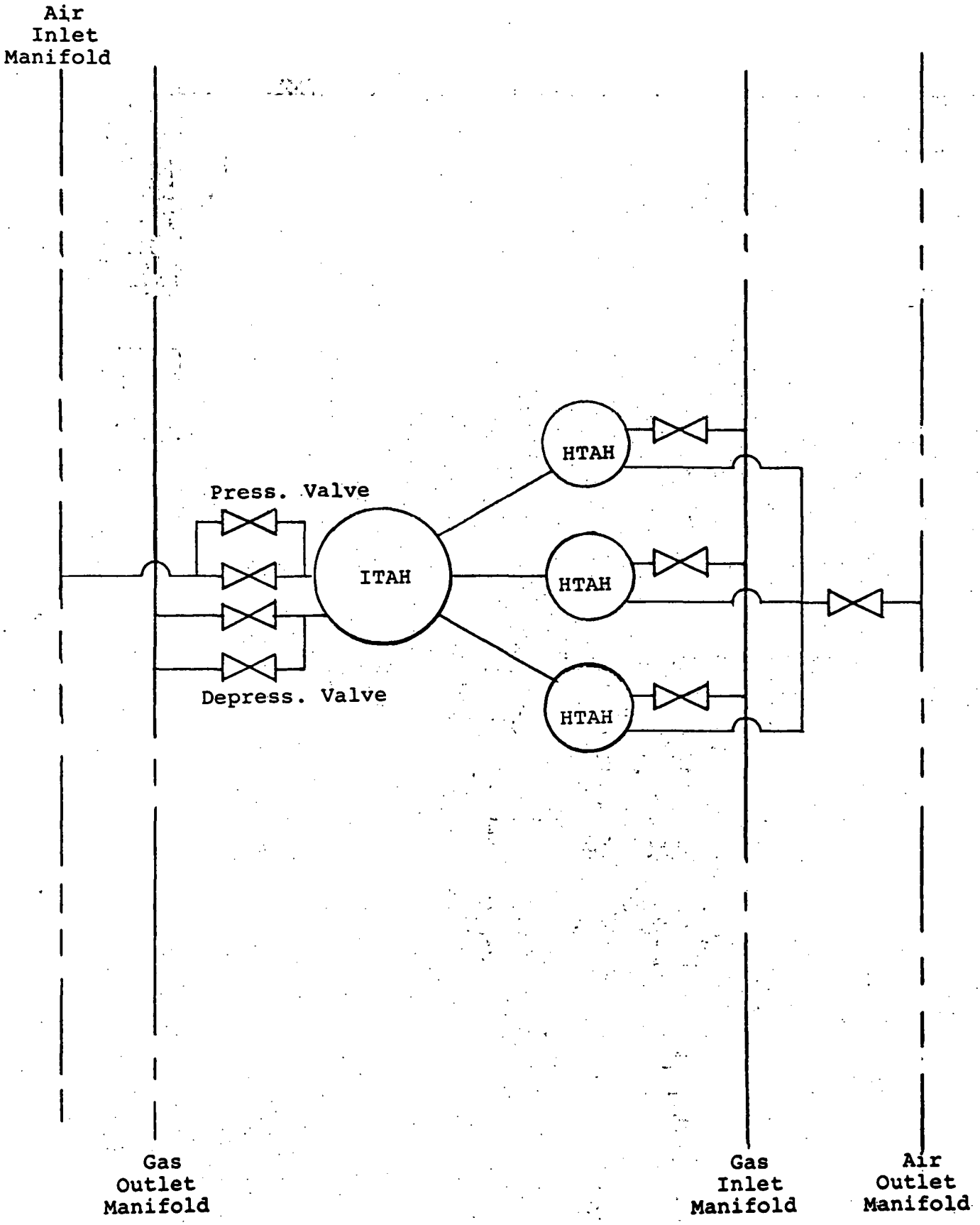

FIGURE 64. SCHEMATIC ARRANGEMENT OF INTEGRATED ITAH/HTAH HEATERS

☆U.S. GOVERNMENT PRINTING OFFICE: 1981-740-145/2127